

Bacterial population and biodegradation potential in chronically crude oil-contaminated marine sediments are strongly linked to temperature

Bargiela, R.; Mapelli, F.; Rojo, D.; Chouaia, B.; Tornés, J.; Borin, S.; Richter, M.; Del Pozo, M.V.; Cappello, S.; Gertler, C.; Genovese, M.; Denaro, R.; Martínez-Martínez, M.; Fodelianakis, S.; Amer, R.A.; Bigazzi, D.; Han, X.; Chen, J.; Chernikova, T.N.; Golyshina, O.V.; Mahjoubi, M.; Jaouanil, A.; Benzha, F.; Magagnini, M.; Hussein, E.; Al-Horani, F.; Cherif, A., [No Value]; Blaghen, M.; Abdel-Fattah, Y.R.; Kalogerakis, N.; Barbas, C.; Malkawi, H.I.; Golyshin, P.N.; Yakimov, M.M.; Daffonchio, D.; Ferrer, M.

Scientific Reports

DOI:
[10.1038/srep11651](https://doi.org/10.1038/srep11651)

Published: 29/06/2015

Publisher's PDF, also known as Version of record

[Cyswllt i'r cyhoeddiad / Link to publication](#)

Dyfyniad o'r fersiwn a gyhoeddwyd / Citation for published version (APA):

Bargiela, R., Mapelli, F., Rojo, D., Chouaia, B., Tornés, J., Borin, S., Richter, M., Del Pozo, M. V., Cappello, S., Gertler, C., Genovese, M., Denaro, R., Martínez-Martínez, M., Fodelianakis, S., Amer, R. A., Bigazzi, D., Han, X., Chen, J., Chernikova, T. N., ... Ferrer, M. (2015). Bacterial population and biodegradation potential in chronically crude oil-contaminated marine sediments are strongly linked to temperature. *Scientific Reports*, 5, Article Number 11651. <https://doi.org/10.1038/srep11651>

Hawliau Cyffredinol / General rights

Copyright and moral rights for the publications made accessible in the public portal are retained by the authors and/or other copyright owners and it is a condition of accessing publications that users recognise and abide by the legal requirements associated with these rights.

- Users may download and print one copy of any publication from the public portal for the purpose of private study or research.
- You may not further distribute the material or use it for any profit-making activity or commercial gain
- You may freely distribute the URL identifying the publication in the public portal ?

Take down policy

If you believe that this document breaches copyright please contact us providing details, and we will remove access to the work immediately and investigate your claim.

**Bacterial population and biodegradation potential in chronically crude oil-contaminated
marine sediments are strongly linked to temperature**

Rafael Bargiela, Francesca Mapelli, David Rojo, Bessem Chouaia, Jesús Tornés, Sara Borin, Michael Richter, Mercedes V. Del Pozo, Simone Cappello, Christoph Gertler, María Genovese, Renata Denaro, Mónica Martínez-Martínez, Stilianos Fodelianakis, Ranya A. Amer, David Bigazzi, Xifang Han, Jianwei Chen, Tatyana N. Chernikova, Olga V. Golyshina, Mouna Mahjoubi, Atef Jaouani, Fatima Benzha, Mirko Magagnini, Emad Hussein, Fuad Al-Horani, Ameer Cherif, Mohamed Blaghen, Yasser R. Abdel-Fattah, Nicolas Kalogerakis, Coral Barbas, Hanan I. Malkawi, Peter N. Golyshin, Michail M. Yakimov, Daniele Daffonchio, Manuel Ferrer

12 SUPPLEMENTARY MATERIAL

14 Supplementary Results and Discussion

Bacterial diversity through 16S rRNA pyrotag analysis: general comments. Overall, Proteobacteria was the most abundant (50–100% total sequences) at all sites with the exception of MCh, which was dominated by Bacteroidetes (77.9% total sequences) (Supplementary Fig. S1). The bacterial community at the AQ site contained the highest percentage of Proteobacteria (100%), whereas this phylum was detected at the lowest level (below 50%) at the MES and MCh sites. Note, that no sequences in our dataset were affiliated with the genus *Alcanivorax* or other typical specialized hydrocarbonoclastic (HCB) bacteria. The lack of detection of such species may be due to the very high relative abundance of other genera, as reported in the Deepwater Horizon oil spill³, that are likely more adapted to the unique environmental constraints characterizing the investigated sites. Note also that, although bacteria of the genus *Alcanivorax* were not enriched during the Deep Horizon Oil Spill, in some cases sequences and/or cultured isolates were detected, which may also be possible to occur in the samples herein analysed.

Among those bacteria belonging to the Proteobacteria phylum, Gammaproteobacteria was the predominant class in the sediments AQ, HAV, PRI, MES, and BIZ (comprising 87.6, 55.8, 33.4, 31.3, and 23.4% of the total bacterial community, respectively) (Supplementary Fig. S1B). In addition, Gammaproteobacteria was also the richest class in term of diversity and was represented by 17 different genera/unclassified families (Supplementary Table S3), including *Marinobacter*, *Pseudoalteromonas*, and *Cycloclasticus*, which comprise populations well known for their oil biodegrading capabilities^{32,33}. The sediment of the AQ site was primarily colonized by the genera *Alteromonas* and *Psychrobacter*, which represented 20.5 and 63.7% of the total bacterial community, respectively. Mercury-resistant *Psychrobacter* strains were previously isolated from the sediment of a coastal lagoon in Italy and have been suggested as a possible tool in the bioremediation of mercury-contaminated sediments³⁴. The adaptation of this genus to a broad class of pollutants is further suggested by the ability of *Psychrobacter* strains isolated from Antarctica to degrade polychlorinated biphenyls (PCB) in the laboratory³⁵. The isolation of strains able to degrade naphthalene, phenanthrene, anthracene, and pyrene during microcosm assays suggests that the genus *Alteromonas* was a key player during the biodegradation of PAH during an oil spill along the Korean shoreline³⁶.

The bacterial community of the polluted sediments collected at site ELF primarily comprised Deltaproteobacteria (47% of the total bacterial community, Supplementary Fig. S1B), which was represented by six different genera (Supplementary Table S3). A high abundance of Deltaproteobacteria primarily represented by sulfate-reducing bacteria (SRB) was previously

reported for other natural environments characterized by the presence of oil hydrocarbons and anoxic conditions. These environmental conditions favor the establishment of bacteria belonging to the cluster *Desulfosarcina-Desulfococcus*, which are involved in oil biodegradation processes^{37,38}, and bacteria belonging to the family *Syntrophobacteraceae*, which has been implicated in metal attenuation and retention in sediments³⁹ and constituted 24.7% of the total community in the ELF site. Deltaproteobacteria were also detected at the HAV site (6.6% of the bacterial community, Supplementary Fig. S1B), where the phylum Proteobacteria comprises 92% of the bacterial community (Supplementary Fig. S1A), encompassing all the known classes except for Zetaproteobacteria. Sequences affiliated with the class Betaproteobacteria were detected exclusively at this site (Supplementary Fig. S1B), where the most abundant class was Gammaproteobacteria, including, among others and in addition to the prevalent group of unclassified sequences (42.1% of the bacterial community), the oil-degrading genera *Pseudoalteromonas* and *Cycloclasticus* (Supplementary Table S3). A similar bacterial community composition was observed at the PRI site, where Delta-, Epsilon-, and Gammaproteobacteria were the major phylogenetic groups (Supplementary Fig. S1B). Moreover, among the most abundant members of the proteobacterial communities at the MCh site, the *Arcobacter* genus, belonging to the Epsilonproteobacteria, represented 7% of the sequences detected by bar-coded pyrosequencing. This genus was recently cultivated from oil-polluted sediments in enrichment cultures supplemented with phenanthrene⁴⁰. Finally, at the ELMAX site, the most abundant class was represented by Alphaproteobacteria (Supplementary Fig. S1B), a phylogenetic class widespread in sea-water samples⁴¹ and comprising, in our dataset, 14 different genera (Supplementary Table S3) that formed 46.3% of the total bacterial community.

Apart from Proteobacteria, we found that other members were significantly enriched. The ELMAX bacterial community also contained a high percentage of sequences affiliated with the genus *Bacillus* (Supplementary Table S3), whose presence has been already reported in several hydrocarbon-degrading consortia^{37,42}. MCh was dominated by the class Flavobacteria of the phylum Bacteroidetes (77.9%; Supplementary Fig. S1A). The Bacteroidetes phylum is frequently found in nutrient-rich habitats and has been recognized as a key actor in the carbon cycle in marine environments due to the ability of its members to degrade high-molecular-weight organic matter and biopolymers such as protein and polysaccharides⁴³. The first genomic data available for the Bacteroidetes group was related to the genus *Gramella*⁴³, which represented 4.1% of the total bacterial community at the MCh site (Supplementary Table S3). Bacteroidetes at the MCh site was primarily represented by the genus *Salinimicrobium* (Supplementary Table S3), formerly isolated from saline soils tidal flat sediments⁴⁴. The Bacteroidetes phylum was also abundantly present at the MES site, together with the classes Planctomycetes (Supplementary Fig. S1A-B)

and Gammaproteobacteria, which belong to the family Piscirickettsiaceae (Supplementary Table S1). A high percentage of the bacteria colonizing the MES sediment belonged to the candidate division OD1 (Supplementary Table S3) that was previously found in anoxic, sulfur-rich aquatic ecosystems⁴⁵ in which their ecological role remains unknown. Finally, Planctomycetes of the order Phycisphaerales was particularly abundant in the MES site (Supplementary Table S3). A preponderance of the Proteobacteria phylum was also observed at the lagoon of BIZ site (Supplementary Fig. S1), although at this site, Flavobacteria was the most abundant class (Supplementary Table S3), similar to MCh.

Biogeography of total and crude oil degrading bacterial populations

Low temperature (here, $\leq 19.3^{\circ}\text{C}$) and restricted oxygen (here, $\leq 6.5\text{ mg/L}$) seems to favour the establishment of bacteria belonging to seven different genera/unclassified families (Supplementary Table S3). Those belonging to the families *Desulfobulbaceae*, *Helicobacteraceae* and *Acidimicrobiales* developed primarily (from 0.33 to 18.09% total sequences) at sites with lower temperature (here, $\leq 19.3^{\circ}\text{C}$) and restricted oxygen (here, $\leq 6.5\text{ mg/L}$), namely, ELF, HAV, PRI and BIZ, which formed the Cluster 1 described in Fig. 1. The low relative representation ($\leq 0.047\%$) of these bacterial families at ELMAX (20.0°C), which had a high O_2 concentration (18.0 mg/L), and their absence in the moderately warmer MES site (23.0°C), which was micro-anaerobic (O_2 : $1.0\text{--}2.2\text{ mg/L}$), support members of these families associated to cold- and O_2 -restricted sediments. In addition, bacteria belonging to the families *Syntrophobacteraceae* and *Thermodesulfovibrionaceae* (from 0.1 to 24.7%) were only found at sites with a temperature $\leq 19.0^{\circ}\text{C}$ (ELF, HAV and PRI), and those belonging to the families *Phycisphaerae* and *Desulfobacteraceae* (from 0.1 to 2.3%) at the sites with temperatures $\leq 15.0^{\circ}\text{C}$ (ELF and PRI).

In addition to temperature, other factors, alone or in combination with temperature, are also important secondary factors that influenced the distribution of particular sets of bacterial groups. As summarized in Supplementary Table S3, ELMAX contained the highest number (14, representing 74.1% total sequences) of habitat-specific groups, followed by HAV and MES (3 each, representing 11.98% and 11.47%, respectively), MCh and AQ (2 each, representing 13.53% and 64.39%, respectively) and BIZ (1, accounting 1.85%), whereas none was exclusive at the PRI and ELF sites. Among habitat-specific groups, members unambiguously classified within the genera/families *Caulobacteraceae*, *Bradyrhizobiaceae*, *Methylobacteriaceae*, *Sinobacteraceae*, TM7, *Propionibacterium*, *Methylobacterium*, *Bradyrhizobium*, *Planomicrobium*, *Chitinophagaceae*, *Staphylococcus*, *Anaerococcus*, *Thiomicrospira*, and *Corynebacterium* (in order from higher to lower percentage of sequences referred to the total) were only found in ELMAX, AB16 in HAV, *Spirochaetes* in BIZ, *Gramella* and *Bacillaceae* in MCh, *Mesorhizobium* and candidate division OD1 in

MES and *Nautella* and *Psychrobacter* in AQ. In addition, notable dominance of members of the genera *Salinimicrobium* at the MCh site (73.8% total sequences), *Alteromonas* (20.5%) at the AQ site and of the class Planctomycetes (15.86%) at the MES site, were also observed (Supplementary Table S3).

Finally, bacteria belonging to the genera *Cycloclasticus* (from 0.19 to 2.97%) and *Sulfuricurvum* (from 0.22 to 10.93%; Supplementary Table S3) were restricted to geographically related sites, namely, sites in the more northern part of the whole marine north-south transect we have considered (HAV, PRI, MES and BIZ). While *Cycloclasticus* appeared to be selected (≥ 6.3 -fold in terms of relative percentage of total sequences) in sites with restricted oxygen (here, ≤ 6.5 mg/L) and higher crude oil input (HAV; tar sample), *Sulfuricurvum* was most abundant (≥ 10.3 -fold) in highly contaminated anoxic sites (PRI; 4,000 ppm total hydrocarbons). Furthermore, bacterial members associated to *Phycisphaerales* and *Piscirickettsiaceae* were only associated with more northern sites, namely HAV, PRI and MES, although it was particularly enriched (24.25%) at the warmer (23.0°C) and micro-aerobic (1.0-2.2 mg/L O₂) MES site.

Degradation efficiency of pollutants in enrichment cultures by targeted metabolomics

Targeted GC-Q-MS and LC-QTOF-MS were used to confirm the degradation of 17 pollutants, expected to be degraded to different extents by each of the microbial populations. For that, we determined their abundance level (Supplementary Table S7A) as well as the presence and abundance of 9 key degradation intermediates produced during their degradation (Supplementary Table S7B), in enrichment cultures performed as described in Supplementary Methods. The extent of the degradation efficiency, by meaning of the remaining concentration of chemical species at the end of the three-week incubation time, as compared to the initial concentration and control tests, was calculated.

As shown in Supplementary Table S7A, for AQ all pollutants were degraded, with relative degradation values ranging from ~99 to 41%, after three-weeks incubations. For BIZ, all tested pollutants were degraded, with relative degradation values ranging from ~97 to 3.7%. For ELMAX, all tested pollutants but one (carbazole) were degraded, with relative degradation values ranging from ~98 to 29%. For HAV, all tested pollutants but four (chlorobenzoate, carbazole, phenol and anthracene) were degraded, with relative degradation values ranging from ~98 to 4.4%. For MCh, all tested pollutants but three (chlorobenzoate, terephthalate and carbazole) were degraded, with relative degradation values ranging from ~96 to 54%. For MES, all tested pollutants but two (anthracene and carbazole) were degraded, with relative degradation values ranging from ~99 to 47%. For PRI, all tested pollutants but four (benzoate, chlorobenzoate, 2,3-

dihydroxibiphenyl and carbazole) were degraded, with relative degradation values ranging from ~89 to 30%.

As shown in Supplementary Table S7B, examination of the production of intermediate species revealed that the 9 selected intermediates were significantly produced in all microcosms, except gentisate, which was not found in HAV, and chlorocatechol which was slightly produced in MCh.

Since the setup microcosms herein might not mimic environmental conditions and not all microbes present in the original community may grow under the culture conditions we cannot rule out the possibility that the experimental measurements of substrate pollutants and intermediates might not be synonymous with the presence of genomic signatures. Having said that by linking the presence of each of the chemical species with the gene encoding catabolic enzymes involved in their transformation, we were able to link metabolite data with sequencing (DNA and 16S rRNA) data sets (Fig. 2), and good agreement with our *in silico* predictions was observed. This demonstrates that the enrichment conditions herein used were appropriate to detect the degradation reactions herein evaluated.

Supplementary Methods

Sampling sites and sample codes. The investigated sites included the following, in order of latitude coordinates: (1) the Gulf of Genoa in the northernmost part of the Ligurian Sea (Genoa, Italy; 44° 22'25.75"N, 8° 41'59.58"E), where the Haven tanker sunk (*HAV*) in 1991⁴⁷. MT Haven, formerly Amoco Milford Haven, was a very large crude carrier, leased to Troodos Shipping. In 1991, while loaded with 144,000 tonnes (1 million barrels) of crude oil, the ship exploded, caught fire and sank off the coast of Genoa (Italy), and flooding the Mediterranean with up to 50,000 tonnes of crude oil. It broke in two and sank after burning for three days and since this event the Mediterranean coast and sediments of Italy and France was polluted, especially around Genoa; (2) the harbor of Messina (*MES*) (Sicily, Italy; 38°11'42.267"N, 15°34'25.014"E), a marine harbor that generally suffers chronic petroleum pollution because of intensive maritime traffic and its limited hydrodynamic regimen and restricted area^{48,49}; (3) the coast adjacent to an oil refinery unit in the Elefsina Bay (*ELF*) northwest of Athens (Greece; 38°2'16.28"N, 23°30'45.85"E), which is a contaminated shallow coast where petroleum hydrocarbons seep out intermittently from an adjacent oil refinery unit⁵⁰; (4) the harbor of Priolo (*PRI*) Gargallo (Siracusa, Italy; 37°10'27.462"N, 15°12'7.505"E), which is characterized by heavy industrialization and intensive tanker traffic transporting both crude and refined oil⁵¹; (5) the Bizerte lagoon (*BIZ*) located in Northern Tunisia (37°16'08.9"N, 9°53'20.1"E), which is highly populated and urbanized and is subject to a pollution load determined by petroleum components in the area adjacent to an oil

refinery^{52,53}; (6) the lagoon of Mar Chica (*MCh*), located on the north-west Mediterranean coast of Morocco ($35^{\circ}11'57,1''\text{N}$, $2^{\circ}55'37,6''\text{O}$), which is among the largest lagoons in the south coast of the Mediterranean Sea and was in the past exposed to continuous pollution by the town of Nador on its southwestern shore^{54–58}; (7) the El-Max (*ELMAX*) site located on the western side of the city of Alexandria, Egypt ($31^{\circ}9'31.20''\text{N}$, $29^{\circ}50'28.20''\text{E}$), which is the most contaminated seashore in the Alexandria region and exceeds legal environmental pollution limits for heavy metals, poly-aromatic hydrocarbons (PAH), and crude oil-derived pollutants⁵⁹; (8) the Gulf of Aqaba (*AQ*) along the Jordanian coast at the northern end of the Red Sea ($30^{\circ}22'42''\text{N}$, $25^{\circ}24'57''\text{E}$), which is the northernmost tropical sea ecosystem and contains a major oil terminal moving between 20–30 million tons yearly characterized by frequent pollution with accidental oil spills at the oil terminal as well as spills (with high sulfur concentrations) during loading and unloading of ships at the industrial jetty^{60–63}. When necessary, the samples were named based on the code 'MGS', which refers to MetaGenome Source, followed by a short name indicating the origin of the sample, as follows: MGS-HAV (Haven tanker at the Gulf of Genoa); MGS-MES (the harbor of Messina); MGS-PRI (the harbor of Priolo Gargallo); MGS-MCh (the lagoon of Mar Chica); MGS-BIZ (the Bizerte lagoon); MGS-ELMAX (El-Max site); MGS-ELF (Elefsina site); and MGS-AQ (Gulf of Aqaba).

Sample collection, environmental measurements, and nucleic acid extraction. Sediment site duplicates (5.0 kg) were collected at a water depth of 1.0 to 78.0 m (October 2011) by scuba. Analytical procedures, in triplicates per each of the duplicates, are as follows. Temperature, salinity, pH, redox potentials and dissolved oxygen were measured immediately by a portable multiparametric probe analyser (WP 600 Series Meters Eutech instruments Pte Ltd Singapore). Determination of oxygen concentration was carried out using the Winkler method with an automatic endpoint detection burette 716 DNS Titrino (Metrohm AG, Herisau, Switzerland). Samples for measurements of NO_3^- , NO_2^- and PO_4^{3-} and nutrient concentrations were stored at -20°C and were determined later in triplicate in the laboratory using a “SEAL AutoAnalyzer Quattro” following classical methods⁶⁴ with slight modifications adapted for sediments. Briefly, 1 kg of melted sediments were placed in the PVC tube of 15 cm diameter and 50 cm length. Holes of 0.1 cm diameter were drilled at the bottom of the tube and sealed with a rubber tape before filling. For the retrieval of porewater the tapes covering the sampling holes were cut open with a paper knife. A MicroRhizon sampler (Rhizosphere Research Products, Wageningen, Netherlands) of 2 cm length and 1 mm diameter connected to a 1 mL syringe was inserted horizontally and porewater were drawn out gently. Conductivity calibration was carried out with a KCl 0.01 mol/L control solution. Reference solutions with pH values of 7.0 and 9.0 were employed for pH

meter. Ammonium was determined using the indophenol blue technique (IOC, 1983). The dissolved organic carbon content was determined by the dichromate wet oxidation method^{65,66}; total organic matter content was calculated by multiplying the values of the organic carbon by 1.8. The amount of total extracted and resolved hydrocarbons (TERHC), was determined as follows. Briefly, TERCH were extracted from sediments following the 3550C EPA (Environmental Protection Agency) procedure. Briefly, 500 mL mixture of CH₂Cl₂:CH₃COCH₃ (1:1, vol/vol) was added to 1,000 x g of dry sediments, sonicated for 2 minutes in ultrasound bath (Branson 1200 Ultrasonic Cleaner, Branson USA). Samples were further shaken at 150 rpm for 30 minutes, centrifuged for 10 minutes at 5,000 x g and the supernatant was passed through a ceramic column filled with anhydrous Na₂SO₄ (Sigma-Aldrich, Milan). Same treatment of sediments was repeated with 500 mL of CH₂Cl₂ and the obtained solvents were combined and volatilized to the dryness. Residues were re-suspended in CH₂Cl₂ prior the gas chromatography (GC) analysis. All measures were performed using a Master GC DANI Instruments (Development Analytical Instruments), equipped with SSL injector and FID detector. Sample (1 µL) was injected in splitless mode at 330 °C. The analytical column was a Restek Rxi-5 Sil MS with Integra-Guard, 30m x 0.25 mm (ID x 0.25 µm film thickness). The helium carrier gas was maintained at a constant flow of 1.5 mL/min. TERCH were calculated using the mean response factors of *n*-alkanes, i.e. individual *n*-alkane concentrations from *n*-C₁₅ to *n*-C₄₀, pristane and phytane were calculated for each sample. The amount of analyzed TERCH was expressed as ppm (part per million) or mg/kg.

Nucleic acid extraction was performed directly from 10 g of sediment duplicate samples using the PowerMaxSoil® DNA Isolation Kit (MoBio, CA, USA) according to supplier's recommendations. Once extracted, DNA concentration was measured by using PicoGreen Quantification Reagent (Invitrogen, ORE, USA), and equal amount of both (1 µg each) was mixed for further analysis (SSU rRNA hypervariable tag analysis and DNA sequencing).

SSU rRNA hypervariable tag analysis. Pyrotag assays were performed using universal-bacterial primers targeting the variable regions of the 16S rRNA, V1-V3 (27 F mod 5' – AGRGTTTGATCMTGGCTCAG – 3'; 519 R mod bio 5' – GTNTTACNGCGGCKGCTG – 3'), amplifying a fragment of approximately 400 bp. The amplified 16S rRNA regions contain sufficient nucleotide variability to enable the identification of bacterial species^{67,68}. Multiplex identifiers (MIDs) specific to each sample were used: TCCAGTAC for HAV, TCCAGGTG for PRI, TCATCTCC for BIZ, TCATGGTT for ELMAX, TCATTGTT for MCh, TCCACGTG for MES, TCAGTAAG for AQ, and TAGGATGA for ELF.

PCR reactions were performed in a final volume of 50 µL with 40 ng of sample DNA, 0.3 µmol/L of each primers, 1× PCR Buffer with 1.5 mmol/L of MgCl₂, 0.2 mmol/L of each dNTP

and 1U of HotStarTaq Plus Master Mix Kit (Qiagen, Valencia, CA, USA). The PCR cycling
 256 procedure was as follows: 94 °C for 3 min followed by 28 cycles at 94 °C for 30 sec, 53 °C for 40
 258 sec and 72 °C for 1min; a final elongation at 72 °C for 5 min was performed. After PCRs, all
 amplicons were purified using Agencourt Ampure beads (Agencourt Bioscience Corporation, MA,
 USA) and an equal amount was sequenced using Roche FLX 454 titanium. PCR and next-
 260 generation 454 pyrosequencing were performed at MR DNA laboratories (Shallowater, TX –
 U.S.).

262 A first-quality filter was applied to remove sequences shorter than 300 bp, longer than 500 bp,
 or with an average quality score (Phred score) of less than 30 (0.1% per-base error probability).
 264 The high-quality 16S rRNA gene sequences obtained by 454 pyrosequencing were then analyzed
 using QIIME⁶⁹ as follows: the sequences were clustered into operational taxonomic units (OTUs)
 266 based on a threshold of 97% for sequence identity using UCLUST⁷⁰. The combination of applied
 quality filtering and clustering threshold at 97% guarantee that the influence of erroneous reads is
 268 minimized⁷¹. A representative sequence from each OTU was selected and aligned to Greengenes
 (13_8 release; <http://greengenes.lbl.gov/>) using PyNast⁷². After OTU clustering, ChimeraSlayer
 270 was used in order to remove all chimeric OTUs from the dataset. Sequence identification was,
 then, conducted using Ribosomal Database Project classifiers with default parameters⁷². For each
 272 sample, the Shannon index and rarefaction curves of the observed species were estimated to
 analyze the species sampling coverage. The OTU diversity within and between samples (alpha
 274 and beta diversity) was estimated using QIIME (<http://qiime.org/>) workflow scripts. The
 QIIME workflow, including the commands used for bacterial SSU rRNA hypervariable tag
 276 analysis, are indicated below:

| | QIIME command |
|---|--|
| #seq filter and sample assign | - split_libraries.py -m *.mapping.txt -f *.fasta -q *.qual -o split_library_output -r -l 300 -L 500 -s 30 -b hamming_8 |
| #otu table creation | - pick_de_novo_otus.py -i split_library_output/seqs.fna -o otus -a -O 4 |
| #Inside the dir otus, remove the file *.tree | |
| #chimera removal | - identify_chimeric_seqs.py -i pynast_aligned_seqs/seqs_rep_set_aligned.fasta -a /home/qiime_software/chimeraslayer-4.29.2010-release/RESOURCES/rRNA16S.gold.NAST_ALIGNED.fasta -m ChimeraSlayer -o otus/chimeric_seqs.txt - filter_fasta.py -f otus/pynast_aligned_seqs/seqs_rep_set_aligned.fasta -o otus/pynast_aligned_seqs/non_chimeric_seqs_rep_set_aligned.fasta -s otus/chimeric_seqs.txt -n - filter_alignment.py -i otus/pynast_aligned_seqs/non_chimeric_rep_set_aligned.fasta -m /home/qiime_software/lanemask_in_1s_and_0s -o otus/pynast_aligned_seqs/ - make_phylogeny.py -i |

| | |
|---|---|
| | otus/pynast_aligned_seqs/non_chimeric_rep_set_aligned_pfiltered.fasta -o otus/rep_phylo.tre - make_otu_table.py -i otus/uclust_picked_otus/seqs_otus.txt -o otus/non_chimeric_otu_table.biom -e otus/chimeric_seqs.txt -t otus/rdp_assigned_taxonomy/seqs_rep_set_tax_assignments.txt |
| #stat | - biom summarize-table -i otus/otu_table.biom -o otus/otu_table_summary.txt |
| #cleaning the OTU table (removing OTUs contaminants) | - biom convert -i otus/non_chimeric_otu_table.biom -o otus/table.from_biom.txt -b #convert the biom to txt - biom convert -i otus/non_chimeric_otu_table.biom -o otus/table.from_biom_w_taxonomy.txt -b --header-key taxonomy - copy table.txt to cleaning directory and use the cleaning script - filter_otus_from_otu_table.py -i otu/non_chimeric_otu_table.biom -o non_chimeric_otu_table_cleaned.biom -e non_chimeric_otu_table_cleaned.txt |
| #taxa summary | - summarize_taxa_through_plots.py -i otus/non_chimeric_otu_table_cleaned.biom -o wf_taxa_summary -m Fasting_Map.txt |
| #alpha div | - echo "alpha_diversity:metrics shannon,PD_whole_tree,chao1,observed_species" > alpha_params.txt - alpha_rarefaction.py -i otus/non_chimeric_otu_table_cleaned.biom -m mapping_file.txt -o wf_arare/ -p alpha_params.txt -t otus/rep_phylo.tre |
| #beta div | - beta_diversity_through_plots.py -i otus/non_chimeric_otu_table_cleaned.biom -m Fasting_Map.txt -o wf_bdiv_even146/ -t otus/rep_phylo.tre -e cutoff_value - make_2d_plots.py -i (un)weighted_unifrac_pc.txt -m Fasting_Map.txt (-e flag [cutoff_value] is 6000) |

278 Beta diversity was assessed after construction of weighted and unweighted Unifrac distances⁷³
 280 with weighted Unifrac accounting for differences in the relative abundance of microbial
 282 community members. To remove noise from the data, including potential rare contaminants, we
 removed OTUs that did not meet the criterion of being present in at least 0.05% of the total
 number of reads using an in-house script, as follows:

```

284 # Remove OTUs present under a fixed threshold
286 # python clean_OTU_mod.py [otu_table] [threshold]
288 import sys
290
292 inF=open(sys.argv[1].strip(),"r")
294 thr=int(sys.argv[2].strip())
296 assert (thr > 0); 'you should enter a positive number'
```

```

298 outname="%s_cleaned" %(sys.argv[1].strip())
300 out=open(outname,"w")
302
304 for oline in inF.readlines():
306     if oline[0]=="#":
308         out.write(oline)
310     else:
312         line=oline.strip().split("\t")
314         line.pop(0)
316         tot=0.0
318         for a in line:
320             tot+=float(a)
322         if tot<float(thr): #this number is the limit of the OUTs number to keep
324             out.write(oline)
326
328 inF.close()
330 out.close()

```

332 The Shannon diversity index was calculated by PAST software⁷². Library coverage was
calculated for each library using the equation $C = [1 - (n1/N)] \times 100$, where n1 is the number of
334 singleton OTUs and N is the total number of reads in the library.

336 **DNA sequencing, assembly, and gene calling.** Sequencing of AQ was performed with a Roche
454 GS FLX Ti sequencer (454 Life Sciences, Branford, CT, USA) at Lifesequencing S.L.
338 (Valencia, Spain) in a single picotiter plate. Assembly was performed using a Roche Newbler
assembler v. 2.5.3 using the default parameters, and potential protein-coding genes were predicted
340 and annotated as described previously⁷⁵. All other DNA samples were sequenced by pair-end
sequencing (Illumina Hiseq 2000) at Beijing Genomics Institute (BGI; China); software

342 MetaGeneMark (version 2.10, default parameters) was used to predict potential protein-coding genes based on the assembly results.

344 For Illumina Hiseq 2000 sequencing and data processing, the DNA samples were sequenced following standard pipelines in Illumina platform. Data filtration was done by in-house scripts, 346 listed as follows:

(1) removing reads with 3 N bases removing reads contaminated by adapter(15 bases overlapped by reads and adapter)

(2) Remove reads with 20 bp low quality (20) bases

350 (3) Remove duplication contamination.

The removal reads process is simultaneously read1 and read2 operation, finally obtained can 352 be used for subsequent analysis to quality data (Clean Data)⁷⁶.

For assembly for Illumina Hiseq 2000 sequences, SOAPdenovo (Version 1.0, 354 <http://soap.genomics.org.cn/soapdenovo.html>) was used to assemble filtered data and assembly results with the best N₅₀ contig length were optimized by in-house scripts previously described⁷⁷.

356 The data statistics, assembly results data, number of open reading frames (ORF) and number of ORF with assigned function for each of set of sequences are shown in Supplementary Table S6.

358

Biodegradation network reconstruction

360 Data for the *in silico* degradation network reconstruction were based in three different sequence datasets, resulting in three different reconstructions. The first dataset was built according with 362 the similarity comparison (score > 45; e-value < 10e⁻³) between the gene sequences from the metagenomes of the samples and the sequences from AromaDeg database^{24,27}. The second dataset 364 was based on the results from the 16S rRNA phylogenetic affiliations, building a putative metagenome for each of the samples based on the detected taxons. For that, we downloaded the 366 genome proteins (from the NCBI website) belonging to one of the closest species inside these taxons, and query sequences that matches a given protein family of the AromaDeg^{24,27} were 368 selected. The last dataset was the result of joining both prior data sets, metagenome-based and 16S rRNA-based data sets. These data sets were used to create a nodes Table (Supplementary 370 Table S5) on the basis of which we develop a network reconstruction under R language^{78,79}, that is described below.

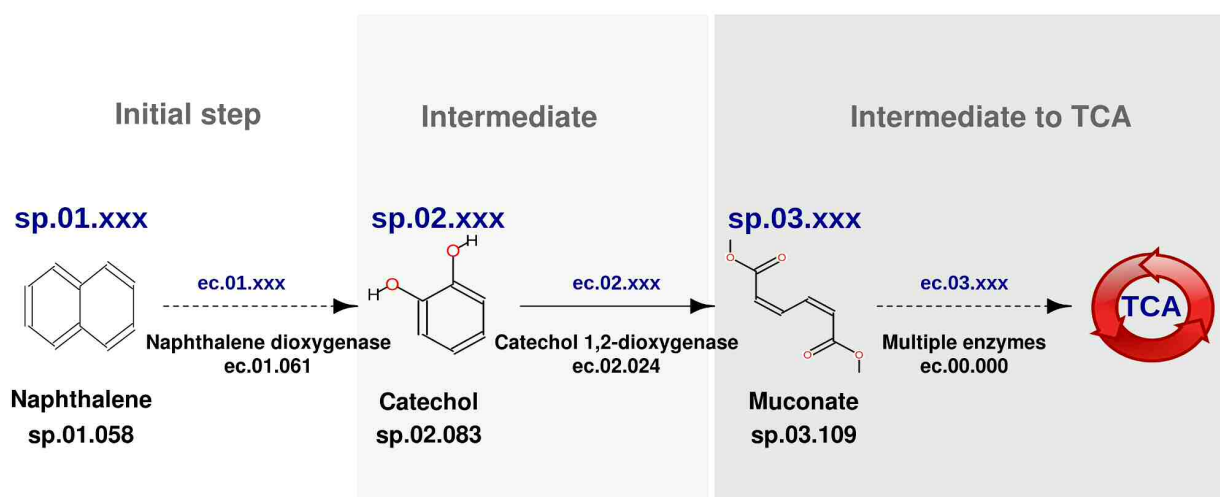
372

Step 1: Creating the nodes Table

374

Each connection in the network represents a step in the degradation pathway (a degradation 376 reaction), connecting a product with its substrate (nodes), which is assigned to a gene encoding a

catabolic enzyme. An in house code is used to identify enzymes and compounds in the Table, formed by two numbers. The first number indicates their location according to the whole degradation pathway: 01 when is an initial or peripheral step, 02 when is a first stage intermediate product, and 03 when is an intermediate product close connected with the tricarboxylic acid (TCA) acid/pathway. The second is an arbitrary number which identify each specific element (catabolic gene/enzyme and reaction substrate or product). The follow scheme (Scheme 1) summarized the codes:



Scheme 1: Description of the codes assignment to catabolic genes/enzymes and compounds in the network.

General pattern for the assignment is highlighted in blue, while in black we described an example with the naphthalene degradation pathway. Code ec.00.000 is assigned to existing reaction/s without any representative sequence in AromaDeg database^{24,27}. Single step reactions are represented by solid lines, while transformations involving multiple reactions are represented by dashed lines.

Relative abundance for each type of gene encoding catabolic enzymes found for each sample (according to the list of detected gene sequences encoding enzymes potentially involved in degradation) is used to set up the nodes Table (Supplementary Table S5A), resulting in a list of weights that specifies the size of the connections in each step of the network for each sample, as exemplified below.

| EC code | Substrate code | Product code | MGS-HAV | MGS-PRI | MGS-MES | MGS-MCH | MGS-BIZ | MGS-ELMAX | MGS-AQ |
|-----------|----------------|--------------|---------|---------|---------|---------|---------|-----------|--------|
| ec.01.061 | sp.01.058 | sp.01.003 | 0,024 | 0,000 | 0,052 | 0,013 | 0,144 | 0,072 | 0,067 |
| ec.01.006 | sp.01.003 | sp.01.014 | 0,000 | 0,000 | 0,000 | 0,000 | 0,000 | 0,000 | 0,000 |
| ec.00.000 | sp.01.014 | sp.01.067 | 0,000 | 0,000 | 0,000 | 0,000 | 0,000 | 0,000 | 0,000 |
| ec.01.023 | sp.01.067 | sp.02.083 | 0,000 | 0,000 | 0,002 | 0,000 | 0,007 | 0,000 | 0,000 |
| ec.02.024 | sp.02.083 | sp.03.109 | 0,000 | 0,000 | 0,015 | 0,007 | 0,004 | 0,008 | 0,011 |
| ec.02.017 | sp.02.083 | sp.03.124 | 0,024 | 0,000 | 0,062 | 0,063 | 0,155 | 0,095 | 0,107 |
| ec.00.000 | sp.03.109 | sp.04.000 | 0,000 | 0,000 | 0,000 | 0,000 | 0,000 | 0,000 | 0,000 |

Example of a part of the nodes Table. Codes for the genes/enzymes, substrates and products (intermediates) are shown in grey. Weights (relative abundance of catabolic genes) for each reaction in each sample are shown in blue. For complete set of data see Supplementary Table S5A.

400 **Step 2: Setting up the nodes of the network**

Network structure is set up under the programming language *R*^{78,79}, using the functions provided
402 by the package *igraph* and the information given in the nodes Table. The process starts calling the
functions of the package, opening the Table under the *R* environment and creating a new graph
404 object with the substrates/products of the Table like nodes:

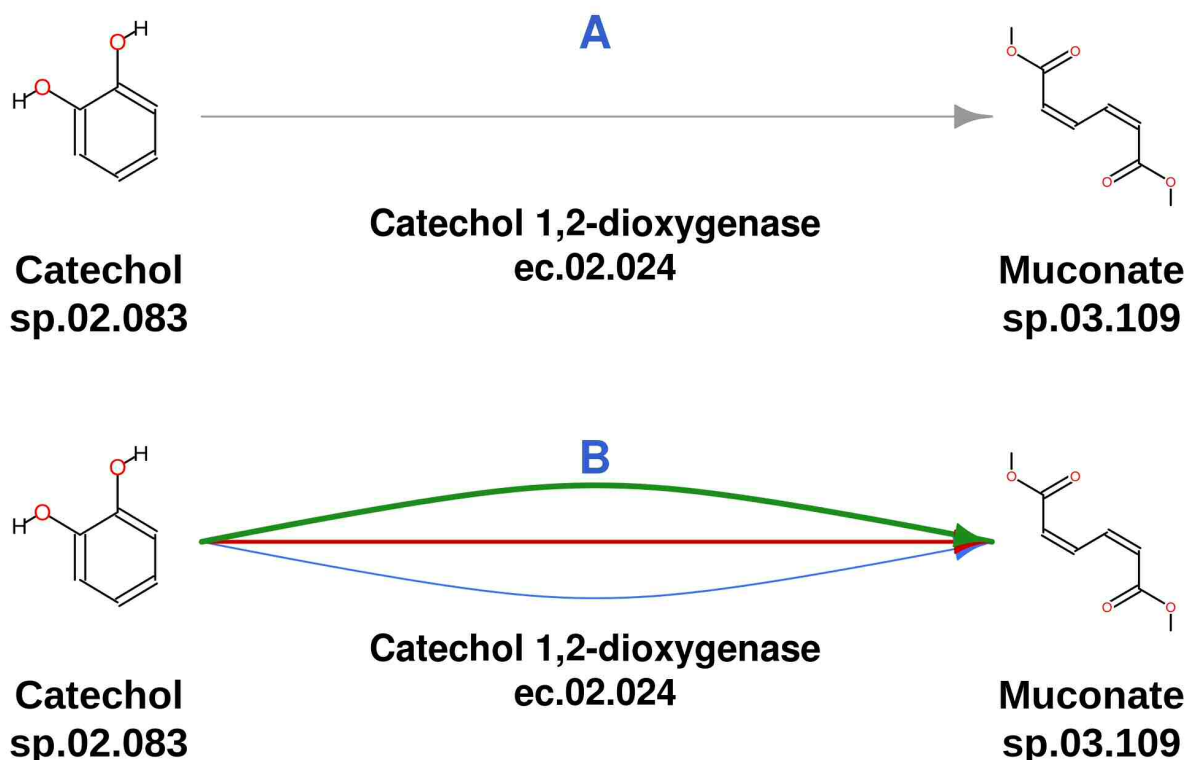
```
406 > library(igraph)
> edgelist <-read.table("NodesTable.txt",
408 +   header=TRUE,dec=" ",sep="\t",check.names=FALSE)
> g <-graph.empty(directed=TRUE)
410 > u <-unique(c(as.character(edgelist[,2]),
+               as.character(edgelist[,3])))
412 > g<-add.vertices(g,length(u),name=u,
+               size=size,degree=degree,dist=dist)
```

414 After creating a new graph with `graph.empty`, all the substrate/product names are listed in a
value with `unique` and added as nodes of the new graph with `add.vertices`, where some
416 attributes like the size of the node or the position for the labels can be set up using values like *size*,
418 *degree* or *dist*.

420 **Step 3: Adding the connections between nodes to the network**

422 There are two different types of connections, those with 0 abundance in all samples (empty
connections) and the connections with at least one sample with an abundance > 0 (positive
424 connections). We make this difference in order to set up independently the drawing attributes of
both types of connections, like the type and curve of the line in the arrows. See scheme 2 below.

426



Scheme 2: Description of the two different types of connections. A, an empty connection with 0 abundance in all the samples. B, a positive connection with abundance >0 in three different samples (represented in green, red and blue line), with the size of the line according to the relative abundance value of catabolic gene for each sample.

Empty connections are added first. A loop checking the data for each sample is needed:

```

428
> for(i in 1:nrow(edgelist)){
430 +   if (sum(edgelist[i,4:ncol(edgelist)])==0){
+       g<- add.edges(g,rbind(edgelist[i,2],edgelist[i,3]),
432 +           attr=list(color="grey60",curve=0,
+           name=as.character(edgelist[i,1])))
434 +   }
+ }
436

```

Connections are introduced in the graph with the function `add.edges`. Calculating the total abundance in each network step (row) from the nodes Table, one can see whether the abundance is 0 in all the samples (from the fourth to the final column in the Table [Supplementary Table S5A]); in this case a simple connection is added to the graph with a grey arrow. Another loop is run to add the positive connections (abundance >0 at least in one sample):

```

442

```



```

> curve<-0
444 > for(i in 4:ncol(edgelist)){
+     from<-NA
446 +     to<-NA
+     weights<-NA
448 +     name<-NA
+     newfrom<-na.omit(from)
450 +     newto<-na.omit(to)
+     weights<-na.omit(weights)
452 +     name<-na.omit(name)

454 +     for(j in 1:nrow(edgelist)){
+         if (edgelist[j,i] > 0){
456 +             from<-append(from,
+                             as.character(edgelist[j,2]),
458 +                             after=length(from))

460 +             to<-append(to,
+                           as.character(edgelist[j,3]),
462 +                           after=length(to))
+             weights<-append(weights,
464 +                             edgelist[j,i],
+                             after=length(weights))
466
+             name<-append(name,
468 +                             as.character(edgelist[j,1]),
+                             after=length(name))
470 +         }
+     }
472 +     g<- add.edges(g, rbind(from,to),
+                     attr=list(weight=weights,
474 +                             color=color, curve=curve), name=name)
+
476 +     if (curve%%2==0){

```

```

+           curve<-abs (curve)
478 +       }
+       else{
480 +           curve<- -curve
+       }
482 +
+       if (curve<0) {
484 +           curve<-curve
+       }
486 +       else{
+           curve<-abs (curve) +0.2
488 +       }
+
490 + }

```

492 In this case (abundance >0 at least in one sample) the loop is more complicated. In the first part,
 empty vectors for each sample (from the fourth to the last column in the Table [Supplementary
 494 Table S5A]) are created to save (using the function `append`) the different attributes of the
 connections in each case (name, weight and nodes of the connections). The connections for each
 496 sample are added to the graph at the final of the loop again with `add.edges`. The attribute *curve*
 is configured before running this step and is changed at the end of the loop to set the curve for the
 498 next sample.

500 Reason for running two independent `for` loops, checking twice the whole table, is simple.
 Checking empty connections needs to look over the table row by row, like in the first loop, but
 502 checking the positive connections needs to look over the table column by column (sample by
 sample), like in the second loop.

504
 Note that the line for empty connections is drawn in grey color, which means that abundance in
 506 this case is 0, and the width of the line is not representing any percentage of gene presence. Also,
 these connections can represent a single step in the pathway (straight line) or multiple reactions
 508 (dashed line).

510 **Step 4: Setting up the coordinates of the nodes in the network**

512 Coordinates of the nodes determine the position of each node (substrate/product) in the final draw
of the network. This coordinates can be set manually, in order to obtain a customized layout for
514 the network, saved in a file and use this file when is needed to draw a new network, without a new
manual set up:

```
516 > p <- tkplot(g)
518 > Coords <- tkplot.getcoords(p)
> write.table(Coords,"Coords.txt",row.names=FALSE,col.names=FALSE)
520 > Coords<- matrix(scan("Coords.txt"),nc=2,byrow=TRUE)
```

522 Function `tkplot` displays a new interactive screen where we can point each node in the desired
position and then save the coordinates in a value with `tkplot.getcoords`. Using
524 `write.table` is possible to print the value with the coordinates in an output file, and read it
again using `matrix` and `scan`.

526

Step 5: Drawing the network

528

Network can be drawn using the coordinates and the configuration in the prior steps:

530

```
> jpeg("Network.jpg",width=5796,height=3561,
532 +   res=300,quality=100,units="px")
```

```
534 > par(mar=c(0,0,0,0),xpd=TRUE)
```

```
> plot.igraph(g,
536 +   layout=Coords,
+   vertex.shape=shape,
538 +   vertex.size=size1,
+   vertex.size2=size2,
540 +   vertex.size2=size2,
+   vertex.label=labels,
542 +   vertex.label.dist=V(g)$dist,
+   vertex.label.degree=V(g)$degree,
544 +   vertex.label.dist=V(g)$dist,
```

```

+ vertex.label.degree=V(g)$degree,
546 + edge.width=ifelse(E(g)$weight<=0.01,1,
+ ifelse(E(g)$weight>0.10,10,E(g)$weight*100)),
548 + edge.lty=lty
+ )
550
+ dev.off()

```

552

Functions `jpeg` and `dev.off` are used to save the plot in a jpeg file. The main function to draw the network is `plot.igraph`, using the coordinates saved before as layout, and the parameters provided when the vertex were added to the graph object to set up the different options of the function. Other options can be modified using vector objects with values for the different vertex/connections. Abundances for each node in each sample are used as the width of the connections (saved as connection *weight* in the step 2) but are adapted, with a conditional loop (`ifelse`), to make them fit in the plot. Herein, an abundance of 0.01 is equal 1 in the *edge.width* parameter, so this value will be the abundance multiply by 100 (0.02 is equal to 2, 0.05 is equal to 5). When the *edge.width* value is higher than 10 (for abundances > 0.1) the value is set in 10, and if the value is lower than 1 (abundances < 0.01) the width is set in 1. For empty connections abundance is set as 0, but in the network will be drawn with a size of 1 as is configured in the parameter *edge.width*. This is because a size > 0 must be indicated in the script in order to draw a visible connection; however a grey color is used in these connections to specify the absence of abundance in these reaction/s.

568 Target metabolomics for experimental validations of predicted biodegradation capacities

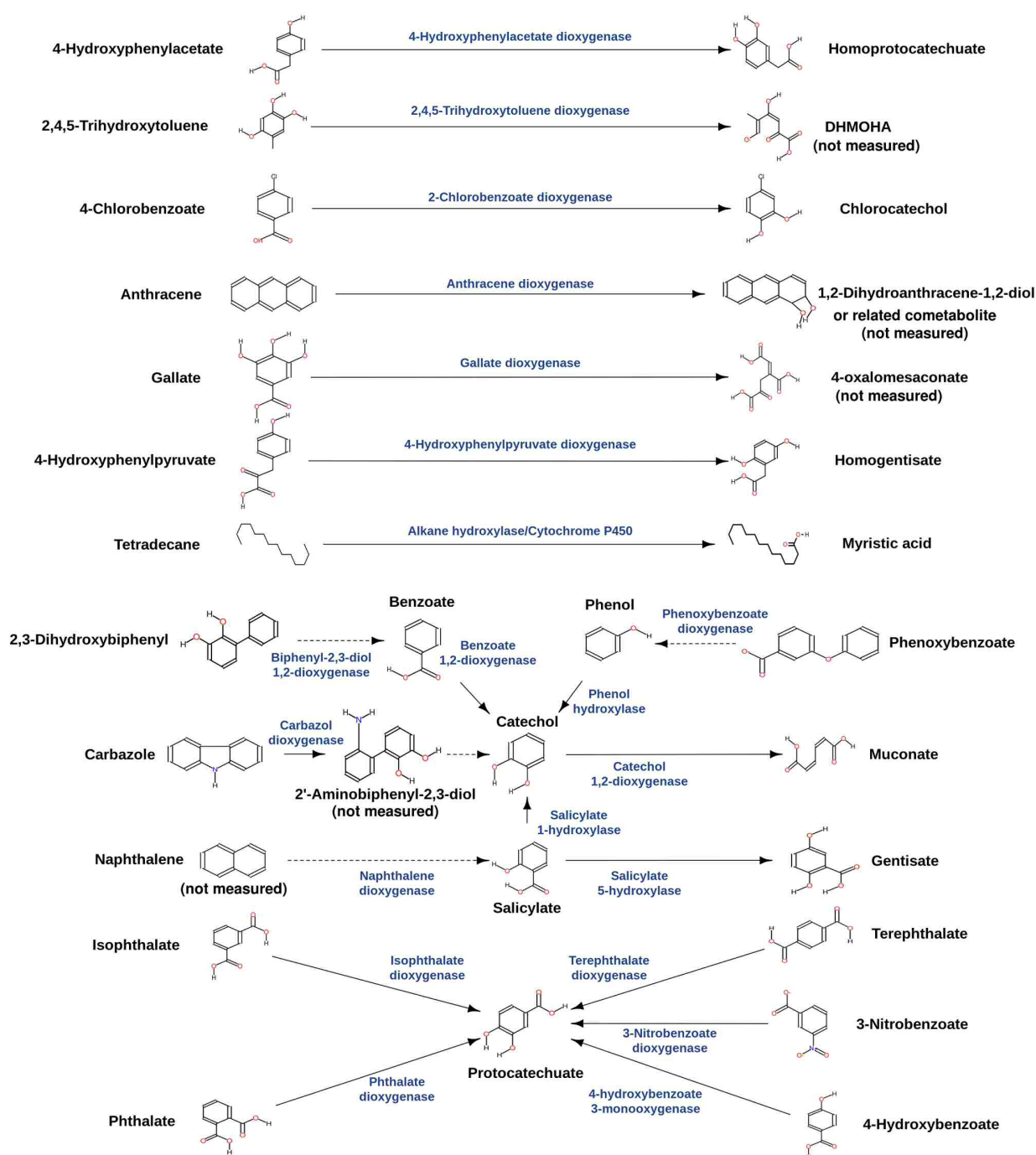
The ability of each of the microbial communities to grow on a mix of distinct pollutants as the sole source of carbon and energy was evaluated in 1 l Erlenmeyer flasks containing 100 mL of ONR7a⁸⁰ minimal medium, supplemented with 10 mM total substrate mix. The sediment samples used for enrichment cultures were exactly the same than those used for environmental measurements and nucleic acid extractions; note that in this case, the sediments were stored at -20 °C prior to use. The following pollutants, all from Fluka-Aldrich-Sigma Chemical Co. (St. Louis, MO, USA), were used: naphthalene, tetradecane, benzoate, 4-chlorobenzoate, 3-nitrobenzoate, 4-hydroxybenzoate, phthalate, isophthalate, terephthalate, anthracene, 2,3-dihydroxybiphenyl, 4-hydroxyphenylpyruvate, 3,4-phenoxybenzoate, carbazole, phenol, 2,4,5-trihydroxytoluene and gallate. One liter Erlenmeyer flasks were filled with 100 mL of sediment,

sterilized, and spiked with 10 mL of sterile-filtered Arabian light crude oil. The sediment sample
was used to inoculate 300 mL of modified ONR7a medium (omitting ammonium chloride and
disodium hydrogen phosphate). We used an amount of sediment corresponding to approximately
2.0e⁺⁰⁵ cells per g, so the same amount of bacterial cells was used in each of the microcosm
experiments. To calculate cell numbers in the sediments, cell counts were performed over fixed
(4% formaldehyde for 4 h at 4°C), 4',6-diamidino-2-phenylindole (DAPI)-stained samples
immobilized onto 8-well teflon printed slides by manual [Cell Counter plugin incorporated in
ImageJ v1.47 (<http://imagej.nih.gov/ij/>)⁸¹] or automated counting of single color images
(ImageJ v1.47), depending on the sample's characteristics. To achieve statistical significance, 50
fields were examined per sample. Cell numbers were obtained by referencing the counts to the
screened area and the amount of sediment used

We added the substrate mix to give a final concentration of 10 mM (from a 100 mM stock
solution each in methanol). A total of 5 mM NH₄Cl and 0.5 mM Na₂HPO₄ to a molar N:P ratio of
approx. 10:1, were added. Enrichment cultures, performed in triplicates per each of the duplicate
sediments, were incubated at 250 rpm for up to 3 weeks. Samples were taken after incubation for 1
day (time zero in our assay) and 3 weeks. Oxygen and temperature concentrations were
maintained at values corresponding to environmental values (see the Supplementary Table S1),
except for sediment sample from Priolo Gargallo for which 1.0 mg L⁻¹ O₂ was used; note that in
this case, the sediment sample was anaerobic and, in order to detect aerobic degradation products,
low O₂ concentration was added for the enrichments. Two control experiments (in triplicates)
were used under each of the conditions tested: i) cultures without the addition of sediments but
with chemicals; ii) cultures plus sediments but without the addition of chemicals. The extent of
degradation and transformation in test and control samples was quantified in a solution
containing 1 mL of the culture medium (previously separated by centrifugation at 13,000 g for 5
min) and 1 mL of a methanol solution prepared as follows. Briefly, microbial cells were harvested
from the enrichment by centrifugation at 13,000 g for 5 min; the metabolites were then extracted
by adding 1.2 mL of cold (-80°C) methanol as previously described⁸². The presence of each of the
17 pollutant molecules as well as key 9 degradation products produced after their degradation,
namely, catechol, chlorocatechol, salicylate, muconate, gentisate, protocatechuate, homogentisate,
myristate and homoprotocatechuate, was determined by target analysis by gas chromatography-
mass spectrometry (GC-Q-MS) and liquid chromatography-mass spectrometry (LC-QTOF-MS)
using the following reagents: O-methoxyamine hydrochloride (Sigma-Aldrich - Taufkirchen,
Germany), 15 mg/mL in pyridine (Silylation grade - Taufkirchen, Germany); N,O-
Bis(trimethylsilyl)trifluoroacetamide (BSTFA) with 1% trimethylchlorosilane (TMCS; Pierce
Chemical Co, Rockford, IL, USA); C18:0 methyl ester (Sigma-Aldrich - Taufkirchen, Germany) in

614 heptane (GC-MS grade – Sigma-Aldrich - Taufkirchen, Germany); and isopropanol (HPLC-MS
grade – Sigma-Aldrich - Taufkirchen, Germany), in addition to the appropriate standards.
616 Napthalene, tetradecane and toluene were added to the assay, but the analytic method used did
not permit the quantification of these compounds, so their relative concentrations during the
618 assay could not be determined; however, the identification and quantification of degradation
intermediates could demonstrate the capacity of microbial communities to degrade them.

620 The presence (no degradation), absence (total degradation) and abundance (partial degradation)
level of mass signatures of all tested pollutants and key degradation intermediates can be linked to
622 the presence of 21 key genes encoding catabolic enzymes involved either in their degradation (in
case of initial pollutants) or their production (in case of intermediates). The links between the
624 presence or absence of substrate pollutants and intermediate (in a degradation reaction), and a
gene encoding a catabolic enzyme assigned to the degradation reactions where both chemical
626 species participates, were established on the basis of AromaDeg²⁴ and nodes described in
Supplementary Table S5A. Links are summarized in the Scheme 3 as follows:



Scheme 3. Association between biodegradation reactions and genes encoding catabolic enzymes. Abbreviations as follows: DHMOHA, 2,4-Dihydroxy-5-methyl-6-oxohexa-2,4-dienoate. Note, that “not measured” indicates metabolites which were not measured by target metabolomics.

We are aware about the fact that in the enrichment assays we used artificial incubations and conditions to determine the catabolic potential of the microbial communities from sediments samples herein investigated. Such enrichment cultures may have a number of limitations to predict the actual catabolic potential or microbial communities as might be expected in the field sediment. However, here we would like to point to the fact that the reason of these experiments

are not to identify the most active genes encoding catabolic enzymes or the abundance level of them in each of the microbial communities after enrichments with particular substrates, but rather to demonstrate the capacity to degrade distinct substrates. Although, the abundance level in field sediments might be different to the one in the enrichments cultures²⁹, it is highly likely that the presence of a catabolic activity in an enrichment culture implies that such activity also exist, albeit at different level, in the natural environment.

Target analysis by GC-Q-MS: Samples for GC-MS analysis were prepared from 100 μ L volumes of the methanol extracts. Blanks reflecting the matrices of the samples were prepared and treated in the same manner as the samples. Standards were prepared at a concentration of 100 ppm. All samples were evaporated to dryness using a Speedvac Concentrator (Thermo Fisher Scientific Inc., Waltham, MA) and derived using a two-stage process of methoximation and silylation. For methoximation, 10 μ L of O-methoxyamine hydrochloride (15 mg/mL) in pyridine was added to each of the samples, which were then subjected to three cycles of vortex mixing and ultra-sonication and kept in the dark at room temperature for 16 h. For silylation, 10 μ L of BSTFA with 1% TMCS was added to the samples, which were then subjected to three cycles of vortex mixing and ultra-sonication before incubation at 70 °C for 1 h. Finally, 100 μ L of 10 ppm C18:0 methyl stearate in heptane (internal standard) was added to each sample, and all samples were vortex mixed for 2 min. The analytical run started with the injection of C18 (10 ppm), followed by three blanks to equilibrate the column. Subsequently, samples were analyzed in random order, followed by the standards. The run terminated with the injection of the final blank. The GC-MS system (Agilent Technologies 7890A) consisted of an autosampler (Agilent Technologies 7693) and an inert mass selective detector (MSD) with Quadrupole (Agilent Technologies 5975). The derived samples were injected in 2 μ L volumes onto a GC-Column DB5-MS (30 m length, 0.25 mm i.d., 0.25 μ m film 95% dimethyl/5% diphenyl polysiloxane) with a pre-column (10 m J&W integrated with Agilent 122-5532G). The helium carrier gas flow rate was set at 1 mL/min, and the injector temperature was set at 250°C. The split ratio was 1:10 flowing into a Restek 20782 deactivated glass-wool split liner. The temperature gradient was programmed as follows: the initial oven temperature was set at 60°C (held for 1 min) and then increased to 325°C at the rate of 10°C/min. Finally, a cool-down period was applied for 10 min before the subsequent injection. The total analysis time for each sample was 37.5 min. The detector transfer line, the filament source, and the quadrupole temperatures were set at 290°C, 230°C, and 150°C, respectively. The electron ionization (EI) source was operated at 70 eV. The mass spectrometer was operated in scan mode over a mass range of m/z 50-600 at a rate of 2 spectra/s. Peak detection and spectra processing were obtained using Agilent ChemStation Software (G1701EA E.02.00.493, Agilent). Compound identification was performed using the NIST 08 Library

(National Institute of Standards and Technology, U.S. Department of Commerce) with ChemStation software (G1701EA E.02.00.493, Agilent). As soon as they were properly characterized in the chromatograms of the standards (retention time and spectrum), a target analysis method was created in the ChemStation software (G1701EA E.02.00.493, Agilent) to identify and integrate the corresponding peaks in the chromatograms of the samples.

Target analysis by LC-QTOF-MS: Samples for LC-MS analysis were prepared by filtering the methanol extracts using 0.2 μm nylon syringe filters (Thermo Scientific, Rockwood, USA). The analytical run began with the analysis of ten QCs, followed by the samples in random order; a QC sample was injected in between blocks of four samples until the end of the run. Finally, the corresponding standards (100 ppm) were analyzed. All vials were maintained at 4°C throughout the run. Each metabolic fingerprint was achieved using a liquid chromatography system consisting of a degasser, binary pump, and autosampler (1290 infinity, Agilent). A total of 0.5 μL was applied to a reverse-phase column (Zorbax Extend C₁₈ 50 \times 2.1 mm, 3 μm ; Agilent), which was maintained at 60°C during the analysis. The system was operated in positive and negative ion mode at a flow rate of 0.6 mL/min with solvent A (water with 0.1% formic acid) and solvent B (acetonitrile with 0.1% formic acid). The gradient was 5% B (0-1 min), 5 to 80% B (1-7 min), 80 to 100% B (7-11.5 min), and 100 to 5% B (11.5-12 min), followed by reequilibration at 5% B for 3 min (15 min of total analysis time). Data were collected in positive and negative ESI mode in separate runs on a QTOF (Agilent 6550 iFunnel). Both ion modes were operated in full scan mode (m/z 50 to 1,000 in positive and m/z 50 to 1,100 in negative ion mode). For each mode, the capillary voltage was 3,000 V, the scan rate was 1.0 spectra/s, the gas temperature was 250°C, the drying gas flow was 12 L/min, and the nebulizer was 52 psi. The MS-TOF parameters for positive ion mode were as follows: fragmentor 175 V, skimmer 65 V, and octopole radio frequency voltage (OCT RF Vpp) 750 V. The same MS-TOF parameters were used in negative ion mode, except the fragmentor, which was set to 250 V. Two reference masses were used for each mode: m/z 121.0509 ($[\text{C}_5\text{H}_4\text{N}_4+\text{H}]^+$) and m/z 922.0098 ($[\text{C}_{18}\text{H}_{18}\text{O}_6\text{N}_3\text{P}_3\text{F}_{24}+\text{H}]^+$) during positive analysis and m/z 112.9855 ($[\text{C}_2\text{O}_2\text{F}_3-\text{H}]^-$) and m/z 1033.9881 ($[\text{C}_{18}\text{H}_{18}\text{O}_6\text{N}_3\text{P}_3\text{F}_{24}+\text{TFA}-\text{H}]^-$) during negative analysis. The reference masses were continuously infused into the system to permit constant mass correction⁸³. Compound identification and peak integration were performed using Mass Hunter Qualitative Analysis (B.05.00, Agilent). Following their identification in the chromatograms of the standards (retention time and spectrum), the molecular ion of each compound that was not previously identified in GC-MS was searched for in the chromatograms of the samples.

Metabolomic fingerprint analysis of sediment samples. The metabolites were extracted in triplicates from sediment samples as follows. In a 100 mL Erlenmeyer flask, 5 g of sediments were mixed with 10 mL of cold (-80°C) HPLC-grade methanol (MeOH). The samples were sonicated for 120 sec (at 15 W) on an ice water bath. This protocol was repeated 4 times, and the samples were kept on ice for at least 2 min between each step. After sonication, the supernatant was removed by centrifugation at 10,000 *g* for 30 min at 4°C, and the supernatant was stored in 20-mL penicillin vials at -80°C. Methanol extracts were filtered using 0.2 µm nylon syringe filters (Thermo Scientific, Rockwood, USA) and analyzed by LC-QTOF-MS as described above.

Supplementary References

32. Hedlund, B. P. & Staley, J. T. Isolation and characterization of *Pseudoalteromonas* strains with divergent polycyclic aromatic hydrocarbon catabolic properties. *Environ. Microbiol.* **8**, 178-182 (2006).
33. Yakimov, M. M., Timmis, K. N. & Golyshin, P. N. Obligate oil-degrading marine bacteria. *Curr. Opin. Biotech.* **18**, 257-266 (2007).
34. Pepi, M. *et al.* Mercury-resistant bacterial strains *Pseudomonas* and *Psychrobacter* spp. isolated from sediments of Orbetello Lagoon (Italy) and their possible use in bioremediation processes. *Int. Biodet. Biodeg.* **65**, 85-91 (2011).
35. Michaud, L., Di Marco, G., Bruni, V. & Lo Giudice, A. Biodegradative potential and characterization of psychrotolerant polychlorinated biphenyl-degrading marine bacteria isolated from a coastal station in the Terra Nova Bay (Ross Sea, Antarctica). *Mar. Pollut. Bull.* **54**, 1754-1761 (2007).
36. Jin, H. M., Kim, J. M., Lee, H. J., Madsen, E. L. & Jeon, C. O. *Alteromonas* as a key agent of polycyclic aromatic hydrocarbon biodegradation in crude oil-contaminated coastal sediment. *Environ. Sci. Technol.* **46**, 7731-7740 (2012).
37. Abed, R. M. M., Musat, N., Musat, F. & Mußmann, M. Structure of microbial communities and hydrocarbon-dependent sulfate reduction in the anoxic layer of a polluted microbial mat. *Mar. Pollut. Bull.* **62**, 539-546 (2011).
38. Jaekel, U., Musat, N., Adam, B., Kuypers, M., Grundmann, O. & Musat, F. Anaerobic degradation of propane and butane by sulfate-reducing bacteria enriched from marine hydrocarbon cold seeps. *ISME J.* **7**, 885-895 (2013).
39. Sitte, J. *et al.* Microbial links between sulfate reduction and metal retention in uranium- and heavy metal-contaminated soil. *Appl. Environ. Microbiol.* **76**, 3143-3152 (2010).

- 740 40. Isaac, P., Sánchez, L. A., Bourguignon, N., Cablar M. E. & Ferrero M. A. Indigenous PAH-
degrading bacteria from oil-polluted sediments in Caleta Cordova, Partagonia Argentina. *Int.*
742 *Biodet. Biodeg.* **82**, 207-214 (2013).
41. Gilbert, J. A. *et al.* Defining seasonal marine microbial community dynamics. *ISME J.* **6**, 298-
744 308 (2012).
42. Zahed, M. A. *et al.* Kinetic modeling and half life study on bioremediation of crude oil
746 dispersed by Corexit 9500. *J. Hazard Mater.* **185**, 1027-1031 (2011).
43. Bauer, M. *et al.* Whole genome analysis of the marine Bacteroidetes ‘*Gramella forsetii*’ reveals
748 adaptations to degradation of polymeric organic matter. *Environ. Microbiol.* **8**, 2201-2213
(2006).
- 750 44. Chen, Y. *et al.* *Salinimicrobium terrae* sp. nov., isolated from saline soil, and emended
description of the genus *Salinimicrobium*. *Int. J. Syst. Evol. Microbiol.* **58**, 2501-2504 (2008).
- 752 45. Peura, S. *et al.* Distinct and diverse anaerobic bacterial communities in boreal lakes dominated
by candidate division OD1. *ISME J.* **6**, 1640-1652 (2012).
- 754 46. Seifert, J. *et al.* Bioinformatic progress and applications in metaproteogenomics for bridging
the gap between genomic sequences and metabolic functions in microbial communities.
756 *Proteomics* **13**, 2786-2804 (2013).
47. Attias, L. *et al.* Crude oil spill in sea water: an assessment of the risk for bathers correlated to
758 benzo(a)pyrene exposure. *Cent. Eur. J. Public. Health* **3**, 142-145 (1995).
48. Genovese, M. *et al.* Effective bioremediation strategy for rapid in situ cleanup of anoxic
760 marine sediments in mesocosm oil spill simulation. *Front. Microbiol.* **5**, 162 (2014).
49. Denaro, R. *et al.* Assessing terminal restriction fragment length polymorphism suitability for
762 the description of bacterial community structure and dynamics in hydrocarbon-polluted
marine environments. *Environ. Microbiol.* **7**, 78-87 (2005).
- 764 50. Nikolopoulou, M., Eickenbusch, P., Pasadakis, N., Venieri, D. & Kalogerakis, N. Microcosm
evaluation of autochthonous bioaugmentation to combat marine oil spills. *N. Biotechnol.* **30**,
766 734-742 (2013).
51. Cappello, S. *et al.* Characterisation of oil-degrading bacteria isolated from Bilge water. *Water*
768 *Air. Soil Poll.* **223**, 3219-3226 (2012).
52. Ben Said, O., Goñi-Urriza, M., El Bour, M., Aissa, P. & Duran, R. Bacterial community
770 structure of sediments of the bizerte lagoon (Tunisia), a southern Mediterranean coastal
anthropized lagoon. *Microb Ecol.* **59**, 445-456 (2010).
- 772 53. Barhoumi, B. *et al.* Polycyclic aromatic hydrocarbons (PAHs) in surface sediments from the
Bizerte Lagoon, Tunisia: levels, sources, and toxicological significance. *Environ. Monit. Assess.*

- 774 **186**, 2653-2669 (2014).
54. Ben Chekroun, K. *et al.* Role of macroalgae in biomonitoring of pollution in «Marchica», the
776 Nador lagoon. *Phyton (B. Aires)* **82**, 31-34 (2013).
55. Ruiz, F., *et al.* (2006). The present environ-mental scenario of the Nador Lagoon (Morocco).
778 *Environ. Res.* **102**, 215-229 (2006).
56. González, I., Águila. E. & Galán E. Partitioning, bioavailability and origin of heavy metals
780 from the Nador Lagoon sedi-ments (Morocco) as a basis for their management. *Environ. Geol.*
 52, 1581-1593 (2007).
- 782 57. Bloundi, M. K., Faure, P. & Duplay, J.Organic contamination identification in sediments from
 a Mediterranean coastal ecosystem: The case of the Nador lagoon (Eastern Morocco). *C. R.*
784 *Geoscience* **340**, 840-849 (2008).
58. Piazza, R. *et al.* Polychlorinated biphenyls in sediments of selected coastal en-vironments in
786 northern Morocco. *Mar. Poll. Bull.* **58**, 431-438 (2009).
59. Ranya, A. *et al.* Hydrocarbonoclastic marine bacteria in Mediterranean Sea, El-Max, Egypt:
788 isolation, identification and site characterization. *JÖKULL* **64**, 223-249 (2014).
60. Ibrahim, H. A., Farag, A. M., Beltagy, E. A. & El-Shenawy, M. A. Microbial pollution
790 indicators along the Egyptian coastal waters of Suez and Aqaba Gulfs and Red Sea. *J. Egypt.*
 Public Health Assoc. **86**, 111-118 (2011).
- 792 61. Al-Rousan, S. A., Al-Shloul, R. N., Al-Horani, F. A. & Abu-Hilal, A. H. Heavy metal contents
 in growth bands of Porites corals: record of anthropogenic and human developments from the
794 Jordanian Gulf of Aqaba. *Mar. Pollut. Bull.* **54**, 1912-1922 (2007).
62. Al-Taani, A. A. *et al.* Status of trace metals in surface seawater of the Gulf of Aqaba, Saudi
796 Arabia. *Mar. Pollut. Bull.* **86**, 582-590 (2014).
63. Al-Najjar, T., Rasheed, M., Ababneh, Z., Ababneh, A. & Al-Omarey, H. Heavy metals
798 pollution in sediment cores from the Gulf of Aqaba, Red Sea. *Natural Science* **3**, 775-782
 (2011).
- 800 64. Grasshoff, K. *et al.* *Methods of Seawater Analysis*, 3rd edn. Weinheim: WILEY-VCH, ch. 10, p.
 162, ch. 11, p. 230, ch. 12, pp. 263-271 (1999).
- 802 65. Menzel, D.W. & Vaccaro R.F. The measurement of dissolved organic and particulate carbon
 in seawater. *Limnol. Oceanog.* **9**, 138-142 (1964).
- 804 66. Kamaruzzaman, B.Y., Siti Waznah, A., Ong, M.C., Shahbudin, S. & Jalal, K.C.A. Variability of
 Organic Carbon Content in Bottom Sediment of Pahang River Estuary, Pahang, Malaysia. *J*
806 *Appl. Sci.* **9**, 4253-4257 (2009).

67. Van de Peer, Y., Chapelle, S. & De Wachter, R. A. Quantitative map of nucleotide substitution
808 rates in bacterial rRNA. *Nucleic Acids Res.* **24**, 3381-3391 (1996).
68. Chakravorty, S., Helb, D., Burday, M., Connell, N. & Alland, D. A detailed analysis of 16S
810 ribosomal gene segments for the diagnosis of pathogenic bacteria. *J. Microbiol. Methods* **69**,
330-339 (2007).
69. Caporaso, J. G. *et al.* QIIME allows analysis of high-throughput community sequencing data.
812 *Nat. Meth.* **7**, 335-336 (2010).
70. Edgar, R. C. Search and clustering orders of magnitude faster than BLAST. *Bioinformatics* **26**,
814 2460-2461 (2010).
71. Kunin, V., Engelbrektson, A., Ochman, H., Hugenholtz, P. Wrinkles in the rare biosphere:
816 pyrosequencing errors can lead to artificial inflation of diversity estimates. *Environ. Microbiol.*
818 **12**, 118-123 (2010).
72. Wang, Q., Garrity, G. M., Tiedje, J. M. & Cole, J. R. Naive Bayesian classifier for rapid
820 assignment of rRNA sequences into the new bacterial taxonomy. *Appl. Environ. Microbiol.* **73**,
5261-5267 (2007).
73. Lozupone, C., Lladser, M. E., Knights, D., Stombaugh, J. & Knight, R. UniFrac: an effective
822 distance metric for microbial community comparison. *ISME J.* **5**, 169-172 (2011).
74. Hammer, Ø., Harper, D. A. T. & Ryan, P. D. PAST: paleontological statistics software
824 package for education and data analysis. *Palaeontol. Electronica* **4**, 1 (2001).
75. Méndez-García, C. *et al.* Microbial stratification in low pH oxic and suboxic macroscopic
826 growths along an acid mine drainage. *ISME J.* **8**, 1259-1274 (2014).
76. Li, R. *et al.* De novo assembly of human genomes with massively parallel short read
828 sequencing. *Genome Res.* **20**, 265-272 (2010).
77. Li, R., Li, Y., Kristiansen, K. & Wang, J. SOAP: short oligonucleotide alignment program.
830 *Bioinformatics* **24**, 713-714 (2008).
78. Csardi, G. & Nepusz T. The igraph software package for complex network research.
832 InterJournal, Complex systems, 1695 (2006).
79. R Development Core Team. R: A language and environment for statistical computing. R
834 Foundation for Statistical Computing, Vienna, Austria. ISBN 3-900051-07-0. 2011;
836 <http://www.R-project.org/>.
80. Rasband, W.S. ImageJ, U. S. National Institutes of Health, Bethesda, Maryland, USA,
838 <http://imagej.nih.gov/ij/>, 1997-2012.
81. Dyksterhouse, S.E., Gray, J.P., Herwig, R.P., Lara, J.C. & Staley, J.T. *Cycloclasticus pugetii* gen.
840 nov., sp. nov., an aromatic hydrocarbon-degrading bacterium from marine sediments. *Int. J.*

Syst. Bacteriol. **45**, 116–123 (1995).

- 842 82. Pérez-Cobas, A. E. *et al.* Gut microbiota disturbance during antibiotic therapy: a multi-omic
approach. *Gut* **62**, 1591–1601 (2013).
- 844 83. Dunn, W. B., *et al.* Procedures for large-scale metabolic profiling of serum and plasma using
gas chromatography and liquid chromatography coupled to mass spectrometry. *Nat. Protoc.* **6**,
846 1060–1083 (2011)

Supplementary Table S1 Overall physico-chemical characteristics of the investigated sediment samples

| Location | Mediterranean Sea | | | | | | | Red Sea |
|--|-------------------------|-------------------------|-------------------------|-------------------------|-------------------------|-------------------------|-------------------------|-------------------------|
| Sample code | ELF | HAV | PRI | BIZ | ELMAX | MCh | MES | AQ |
| Depth (m) | 15.7 | 78.0 | 6.0 | 1.0 | 9.2 | 32.0 | 1.0 | 18.0 |
| [Pet Hyd] (ppm) ^{1,2} | 500 | 260,000 | 4,000 | 116 | 1,822 | 5,100 | 1,000 | 2,400 |
| Temperature (°C) | 13.0 | 15.0 | 19.0 | 19.3 | 20.0 | 21.3 | 23.0 | 26.5 |
| Dissolved O ₂ (mg/L) ³ | 6.04 | 6.0–6.5 | 0 ³ | 3.0 | 18.0 | 22.0 | 1.0–2.2 ³ | 20.0 |
| pH | 7.5 | 8.05 | 6.85 | 7.76 | 7.59 | 8.62 | 7.37 | 8.30 |
| Conductivity (Ms/cm) | 57.0 | 49.0 | 49.0 | 13.1 | 77.0 | 53.6 | 70.0 | 89.0 |
| Ammonium (mkmol/L) | 20.18 | 0.6–0.7 | 420 | 8.4 | 8.8 | 60.0 | 7.0 | 8.5 |
| Calcium (mg/L) | 50.94 | 420 | 408 | 35.80 | 71.3 | 87.37 | 430 | 125.78 |
| Diss_org_carb (mg/L) | 143.0 | 5.00 | 125.00 | 1.00 | 59.53 | 130.00 | 50.00 | 26.00 |
| Part_org_carb (μM) | 1.20 | 1.40 | 1.89 | 2.80 | 1.37 | 2.01 | 1.44 | 2.29 |
| [Microelements] (nM) ⁴ | 150.3 | 392.0 | 883.0 | 238.03 | 411.0 | 67.3 | 408.0 | 238.03 |
| Cells per g of sediment ⁵ | ~2.30e+08 (1.40e+08) | ~1.90e+09 (1.15e+09) | ~4.04e+08 (3.67e+08) | ~2.63e+08 (1.44e+08) | ~3.03e+08 (1.98e+08) | ~2.63e+08 (2.29e+08) | ~2.22e+08 (1.41e+08) | ~3.43e+08 (1.93e+08) |

¹Total petroleum hydrocarbon concentration

²BIZ site is chronically polluted; however, total hydrocarbon concentration is low as compared to other highly polluted sites herein investigated. BIZ sediments were collected near an Oil Refinery Industry. The site is characterized by a marked pollution due to the release of the refinery wastewater containing residual hydrocarbons. Since this is the seashore/beach, the sea waves could have an influence on the turnover of the pollutants, that can be spread through the seawater more rapidly, compared to common chronically polluted sediment, thus explaining the low total hydrocarbon concentration.

³Oxygen concentration as measured in the seawater immediately above the sediment sample. PRI is an anoxic site; MES is a micro-anaerobic environment.

⁴Microelements include Sc, Cr, Mn, Fe, Ni, Co, As, Se, Mo, Ag, Sn, Sb, Ba, La, Ce, Sm, Eu, Tb, Hf, Au, Hg, as well as heavy metals such as Zn, Cd, Pb and Cu.

⁵Standard deviation of triplicates per each of the duplicates is shown in brackets. For all other parameters, triplicate measurements per each of the sediment site duplicates were performed, with standard deviations lower than 5%.

Supplementary Table S2 Library coverage estimation and sequence diversity of 16S rRNA

| Sample | Nr. reads per sample | N. OTU ₉₇ | % Coverage* | Shannon index** |
|--------|----------------------|----------------------|-------------|-----------------|
| ELF | 20454 | 7679 | 0.79 | 8.10 |
| PRI | 6303 | 3012 | 0.69 | 7.39 |
| HAV | 7365 | 3054 | 0.75 | 7.32 |
| MES | 8772 | 1858 | 0.88 | 5.73 |
| BIZ | 9972 | 3058 | 0.81 | 6.75 |
| AQ | 6816 | 406 | 0.97 | 3.18 |
| ElMAX | 8243 | 478 | 0.98 | 4.24 |
| MCh | 14535 | 1065 | 0.96 | 4.07 |

*Library coverage was calculated as $C = 1 - n/N$, where n is the number of OTUs without a replicate, and N is the total number of sequences; **Shannon diversity index calculated using PAST

Supplementary Table S3 List of the taxonomic groups, identified based on the results of 16S rRNA pyrosequencing, composing the bacterial communities in the polluted sediments collected in the Mediterranean Sea and the Aqaba Gulf (Red Sea). Data indicate the relative percentage of sequences associated to each taxonomic group referred to the total number of sequences.

| TAXONOMIC CLASSIFICATION | Mediterranean Sea | | | | | | | Red Sea |
|--|-------------------|-------|--------|--------|--------|--------|--------|---------|
| | ELF | HAV | PRI | BIZ | ELMAX | MCh | MES | AQ |
| Temperature (°C) | 13.0 | 15.0 | 19.0 | 19.3 | 20.0 | 21.3 | 23.0 | 26.5 |
| Uncl. Acidimicrobiales | 0.326 | 0.186 | 0.377 | 2.698 | 1.638 | 0.000 | 0.000 | 0.000 |
| <i>Corynebacterium</i> | 0.000 | 0.000 | 0.000 | 0.000 | 0.646 | 0.000 | 0.000 | 0.000 |
| <i>Propionibacterium</i> | 0.000 | 0.000 | 0.000 | 0.000 | 4.267 | 0.000 | 0.000 | 0.000 |
| Uncl. Bacteroidales | 0.148 | 0.371 | 1.508 | 0.502 | 0.000 | 0.000 | 1.308 | 0.000 |
| Uncl. <i>Flavobacteriaceae</i> | 2.370 | 2.414 | 3.676 | 37.527 | 1.181 | 0.000 | 21.661 | 0.000 |
| <i>Arenibacter</i> | 0.000 | 0.000 | 0.094 | 0.000 | 0.000 | 0.000 | 1.629 | 0.000 |
| <i>Gramella</i> | 0.000 | 0.000 | 0.000 | 0.000 | 0.000 | 4.152 | 0.000 | 0.000 |
| <i>Salinimicrobium</i> | 0.000 | 0.000 | 0.000 | 0.000 | 0.441 | 73.791 | 0.000 | 0.000 |
| Uncl. <i>Chitinophagaceae</i> | 0.000 | 0.000 | 0.000 | 0.000 | 2.267 | 0.000 | 0.000 | 0.000 |
| Uncl. Ignavibacteriales | 0.000 | 0.000 | 0.000 | 2.165 | 0.803 | 0.000 | 0.115 | 0.000 |
| Uncl. Cyanobacteria | 0.237 | 0.000 | 0.000 | 1.224 | 1.102 | 0.000 | 0.000 | 0.000 |
| Uncl. <i>Bacillaceae</i> | 0.000 | 0.000 | 0.000 | 0.000 | 0.000 | 9.376 | 0.000 | 0.000 |
| <i>Bacillus</i> | 0.000 | 0.000 | 0.000 | 0.000 | 13.998 | 1.162 | 0.000 | 0.000 |
| <i>Planomicrobium</i> | 0.000 | 0.000 | 0.000 | 0.000 | 2.724 | 0.000 | 0.000 | 0.000 |
| <i>Staphylococcus</i> | 0.000 | 0.000 | 0.000 | 0.000 | 1.417 | 0.000 | 0.000 | 0.000 |
| Uncl. <i>Clostridiaceae</i> | 0.000 | 0.000 | 0.094 | 0.000 | 0.756 | 2.225 | 0.344 | 0.000 |
| <i>Anaerococcus</i> | 0.000 | 0.000 | 0.000 | 0.000 | 1.086 | 0.000 | 0.000 | 0.000 |
| Uncl. <i>Peptostreptococcaceae</i> | 0.000 | 0.093 | 0.000 | 0.000 | 0.724 | 0.000 | 0.000 | 0.000 |
| <i>Propionigenium</i> | 1.303 | 0.000 | 0.377 | 0.000 | 0.000 | 0.000 | 0.000 | 0.000 |
| <i>Psychrilyobacter</i> | 0.415 | 0.186 | 4.147 | 0.000 | 0.000 | 0.000 | 0.023 | 0.000 |
| Uncl. <i>Thermodesulfovibrionaceae</i> | 1.244 | 0.093 | 0.754 | 0.000 | 0.000 | 0.000 | 0.000 | 0.000 |
| Uncl. <i>Phycisphaerae</i> | 3.110 | 0.093 | 0.000 | 0.000 | 0.000 | 0.000 | 0.000 | 0.000 |
| Uncl. Phycisphaerales | 0.000 | 0.650 | 13.666 | 0.000 | 0.000 | 0.000 | 9.890 | 0.000 |
| Uncl. <i>Pirellulaceae</i> | 0.000 | 0.000 | 0.000 | 0.031 | 2.047 | 0.000 | 0.000 | 0.000 |
| Planctomyces | 0.000 | 0.093 | 0.000 | 0.000 | 0.000 | 0.000 | 15.856 | 0.000 |
| Uncl. Alphaproteobacteria | 0.000 | 3.993 | 0.000 | 0.000 | 0.000 | 0.000 | 0.000 | 0.000 |
| Uncl. <i>Caulobacteraceae</i> | 0.000 | 0.000 | 0.000 | 0.000 | 21.083 | 0.000 | 0.000 | 0.000 |
| Uncl. <i>Bradyrhizobiaceae</i> | 0.000 | 0.000 | 0.000 | 0.000 | 10.219 | 0.000 | 0.000 | 0.000 |
| <i>Bradyrhizobium</i> | 0.000 | 0.000 | 0.000 | 0.000 | 3.196 | 0.000 | 0.000 | 0.000 |

| | | | | | | | | |
|-----------------------------------|--------|--------|--------|--------|-------|-------|--------|--------|
| Uncl. <i>Methylobacteriaceae</i> | 0.000 | 0.000 | 0.000 | 0.000 | 8.235 | 0.000 | 0.000 | 0.000 |
| <i>Methylobacterium</i> | 0.000 | 0.000 | 0.000 | 0.000 | 3.527 | 0.000 | 0.000 | 0.000 |
| <i>Mesorhizobium</i> | 0.000 | 0.000 | 0.000 | 0.000 | 0.000 | 0.000 | 0.918 | 0.000 |
| Uncl. <i>Rhodobacteraceae</i> | 1.037 | 1.114 | 0.471 | 6.997 | 0.047 | 0.000 | 0.780 | 2.111 |
| <i>Nautella</i> | 0.000 | 0.000 | 0.000 | 0.000 | 0.000 | 0.000 | 0.000 | 0.704 |
| <i>Paracoccus</i> | 0.000 | 0.000 | 0.189 | 0.000 | 0.000 | 0.018 | 0.000 | 6.668 |
| <i>Phaeobacter</i> | 0.000 | 0.093 | 0.094 | 0.345 | 0.000 | 0.000 | 0.023 | 1.689 |
| <i>Ruegeria</i> | 0.237 | 0.093 | 0.283 | 1.130 | 0.000 | 0.000 | 0.000 | 0.018 |
| <i>Thalassobius</i> | 0.000 | 4.457 | 0.000 | 0.000 | 0.000 | 0.000 | 3.006 | 1.161 |
| Uncl. <i>Rhodospirillaceae</i> | 0.977 | 0.464 | 0.189 | 0.000 | 0.000 | 0.000 | 0.000 | 0.000 |
| Uncl. Betaproteobacteria | 0.000 | 4.271 | 0.000 | 0.000 | 0.000 | 0.000 | 0.000 | 0.000 |
| Uncl. <i>Desulfobulbaceae</i> | 6.309 | 1.021 | 11.027 | 1.255 | 0.047 | 0.000 | 0.000 | 0.000 |
| Uncl. <i>Desulfuromonadaceae</i> | 0.415 | 2.693 | 0.189 | 2.071 | 0.000 | 0.000 | 0.000 | 0.000 |
| Uncl. <i>Desulfobacteraceae</i> | 2.281 | 0.279 | 0.000 | 0.000 | 0.000 | 0.000 | 0.000 | 0.000 |
| <i>Desulfococcus</i> | 11.463 | 1.764 | 1.885 | 0.063 | 0.000 | 0.000 | 0.000 | 0.000 |
| <i>Desulfosarcina</i> | 1.866 | 0.650 | 4.430 | 3.765 | 0.000 | 0.000 | 0.000 | 0.000 |
| Uncl. <i>Syntrophobacteraceae</i> | 24.704 | 0.186 | 0.566 | 0.000 | 0.000 | 0.000 | 0.000 | 0.000 |
| <i>Arcobacter</i> | 2.251 | 0.093 | 0.000 | 0.000 | 0.000 | 7.106 | 0.000 | 0.000 |
| Uncl. <i>Helicobacteraceae</i> | 2.607 | 14.578 | 18.096 | 3.044 | 0.031 | 0.000 | 0.000 | 0.000 |
| <i>Sulfuricurvum</i> | 0.000 | 0.464 | 10.933 | 0.220 | 0.000 | 0.000 | 1.056 | 0.000 |
| <i>Sulfurimonas</i> | 0.000 | 0.000 | 4.430 | 11.672 | 0.000 | 0.000 | 0.000 | 0.000 |
| Uncl. Gammaproteobacteria | 4.532 | 42.154 | 9.331 | 0.157 | 0.000 | 0.000 | 0.184 | 0.000 |
| <i>Alteromonas</i> | 0.000 | 0.000 | 0.000 | 0.000 | 0.000 | 0.036 | 0.000 | 20.549 |
| <i>Marinobacter</i> | 0.000 | 0.000 | 0.000 | 2.855 | 0.000 | 0.000 | 0.207 | 0.000 |
| <i>Pseudoalteromonas</i> | 0.000 | 1.671 | 0.000 | 0.000 | 0.000 | 0.000 | 0.000 | 1.970 |
| Uncl. Chromatiales | 8.916 | 0.557 | 4.713 | 13.367 | 0.047 | 0.000 | 0.115 | 0.000 |
| Uncl. Methylococcales | 2.873 | 0.093 | 1.225 | 1.067 | 0.000 | 0.000 | 1.446 | 0.000 |
| Uncl. <i>Halomonadaceae</i> | 0.000 | 0.000 | 0.000 | 0.000 | 0.000 | 0.703 | 0.000 | 0.035 |
| <i>Psychrobacter</i> | 0.000 | 0.000 | 0.000 | 0.000 | 0.000 | 0.000 | 0.000 | 63.688 |
| <i>Pseudomonas</i> | 0.000 | 0.000 | 0.000 | 0.000 | 0.031 | 1.045 | 0.069 | 1.390 |
| Uncl. <i>Piscirickettsiaceae</i> | 0.000 | 4.550 | 0.943 | 0.000 | 0.000 | 0.000 | 24.254 | 0.000 |
| <i>Cycloclasticus</i> | 0.000 | 2.971 | 0.189 | 0.471 | 0.000 | 0.000 | 0.413 | 0.000 |
| <i>Methylophaga</i> | 0.000 | 0.371 | 0.000 | 0.031 | 0.000 | 0.000 | 3.580 | 0.000 |
| <i>Thiomicrospira</i> | 0.000 | 0.000 | 0.000 | 0.000 | 0.661 | 0.000 | 0.000 | 0.000 |
| Uncl. <i>Vibrionaceae</i> | 2.518 | 0.000 | 0.000 | 0.000 | 0.000 | 0.000 | 0.046 | 0.000 |
| <i>Vibrio</i> | 0.030 | 0.000 | 0.000 | 0.031 | 0.000 | 0.387 | 0.000 | 0.018 |
| Uncl. Xanthomonadales | 17.832 | 3.528 | 6.126 | 5.460 | 0.031 | 0.000 | 1.056 | 0.000 |

| | | | | | | | | |
|------------------------------|-------|-------|-------|-------|-------|-------|-------|-------|
| Uncl. <i>Sinobacteraceae</i> | 0.000 | 0.000 | 0.000 | 0.000 | 7.794 | 0.000 | 0.000 | 0.000 |
| Uncl. Spirochaetes | 0.000 | 0.000 | 0.000 | 1.851 | 0.000 | 0.000 | 0.000 | 0.000 |
| Uncl. OD1 | 0.000 | 0.000 | 0.000 | 0.000 | 0.000 | 0.000 | 10.55 | 0.000 |
| Uncl. TM7 | 0.000 | 0.000 | 0.000 | 0.000 | 4.282 | 0.000 | 0.000 | 0.000 |
| Uncl. AB16 | 0.000 | 3.714 | 0.000 | 0.000 | 0.000 | 0.000 | 0.000 | 0.000 |
| Uncl. Bacteria | 0.000 | 0.000 | 0.000 | 0.000 | 5.668 | 0.000 | 1.469 | 0.000 |

Supplementary Table S4 Enrichment in KEGG functional classes by meaning of the percentage of genes belonging to KEGG categories based on PICRUST's prediction. As shown, no significant differences, including in biodegradation pathways (see in grey and bold), were observed.

| KEGG PATHWAY | KEGG PATHWAY | METABOLISM | PERCENTAGE OF GENES | | | | | | | |
|--------------------------------------|--------------------------|----------------------------------|---------------------|--------|--------|--------|--------|--------|--------|--------|
| | | | ELF | HAV | PRI | BIZ | ELMAX | MCh | MES | AQ |
| Cellular Processes | Cell Communication | Adherens junction | 0,0000 | 0,0000 | 0,0000 | 0,0000 | 0,0000 | 0,0000 | 0,0000 | 0,0000 |
| Cellular Processes | Cell Communication | Focal adhesion | 0,0000 | 0,0000 | 0,0000 | 0,0001 | 0,0000 | 0,0000 | 0,0000 | 0,0000 |
| Cellular Processes | Cell Communication | Tight junction | 0,0000 | 0,0000 | 0,0000 | 0,0000 | 0,0000 | 0,0000 | 0,0000 | 0,0000 |
| Cellular Processes | Cell Growth and Death | Apoptosis | 0,0042 | 0,0314 | 0,0080 | 0,0210 | 0,0336 | 0,0340 | 0,0230 | 0,0527 |
| Cellular Processes | Cell Growth and Death | Cell cycle | 0,0000 | 0,0000 | 0,0000 | 0,0000 | 0,0000 | 0,0000 | 0,0000 | 0,0000 |
| Cellular Processes | Cell Growth and Death | Cell cycle - Caulobacter | 0,4735 | 0,5461 | 0,4866 | 0,4529 | 0,3920 | 0,4294 | 0,4902 | 0,3911 |
| Cellular Processes | Cell Growth and Death | Cell cycle - yeast | 0,0000 | 0,0000 | 0,0000 | 0,0000 | 0,0000 | 0,0000 | 0,0000 | 0,0000 |
| Cellular Processes | Cell Growth and Death | Meiosis - yeast | 0,0452 | 0,0400 | 0,0360 | 0,0415 | 0,0575 | 0,0324 | 0,0308 | 0,0333 |
| Cellular Processes | Cell Growth and Death | Oocyte meiosis | 0,0000 | 0,0000 | 0,0000 | 0,0000 | 0,0000 | 0,0000 | 0,0000 | 0,0000 |
| Cellular Processes | Cell Growth and Death | p53 signaling pathway | 0,0044 | 0,0314 | 0,0092 | 0,0210 | 0,0336 | 0,0340 | 0,0243 | 0,0527 |
| Cellular Processes | Cell Motility | Bacterial chemotaxis | 0,8726 | 0,7980 | 0,8039 | 0,5265 | 0,5051 | 0,2429 | 0,8249 | 0,5801 |
| Cellular Processes | Cell Motility | Bacterial motility proteins | 2,5071 | 2,0881 | 2,1701 | 1,3529 | 1,1616 | 0,3788 | 2,0324 | 1,4942 |
| Cellular Processes | Cell Motility | Cytoskeleton proteins | 0,2376 | 0,2165 | 0,2271 | 0,1975 | 0,2005 | 0,2137 | 0,2305 | 0,2323 |
| Cellular Processes | Cell Motility | Flagellar assembly | 1,0149 | 0,9070 | 0,8821 | 0,5533 | 0,5864 | 0,2099 | 0,7631 | 0,7310 |
| Cellular Processes | Cell Motility | Regulation of actin cytoskeleton | 0,0000 | 0,0000 | 0,0000 | 0,0000 | 0,0000 | 0,0000 | 0,0000 | 0,0000 |
| Cellular Processes | Transport and Catabolism | Endocytosis | 0,0005 | 0,0026 | 0,0018 | 0,0019 | 0,0061 | 0,0005 | 0,0030 | 0,0243 |
| Cellular Processes | Transport and Catabolism | Lysosome | 0,0269 | 0,1008 | 0,0408 | 0,0837 | 0,0383 | 0,1254 | 0,0652 | 0,0119 |
| Cellular Processes | Transport and Catabolism | Peroxisome | 0,2392 | 0,2077 | 0,2437 | 0,2455 | 0,2598 | 0,2541 | 0,2173 | 0,2680 |
| Cellular Processes | Transport and Catabolism | Phagosome | 0,0000 | 0,0000 | 0,0000 | 0,0000 | 0,0000 | 0,0000 | 0,0000 | 0,0000 |
| Environmental Information Processing | Membrane Transport | ABC transporters | 2,5575 | 2,8415 | 2,7343 | 2,6935 | 4,2431 | 1,2844 | 2,5389 | 3,7578 |
| Environmental Information Processing | Membrane Transport | Bacterial secretion system | 0,8171 | 0,8650 | 0,7856 | 0,7404 | 0,7023 | 0,5415 | 0,9955 | 0,7248 |
| Environmental Information Processing | Membrane Transport | Phosphotransferase system (PTS) | 0,0989 | 0,1074 | 0,0967 | 0,0622 | 0,1308 | 0,0299 | 0,0853 | 0,0811 |
| Environmental Information Processing | Membrane Transport | Secretion system | 2,0251 | 1,9260 | 1,8174 | 1,4516 | 1,3307 | 0,7669 | 2,0641 | 1,6424 |
| Environmental Information Processing | Membrane Transport | Transporters | 3,8496 | 4,2962 | 4,1925 | 4,2195 | 6,5019 | 2,2727 | 3,9000 | 5,6296 |
| Environmental Information Processing | Signal Transduction | Calcium signaling pathway | 0,0001 | 0,0002 | 0,0000 | 0,0000 | 0,0000 | 0,0000 | 0,0003 | 0,0000 |

| | | | | | | | | | | |
|--------------------------------------|-------------------------------------|--|--------|--------|--------|--------|--------|--------|--------|--------|
| Environmental Information Processing | Signal Transduction | ErbB signaling pathway | 0,0000 | 0,0000 | 0,0000 | 0,0000 | 0,0000 | 0,0000 | 0,0000 | 0,0000 |
| Environmental Information Processing | Signal Transduction | Hedgehog signaling pathway | 0,0000 | 0,0000 | 0,0000 | 0,0000 | 0,0000 | 0,0000 | 0,0000 | 0,0000 |
| Environmental Information Processing | Signal Transduction | MAPK signaling pathway | 0,0000 | 0,0000 | 0,0000 | 0,0000 | 0,0000 | 0,0000 | 0,0000 | 0,0000 |
| Environmental Information Processing | Signal Transduction | MAPK signaling pathway - yeast | 0,0294 | 0,0346 | 0,0272 | 0,0458 | 0,0523 | 0,0703 | 0,0335 | 0,0462 |
| Environmental Information Processing | Signal Transduction | Notch signaling pathway | 0,0000 | 0,0000 | 0,0000 | 0,0000 | 0,0000 | 0,0000 | 0,0000 | 0,0000 |
| Environmental Information Processing | Signal Transduction | Phosphatidylinositol signaling system | 0,1007 | 0,1094 | 0,1030 | 0,1040 | 0,1154 | 0,0767 | 0,1240 | 0,0928 |
| Environmental Information Processing | Signal Transduction | TGF-beta signaling pathway | 0,0000 | 0,0000 | 0,0000 | 0,0000 | 0,0000 | 0,0000 | 0,0000 | 0,0000 |
| Environmental Information Processing | Signal Transduction | Two-component system | 2,2834 | 2,1741 | 2,1898 | 1,7531 | 1,8288 | 1,1684 | 2,3171 | 2,0243 |
| Environmental Information Processing | Signal Transduction | VEGF signaling pathway | 0,0000 | 0,0000 | 0,0000 | 0,0002 | 0,0028 | 0,0000 | 0,0000 | 0,0000 |
| Environmental Information Processing | Signal Transduction | Wnt signaling pathway | 0,0000 | 0,0000 | 0,0000 | 0,0000 | 0,0000 | 0,0000 | 0,0000 | 0,0000 |
| Environmental Information Processing | Signal Transduction | mTOR signaling pathway | 0,0000 | 0,0000 | 0,0000 | 0,0000 | 0,0000 | 0,0000 | 0,0000 | 0,0000 |
| Environmental Information Processing | Signaling Molecules and Interaction | Bacterial toxins | 0,0329 | 0,0369 | 0,0397 | 0,0397 | 0,0472 | 0,0372 | 0,0278 | 0,0254 |
| Environmental Information Processing | Signaling Molecules and Interaction | CAM ligands | 0,0000 | 0,0000 | 0,0000 | 0,0001 | 0,0000 | 0,0000 | 0,0000 | 0,0000 |
| Environmental Information Processing | Signaling Molecules and Interaction | Cell adhesion molecules (CAMs) | 0,0000 | 0,0000 | 0,0000 | 0,0000 | 0,0000 | 0,0000 | 0,0000 | 0,0000 |
| Environmental Information Processing | Signaling Molecules and Interaction | Cellular antigens | 0,0602 | 0,0549 | 0,0555 | 0,0998 | 0,0869 | 0,1646 | 0,0856 | 0,0971 |
| Environmental Information Processing | Signaling Molecules and Interaction | Cytokine receptors | 0,0000 | 0,0000 | 0,0000 | 0,0000 | 0,0000 | 0,0000 | 0,0000 | 0,0000 |
| Environmental Information Processing | Signaling Molecules and Interaction | Cytokine-cytokine receptor interaction | 0,0000 | 0,0000 | 0,0000 | 0,0000 | 0,0000 | 0,0000 | 0,0000 | 0,0000 |
| Environmental Information Processing | Signaling Molecules and Interaction | ECM-receptor interaction | 0,0000 | 0,0000 | 0,0000 | 0,0001 | 0,0000 | 0,0000 | 0,0000 | 0,0000 |
| Environmental Information Processing | Signaling Molecules and Interaction | G protein-coupled receptors | 0,0000 | 0,0000 | 0,0000 | 0,0000 | 0,0000 | 0,0000 | 0,0000 | 0,0000 |
| Environmental Information Processing | Signaling Molecules and Interaction | GTP-binding proteins | 0,0000 | 0,0000 | 0,0000 | 0,0000 | 0,0000 | 0,0000 | 0,0000 | 0,0089 |
| Environmental Information Processing | Signaling Molecules and Interaction | Glycan binding proteins | 0,0000 | 0,0000 | 0,0000 | 0,0000 | 0,0000 | 0,0000 | 0,0000 | 0,0000 |

| | | | | | | | | | | |
|--------------------------------------|-------------------------------------|---|--------|--------|--------|--------|--------|--------|--------|--------|
| Environmental Information Processing | Signaling Molecules and Interaction | Ion channels | 0,0033 | 0,0053 | 0,0045 | 0,0243 | 0,0126 | 0,0340 | 0,0066 | 0,0103 |
| Environmental Information Processing | Signaling Molecules and Interaction | Neuroactive ligand-receptor interaction | 0,0000 | 0,0000 | 0,0000 | 0,0000 | 0,0000 | 0,0000 | 0,0000 | 0,0000 |
| Genetic Information Processing | Folding, Sorting and Degradation | Chaperones and folding catalysts | 1,0328 | 0,9356 | 0,9794 | 0,8937 | 0,7336 | 0,7630 | 1,0505 | 0,7924 |
| Genetic Information Processing | Folding, Sorting and Degradation | Proteasome | 0,0313 | 0,0246 | 0,0291 | 0,0270 | 0,0164 | 0,0340 | 0,0287 | 0,0108 |
| Genetic Information Processing | Folding, Sorting and Degradation | Protein export | 0,5455 | 0,5653 | 0,5511 | 0,5446 | 0,4635 | 0,5022 | 0,5518 | 0,4424 |
| Genetic Information Processing | Folding, Sorting and Degradation | Protein processing in endoplasmic reticulum | 0,0679 | 0,0474 | 0,0635 | 0,0510 | 0,0364 | 0,0348 | 0,0467 | 0,0105 |
| Genetic Information Processing | Folding, Sorting and Degradation | RNA degradation | 0,4672 | 0,4786 | 0,4553 | 0,4532 | 0,3836 | 0,5199 | 0,4869 | 0,3819 |
| Genetic Information Processing | Folding, Sorting and Degradation | Sulfur relay system | 0,3759 | 0,3454 | 0,3381 | 0,3177 | 0,2804 | 0,1686 | 0,4082 | 0,2902 |
| Genetic Information Processing | Folding, Sorting and Degradation | Ubiquitin system | 0,0029 | 0,0035 | 0,0035 | 0,0059 | 0,0051 | 0,0002 | 0,0123 | 0,0097 |
| Genetic Information Processing | RNA family | Non-coding RNAs | 0,0000 | 0,0000 | 0,0000 | 0,0000 | 0,0009 | 0,0000 | 0,0000 | 0,0000 |
| Genetic Information Processing | Replication and Repair | Base excision repair | 0,3198 | 0,3717 | 0,3435 | 0,3610 | 0,3771 | 0,3620 | 0,3783 | 0,3091 |
| Genetic Information Processing | Replication and Repair | Chromosome | 1,3403 | 1,2858 | 1,2872 | 1,1837 | 1,0976 | 1,2343 | 1,3636 | 1,1835 |
| Genetic Information Processing | Replication and Repair | DNA repair and recombination proteins | 2,2391 | 2,2973 | 2,2780 | 2,2546 | 1,9933 | 2,6049 | 2,3406 | 1,9101 |
| Genetic Information Processing | Replication and Repair | DNA replication | 0,5098 | 0,5168 | 0,5184 | 0,5602 | 0,4542 | 0,6911 | 0,5270 | 0,4176 |
| Genetic Information Processing | Replication and Repair | DNA replication proteins | 0,8641 | 0,9029 | 0,8716 | 0,8965 | 0,7336 | 1,0523 | 0,9260 | 0,7259 |
| Genetic Information Processing | Replication and Repair | Homologous recombination | 0,7254 | 0,7207 | 0,7273 | 0,7528 | 0,5929 | 0,8637 | 0,7291 | 0,5714 |
| Genetic Information Processing | Replication and Repair | Mismatch repair | 0,6012 | 0,6072 | 0,6193 | 0,6290 | 0,5261 | 0,7342 | 0,6561 | 0,4938 |
| Genetic Information Processing | Replication and Repair | Non-homologous end-joining | 0,0090 | 0,0244 | 0,0137 | 0,0187 | 0,0397 | 0,0353 | 0,0155 | 0,0289 |
| Genetic Information Processing | Replication and Repair | Nucleotide excision repair | 0,2965 | 0,3003 | 0,3011 | 0,2849 | 0,2570 | 0,3177 | 0,2694 | 0,2147 |
| Genetic Information Processing | Transcription | Basal transcription factors | 0,0004 | 0,0005 | 0,0006 | 0,0018 | 0,0009 | 0,0015 | 0,0005 | 0,0003 |
| Genetic Information Processing | Transcription | RNA polymerase | 0,1320 | 0,1410 | 0,1339 | 0,1288 | 0,1149 | 0,1098 | 0,1410 | 0,1039 |
| Genetic Information Processing | Transcription | Spliceosome | 0,0001 | 0,0002 | 0,0004 | 0,0009 | 0,0000 | 0,0000 | 0,0047 | 0,0000 |

| | | | | | | | | | | |
|--------------------------------|-------------------------|--|--------|--------|--------|--------|--------|--------|--------|--------|
| Genetic Information Processing | Transcription | Transcription factors | 1,0167 | 1,0460 | 1,0523 | 1,2022 | 1,4289 | 1,1971 | 1,2313 | 1,5142 |
| Genetic Information Processing | Transcription | Transcription machinery | 0,7184 | 0,7328 | 0,7445 | 0,8303 | 0,6733 | 1,0922 | 0,7833 | 0,5241 |
| Genetic Information Processing | Translation | Aminoacyl-tRNA biosynthesis | 1,0350 | 1,0745 | 1,0556 | 0,9693 | 0,8738 | 0,8387 | 1,0024 | 0,8062 |
| Genetic Information Processing | Translation | RNA transport | 0,1155 | 0,0862 | 0,1088 | 0,1145 | 0,0799 | 0,2013 | 0,1186 | 0,0608 |
| Genetic Information Processing | Translation | Ribosome | 1,8221 | 1,9109 | 1,8719 | 1,8059 | 1,5176 | 1,9261 | 1,8525 | 1,3974 |
| Genetic Information Processing | Translation | Ribosome Biogenesis | 1,1894 | 1,1516 | 1,1508 | 1,1324 | 0,9518 | 1,1769 | 1,3417 | 1,0904 |
| Genetic Information Processing | Translation | Ribosome biogenesis in eukaryotes | 0,0478 | 0,0399 | 0,0434 | 0,0439 | 0,0322 | 0,0369 | 0,0610 | 0,0362 |
| Genetic Information Processing | Translation | Translation factors | 0,4433 | 0,4502 | 0,4522 | 0,4143 | 0,3402 | 0,4166 | 0,4229 | 0,3267 |
| Genetic Information Processing | Translation | mRNA surveillance pathway | 0,0021 | 0,0019 | 0,0023 | 0,0000 | 0,0000 | 0,0000 | 0,0000 | 0,0000 |
| Human Diseases | Cancers | Bladder cancer | 0,0019 | 0,0051 | 0,0043 | 0,0077 | 0,0150 | 0,0024 | 0,0204 | 0,0146 |
| Human Diseases | Cancers | Chronic myeloid leukemia | 0,0000 | 0,0000 | 0,0000 | 0,0000 | 0,0000 | 0,0000 | 0,0000 | 0,0000 |
| Human Diseases | Cancers | Colorectal cancer | 0,0040 | 0,0310 | 0,0078 | 0,0109 | 0,0308 | 0,0028 | 0,0213 | 0,0438 |
| Human Diseases | Cancers | Glioma | 0,0000 | 0,0000 | 0,0000 | 0,0000 | 0,0000 | 0,0000 | 0,0000 | 0,0000 |
| Human Diseases | Cancers | Pancreatic cancer | 0,0000 | 0,0000 | 0,0000 | 0,0000 | 0,0000 | 0,0000 | 0,0000 | 0,0000 |
| Human Diseases | Cancers | Pathways in cancer | 0,0599 | 0,0806 | 0,0602 | 0,0652 | 0,0710 | 0,0720 | 0,0832 | 0,0795 |
| Human Diseases | Cancers | Prostate cancer | 0,0247 | 0,0187 | 0,0217 | 0,0236 | 0,0136 | 0,0340 | 0,0275 | 0,0097 |
| Human Diseases | Cancers | Renal cell carcinoma | 0,0312 | 0,0310 | 0,0307 | 0,0304 | 0,0238 | 0,0351 | 0,0344 | 0,0260 |
| Human Diseases | Cancers | Small cell lung cancer | 0,0040 | 0,0310 | 0,0078 | 0,0112 | 0,0336 | 0,0028 | 0,0213 | 0,0438 |
| Human Diseases | Cardiovascular Diseases | Arrhythmogenic right ventricular cardiomyopathy (ARVC) | 0,0000 | 0,0000 | 0,0000 | 0,0000 | 0,0000 | 0,0000 | 0,0000 | 0,0000 |
| Human Diseases | Cardiovascular Diseases | Dilated cardiomyopathy (DCM) | 0,0000 | 0,0000 | 0,0000 | 0,0000 | 0,0000 | 0,0000 | 0,0000 | 0,0000 |
| Human Diseases | Cardiovascular Diseases | Hypertrophic cardiomyopathy (HCM) | 0,0005 | 0,0011 | 0,0012 | 0,0005 | 0,0000 | 0,0000 | 0,0060 | 0,0089 |
| Human Diseases | Cardiovascular Diseases | Viral myocarditis | 0,0040 | 0,0310 | 0,0078 | 0,0109 | 0,0308 | 0,0028 | 0,0213 | 0,0438 |
| Human Diseases | Immune System Diseases | Primary immunodeficiency | 0,0216 | 0,0215 | 0,0330 | 0,0376 | 0,0392 | 0,0368 | 0,0395 | 0,0495 |
| Human Diseases | Immune System Diseases | Rheumatoid arthritis | 0,0000 | 0,0000 | 0,0000 | 0,0000 | 0,0000 | 0,0000 | 0,0000 | 0,0000 |
| Human Diseases | Immune System Diseases | Systemic lupus erythematosus | 0,0004 | 0,0006 | 0,0000 | 0,0005 | 0,0000 | 0,0000 | 0,0014 | 0,0000 |
| Human Diseases | Infectious Diseases | African trypanosomiasis | 0,0013 | 0,0123 | 0,0025 | 0,0115 | 0,0093 | 0,0334 | 0,0117 | 0,0222 |
| Human Diseases | Infectious Diseases | Amoebiasis | 0,0011 | 0,0016 | 0,0010 | 0,0058 | 0,0154 | 0,0013 | 0,0030 | 0,0133 |
| Human Diseases | Infectious Diseases | Bacterial invasion of epithelial cells | 0,0043 | 0,0016 | 0,0049 | 0,0018 | 0,0000 | 0,0000 | 0,0000 | 0,0000 |
| Human Diseases | Infectious Diseases | Chagas disease (American trypanosomiasis) | 0,0017 | 0,0132 | 0,0037 | 0,0120 | 0,0084 | 0,0333 | 0,0177 | 0,0216 |

| | | | | | | | | | | |
|----------------|----------------------------|--|--------|--------|--------|--------|--------|--------|--------|--------|
| Human Diseases | Infectious Diseases | Epithelial cell signaling in Helicobacter pylori infection | 0,0483 | 0,0375 | 0,0428 | 0,0400 | 0,0355 | 0,0056 | 0,0372 | 0,0360 |
| Human Diseases | Infectious Diseases | Hepatitis C | 0,0000 | 0,0000 | 0,0000 | 0,0000 | 0,0000 | 0,0000 | 0,0000 | 0,0000 |
| Human Diseases | Infectious Diseases | Influenza A | 0,0043 | 0,0310 | 0,0098 | 0,0111 | 0,0318 | 0,0029 | 0,0216 | 0,0438 |
| Human Diseases | Infectious Diseases | Leishmaniasis | 0,0000 | 0,0000 | 0,0000 | 0,0002 | 0,0028 | 0,0000 | 0,0000 | 0,0089 |
| Human Diseases | Infectious Diseases | Measles | 0,0000 | 0,0000 | 0,0000 | 0,0000 | 0,0000 | 0,0000 | 0,0000 | 0,0000 |
| Human Diseases | Infectious Diseases | Pathogenic Escherichia coli infection | 0,0000 | 0,0000 | 0,0000 | 0,0000 | 0,0000 | 0,0000 | 0,0000 | 0,0000 |
| Human Diseases | Infectious Diseases | Pertussis | 0,0385 | 0,0343 | 0,0387 | 0,0459 | 0,0313 | 0,0680 | 0,0511 | 0,0311 |
| Human Diseases | Infectious Diseases | Shigellosis | 0,0000 | 0,0000 | 0,0000 | 0,0000 | 0,0000 | 0,0000 | 0,0000 | 0,0000 |
| Human Diseases | Infectious Diseases | Staphylococcus aureus infection | 0,0001 | 0,0005 | 0,0025 | 0,0001 | 0,0065 | 0,0023 | 0,0021 | 0,0005 |
| Human Diseases | Infectious Diseases | Toxoplasmosis | 0,0040 | 0,0310 | 0,0078 | 0,0109 | 0,0308 | 0,0028 | 0,0213 | 0,0438 |
| Human Diseases | Infectious Diseases | Tuberculosis | 0,1501 | 0,1715 | 0,1491 | 0,1228 | 0,1341 | 0,0797 | 0,1346 | 0,1460 |
| Human Diseases | Infectious Diseases | Vibrio cholerae infection | 0,0005 | 0,0011 | 0,0012 | 0,0006 | 0,0000 | 0,0000 | 0,0059 | 0,0008 |
| Human Diseases | Infectious Diseases | Vibrio cholerae pathogenic cycle | 0,1386 | 0,0937 | 0,1147 | 0,0865 | 0,0579 | 0,0489 | 0,1370 | 0,1163 |
| Human Diseases | Metabolic Diseases | Type I diabetes mellitus | 0,0492 | 0,0472 | 0,0543 | 0,0462 | 0,0425 | 0,0355 | 0,0404 | 0,0352 |
| Human Diseases | Metabolic Diseases | Type II diabetes mellitus | 0,0491 | 0,0399 | 0,0438 | 0,0506 | 0,0341 | 0,0370 | 0,0466 | 0,0249 |
| Human Diseases | Neurodegenerative Diseases | Alzheimer's disease | 0,1304 | 0,1631 | 0,1264 | 0,1478 | 0,1439 | 0,1165 | 0,1801 | 0,1915 |
| Human Diseases | Neurodegenerative Diseases | Amyotrophic lateral sclerosis (ALS) | 0,0115 | 0,0420 | 0,0178 | 0,0188 | 0,0570 | 0,0707 | 0,0419 | 0,0879 |
| Human Diseases | Neurodegenerative Diseases | Huntington's disease | 0,0966 | 0,1382 | 0,0985 | 0,0897 | 0,1149 | 0,0817 | 0,1596 | 0,1688 |
| Human Diseases | Neurodegenerative Diseases | Parkinson's disease | 0,0685 | 0,1035 | 0,0672 | 0,0592 | 0,0818 | 0,0118 | 0,1159 | 0,1268 |
| Human Diseases | Neurodegenerative Diseases | Prion diseases | 0,0005 | 0,0016 | 0,0018 | 0,0009 | 0,0042 | 0,0324 | 0,0041 | 0,0165 |
| Metabolism | Amino Acid Metabolism | Alanine, aspartate and glutamate metabolism | 0,9059 | 0,9043 | 0,8966 | 0,9095 | 0,8541 | 1,0603 | 0,9137 | 0,8714 |
| Metabolism | Amino Acid Metabolism | Amino acid related enzymes | 1,3214 | 1,3183 | 1,3273 | 1,2839 | 1,1406 | 1,3191 | 1,2873 | 1,1018 |
| Metabolism | Amino Acid Metabolism | Arginine and proline metabolism | 1,1807 | 1,2406 | 1,1803 | 1,3513 | 1,3952 | 1,3716 | 1,3701 | 1,5088 |
| Metabolism | Amino Acid Metabolism | Cysteine and methionine metabolism | 0,7235 | 0,7246 | 0,7230 | 0,7685 | 0,6668 | 0,9166 | 0,7833 | 0,6829 |
| Metabolism | Amino Acid Metabolism | Glycine, serine and threonine metabolism | 0,7753 | 0,8647 | 0,7787 | 0,9992 | 1,0214 | 1,1366 | 0,9236 | 1,1956 |
| Metabolism | Amino Acid Metabolism | Histidine metabolism | 0,5248 | 0,5579 | 0,5739 | 0,6484 | 0,6341 | 0,8930 | 0,5887 | 0,6469 |
| Metabolism | Amino Acid Metabolism | Lysine biosynthesis | 0,6140 | 0,6765 | 0,6347 | 0,6237 | 0,5892 | 0,6734 | 0,6446 | 0,5904 |
| Metabolism | Amino Acid Metabolism | Lysine degradation | 0,5590 | 0,5830 | 0,5954 | 0,6336 | 0,7079 | 0,8030 | 0,6019 | 0,7851 |
| Metabolism | Amino Acid Metabolism | Phenylalanine metabolism | 0,3067 | 0,3499 | 0,3213 | 0,3793 | 0,4472 | 0,3925 | 0,3544 | 0,4186 |

| | | | | | | | | | | |
|------------|---|---|--------|--------|--------|--------|--------|--------|--------|--------|
| Metabolism | Amino Acid Metabolism | Phenylalanine, tyrosine and tryptophan biosynthesis | 0,8067 | 0,7814 | 0,7942 | 0,7740 | 0,6186 | 0,7425 | 0,7482 | 0,6412 |
| Metabolism | Amino Acid Metabolism | Tryptophan metabolism | 0,5812 | 0,6265 | 0,6337 | 0,7052 | 0,8612 | 0,7203 | 0,6438 | 0,9287 |
| Metabolism | Amino Acid Metabolism | Tyrosine metabolism | 0,3807 | 0,4630 | 0,4330 | 0,4939 | 0,5406 | 0,8599 | 0,4657 | 0,5733 |
| Metabolism | Amino Acid Metabolism | Valine, leucine and isoleucine biosynthesis | 0,6730 | 0,7087 | 0,6978 | 0,7712 | 0,7364 | 0,6824 | 0,6576 | 0,6837 |
| Metabolism | Amino Acid Metabolism | Valine, leucine and isoleucine degradation | 0,8343 | 0,9388 | 0,9239 | 1,0488 | 1,2695 | 1,0021 | 0,8910 | 1,4050 |
| Metabolism | Biosynthesis of Other Secondary Metabolites | Betalain biosynthesis | 0,0046 | 0,0038 | 0,0059 | 0,0036 | 0,0112 | 0,0003 | 0,0036 | 0,0076 |
| Metabolism | Biosynthesis of Other Secondary Metabolites | Butirosin and neomycin biosynthesis | 0,0401 | 0,0386 | 0,0453 | 0,0388 | 0,0374 | 0,0039 | 0,0315 | 0,0233 |
| Metabolism | Biosynthesis of Other Secondary Metabolites | Caffeine metabolism | 0,0003 | 0,0003 | 0,0012 | 0,0045 | 0,0033 | 0,0002 | 0,0051 | 0,0008 |
| Metabolism | Biosynthesis of Other Secondary Metabolites | Clavulanic acid biosynthesis | 0,0000 | 0,0000 | 0,0000 | 0,0000 | 0,0000 | 0,0000 | 0,0000 | 0,0003 |
| Metabolism | Biosynthesis of Other Secondary Metabolites | Flavone and flavonol biosynthesis | 0,0002 | 0,0026 | 0,0004 | 0,0004 | 0,0028 | 0,0311 | 0,0003 | 0,0000 |
| Metabolism | Biosynthesis of Other Secondary Metabolites | Flavonoid biosynthesis | 0,0215 | 0,0096 | 0,0172 | 0,0085 | 0,0206 | 0,0634 | 0,0117 | 0,0024 |
| Metabolism | Biosynthesis of Other Secondary Metabolites | Indole alkaloid biosynthesis | 0,0046 | 0,0038 | 0,0059 | 0,0036 | 0,0112 | 0,0003 | 0,0036 | 0,0076 |
| Metabolism | Biosynthesis of Other Secondary Metabolites | Isoflavonoid biosynthesis | 0,0000 | 0,0000 | 0,0000 | 0,0000 | 0,0009 | 0,0001 | 0,0000 | 0,0000 |
| Metabolism | Biosynthesis of Other Secondary Metabolites | Isoquinoline alkaloid biosynthesis | 0,0604 | 0,0637 | 0,0643 | 0,0633 | 0,0687 | 0,0687 | 0,0637 | 0,0654 |
| Metabolism | Biosynthesis of Other Secondary Metabolites | Novobiocin biosynthesis | 0,1544 | 0,1428 | 0,1475 | 0,1487 | 0,1257 | 0,1390 | 0,1437 | 0,1477 |
| Metabolism | Biosynthesis of Other Secondary Metabolites | Penicillin and cephalosporin biosynthesis | 0,0244 | 0,0289 | 0,0324 | 0,0401 | 0,0392 | 0,0389 | 0,0324 | 0,0446 |
| Metabolism | Biosynthesis of Other Secondary Metabolites | Phenylpropanoid biosynthesis | 0,0686 | 0,0735 | 0,0793 | 0,0973 | 0,0860 | 0,1998 | 0,0797 | 0,0938 |
| Metabolism | Biosynthesis of Other Secondary Metabolites | Stilbenoid, diarylheptanoid and gingerol | 0,0203 | 0,0266 | 0,0176 | 0,0391 | 0,0425 | 0,0978 | 0,0228 | 0,0433 |

| | | | | | | | | | | |
|------------|---|--|--------|--------|--------|--------|--------|--------|--------|--------|
| | Secondary Metabolites | biosynthesis | | | | | | | | |
| Metabolism | Biosynthesis of Other Secondary Metabolites | Streptomycin biosynthesis | 0,3009 | 0,2891 | 0,3136 | 0,2877 | 0,2589 | 0,2445 | 0,2454 | 0,1972 |
| Metabolism | Biosynthesis of Other Secondary Metabolites | Tropane, piperidine and pyridine alkaloid biosynthesis | 0,1482 | 0,1385 | 0,1497 | 0,1669 | 0,1346 | 0,1439 | 0,1635 | 0,1588 |
| Metabolism | Biosynthesis of Other Secondary Metabolites | beta-Lactam resistance | 0,0078 | 0,0147 | 0,0115 | 0,0175 | 0,0215 | 0,0355 | 0,0212 | 0,0119 |
| Metabolism | Carbohydrate Metabolism | Amino sugar and nucleotide sugar metabolism | 0,9509 | 0,9354 | 0,9730 | 0,9435 | 0,8481 | 1,0119 | 0,7987 | 0,7348 |
| Metabolism | Carbohydrate Metabolism | Ascorbate and aldarate metabolism | 0,1082 | 0,1294 | 0,1227 | 0,1327 | 0,1846 | 0,1851 | 0,1239 | 0,1693 |
| Metabolism | Carbohydrate Metabolism | Butanoate metabolism | 1,1473 | 1,1235 | 1,1846 | 1,1952 | 1,3163 | 0,9799 | 0,9627 | 1,2495 |
| Metabolism | Carbohydrate Metabolism | C5-Branched dibasic acid metabolism | 0,3113 | 0,3267 | 0,3285 | 0,3360 | 0,3355 | 0,2878 | 0,2998 | 0,3005 |
| Metabolism | Carbohydrate Metabolism | Citrate cycle (TCA cycle) | 0,8769 | 0,8813 | 0,8895 | 0,9371 | 0,8612 | 0,8804 | 0,8786 | 0,7242 |
| Metabolism | Carbohydrate Metabolism | Fructose and mannose metabolism | 0,5845 | 0,6283 | 0,6046 | 0,6321 | 0,5710 | 1,0648 | 0,5279 | 0,5512 |
| Metabolism | Carbohydrate Metabolism | Galactose metabolism | 0,2485 | 0,2578 | 0,3017 | 0,3228 | 0,3000 | 0,2849 | 0,2078 | 0,2650 |
| Metabolism | Carbohydrate Metabolism | Glycolysis / Gluconeogenesis | 1,0031 | 1,0330 | 1,0242 | 1,1208 | 1,1032 | 1,1666 | 0,9711 | 0,9747 |
| Metabolism | Carbohydrate Metabolism | Glyoxylate and dicarboxylate metabolism | 0,8344 | 0,7708 | 0,7926 | 0,8650 | 0,8644 | 0,7233 | 0,6904 | 0,8892 |
| Metabolism | Carbohydrate Metabolism | Inositol phosphate metabolism | 0,1060 | 0,1343 | 0,1227 | 0,1338 | 0,2056 | 0,0605 | 0,1194 | 0,1836 |
| Metabolism | Carbohydrate Metabolism | Pentose and glucuronate interconversions | 0,2119 | 0,2926 | 0,2566 | 0,4091 | 0,4163 | 0,4391 | 0,2688 | 0,4368 |
| Metabolism | Carbohydrate Metabolism | Pentose phosphate pathway | 0,5899 | 0,5830 | 0,6263 | 0,6415 | 0,6229 | 0,7813 | 0,5147 | 0,5655 |
| Metabolism | Carbohydrate Metabolism | Propanoate metabolism | 1,0416 | 1,0634 | 1,0920 | 1,1243 | 1,2807 | 0,8715 | 1,0035 | 1,2938 |
| Metabolism | Carbohydrate Metabolism | Pyruvate metabolism | 1,2236 | 1,1888 | 1,1985 | 1,2954 | 1,2775 | 1,2602 | 1,1181 | 1,2311 |
| Metabolism | Carbohydrate Metabolism | Starch and sucrose metabolism | 0,4850 | 0,4217 | 0,5024 | 0,5109 | 0,4173 | 0,7800 | 0,3923 | 0,3959 |
| Metabolism | Energy Metabolism | Carbon fixation in photosynthetic organisms | 0,5715 | 0,5476 | 0,5585 | 0,5603 | 0,4953 | 0,5942 | 0,4852 | 0,4373 |
| Metabolism | Energy Metabolism | Carbon fixation pathways in prokaryotes | 1,3421 | 1,2524 | 1,3656 | 1,3221 | 1,1952 | 1,0826 | 1,1621 | 1,1583 |
| Metabolism | Energy Metabolism | Methane metabolism | 1,1283 | 1,0249 | 1,1217 | 1,0117 | 1,0513 | 0,6871 | 0,9296 | 1,0015 |
| Metabolism | Energy Metabolism | Nitrogen metabolism | 0,7525 | 0,7521 | 0,7375 | 0,8545 | 0,7714 | 0,8184 | 0,8607 | 0,7508 |
| Metabolism | Energy Metabolism | Oxidative phosphorylation | 1,6082 | 1,6521 | 1,5227 | 1,3937 | 1,3214 | 1,0390 | 1,5134 | 1,2335 |
| Metabolism | Energy Metabolism | Photosynthesis | 0,3883 | 0,3740 | 0,3465 | 0,3084 | 0,2504 | 0,2823 | 0,2922 | 0,2277 |
| Metabolism | Energy Metabolism | Photosynthesis - antenna proteins | 0,0134 | 0,0000 | 0,0000 | 0,0000 | 0,0000 | 0,0000 | 0,0000 | 0,0000 |

| | | | | | | | | | | |
|------------|------------------------------------|--|--------|--------|--------|--------|--------|--------|--------|--------|
| Metabolism | Energy Metabolism | Photosynthesis proteins | 0,4328 | 0,4121 | 0,3727 | 0,3286 | 0,2696 | 0,2861 | 0,3229 | 0,2596 |
| Metabolism | Energy Metabolism | Sulfur metabolism | 0,3261 | 0,3218 | 0,3009 | 0,3284 | 0,2509 | 0,3539 | 0,3522 | 0,2761 |
| Metabolism | Enzyme Families | Cytochrome P450 | 0,0001 | 0,0000 | 0,0004 | 0,0000 | 0,0000 | 0,0002 | 0,0000 | 0,0005 |
| Metabolism | Enzyme Families | Peptidases | 1,4152 | 1,3429 | 1,4101 | 1,4870 | 1,3097 | 1,6304 | 1,4585 | 1,2981 |
| Metabolism | Enzyme Families | Protein kinases | 0,3670 | 0,3132 | 0,3344 | 0,2783 | 0,2827 | 0,1153 | 0,4180 | 0,3235 |
| Metabolism | Glycan Biosynthesis and Metabolism | Glycosaminoglycan biosynthesis - chondroitin sulfate | 0,0000 | 0,0000 | 0,0000 | 0,0000 | 0,0000 | 0,0000 | 0,0000 | 0,0000 |
| Metabolism | Glycan Biosynthesis and Metabolism | Glycosaminoglycan biosynthesis - heparan sulfate | 0,0000 | 0,0000 | 0,0000 | 0,0000 | 0,0000 | 0,0000 | 0,0000 | 0,0000 |
| Metabolism | Glycan Biosynthesis and Metabolism | Glycosaminoglycan degradation | 0,0137 | 0,0475 | 0,0193 | 0,0420 | 0,0229 | 0,0628 | 0,0314 | 0,0108 |
| Metabolism | Glycan Biosynthesis and Metabolism | Glycosphingolipid biosynthesis - ganglio series | 0,0009 | 0,0034 | 0,0020 | 0,0245 | 0,0173 | 0,0316 | 0,0047 | 0,0019 |
| Metabolism | Glycan Biosynthesis and Metabolism | Glycosphingolipid biosynthesis - globo series | 0,0079 | 0,0140 | 0,0182 | 0,0459 | 0,0341 | 0,0325 | 0,0083 | 0,0081 |
| Metabolism | Glycan Biosynthesis and Metabolism | Glycosphingolipid biosynthesis - lacto and neolacto series | 0,0000 | 0,0000 | 0,0000 | 0,0000 | 0,0000 | 0,0000 | 0,0000 | 0,0000 |
| Metabolism | Glycan Biosynthesis and Metabolism | Glycosylphosphatidylinositol(GPI)-anchor biosynthesis | 0,0089 | 0,0019 | 0,0029 | 0,0008 | 0,0000 | 0,0000 | 0,0002 | 0,0000 |
| Metabolism | Glycan Biosynthesis and Metabolism | Glycosyltransferases | 0,4314 | 0,3733 | 0,4366 | 0,3594 | 0,3121 | 0,3741 | 0,3511 | 0,2934 |
| Metabolism | Glycan Biosynthesis and Metabolism | Lipopolysaccharide biosynthesis | 0,5610 | 0,5123 | 0,5335 | 0,4284 | 0,3121 | 0,4486 | 0,5187 | 0,2956 |
| Metabolism | Glycan Biosynthesis and Metabolism | Lipopolysaccharide biosynthesis proteins | 0,6768 | 0,5988 | 0,6427 | 0,5271 | 0,3920 | 0,5507 | 0,6082 | 0,3619 |
| Metabolism | Glycan Biosynthesis and Metabolism | N-Glycan biosynthesis | 0,0355 | 0,0408 | 0,0442 | 0,0357 | 0,0332 | 0,0323 | 0,0329 | 0,0114 |
| Metabolism | Glycan Biosynthesis and Metabolism | Other glycan degradation | 0,0120 | 0,0268 | 0,0242 | 0,0945 | 0,0635 | 0,1882 | 0,0207 | 0,0262 |
| Metabolism | Glycan Biosynthesis and Metabolism | Other types of O-glycan biosynthesis | 0,0057 | 0,0016 | 0,0049 | 0,0018 | 0,0000 | 0,0000 | 0,0000 | 0,0000 |

| | | | | | | | | | | |
|------------|--------------------------------------|--|--------|--------|--------|--------|--------|--------|--------|--------|
| Metabolism | Glycan Biosynthesis and Metabolism | Peptidoglycan biosynthesis | 0,6444 | 0,6138 | 0,6449 | 0,6663 | 0,5504 | 0,6390 | 0,6177 | 0,4995 |
| Metabolism | Glycan Biosynthesis and Metabolism | Various types of N-glycan biosynthesis | 0,0001 | 0,0005 | 0,0012 | 0,0038 | 0,0056 | 0,0002 | 0,0048 | 0,0000 |
| Metabolism | Lipid Metabolism | Arachidonic acid metabolism | 0,0572 | 0,0592 | 0,0483 | 0,0540 | 0,0720 | 0,0744 | 0,0698 | 0,0960 |
| Metabolism | Lipid Metabolism | Biosynthesis of unsaturated fatty acids | 0,2721 | 0,2650 | 0,2679 | 0,3121 | 0,2958 | 0,2930 | 0,3166 | 0,3345 |
| Metabolism | Lipid Metabolism | Ether lipid metabolism | 0,0084 | 0,0051 | 0,0109 | 0,0143 | 0,0182 | 0,0008 | 0,0048 | 0,0252 |
| Metabolism | Lipid Metabolism | Fatty acid biosynthesis | 0,5446 | 0,6111 | 0,5763 | 0,6144 | 0,5378 | 0,7288 | 0,5581 | 0,4673 |
| Metabolism | Lipid Metabolism | Fatty acid elongation in mitochondria | 0,0089 | 0,0211 | 0,0139 | 0,0158 | 0,0290 | 0,0333 | 0,0162 | 0,0311 |
| Metabolism | Lipid Metabolism | Fatty acid metabolism | 0,8439 | 0,8754 | 0,9024 | 0,9009 | 1,1074 | 0,6204 | 0,7577 | 1,1756 |
| Metabolism | Lipid Metabolism | Glycerolipid metabolism | 0,2919 | 0,2818 | 0,3047 | 0,3136 | 0,3233 | 0,2706 | 0,2879 | 0,3132 |
| Metabolism | Lipid Metabolism | Glycerophospholipid metabolism | 0,5293 | 0,5123 | 0,5141 | 0,4831 | 0,4616 | 0,3855 | 0,5512 | 0,4497 |
| Metabolism | Lipid Metabolism | Linoleic acid metabolism | 0,0578 | 0,0831 | 0,0731 | 0,0941 | 0,0827 | 0,1667 | 0,0951 | 0,0852 |
| Metabolism | Lipid Metabolism | Lipid biosynthesis proteins | 0,8850 | 0,8437 | 0,8927 | 0,8713 | 0,8448 | 0,7957 | 0,7805 | 0,7464 |
| Metabolism | Lipid Metabolism | Primary bile acid biosynthesis | 0,0116 | 0,0101 | 0,0127 | 0,0146 | 0,0168 | 0,0022 | 0,0081 | 0,0065 |
| Metabolism | Lipid Metabolism | Secondary bile acid biosynthesis | 0,0041 | 0,0053 | 0,0049 | 0,0053 | 0,0093 | 0,0015 | 0,0047 | 0,0003 |
| Metabolism | Lipid Metabolism | Sphingolipid metabolism | 0,0515 | 0,1149 | 0,0758 | 0,1075 | 0,0701 | 0,0960 | 0,0656 | 0,0468 |
| Metabolism | Lipid Metabolism | Steroid biosynthesis | 0,0289 | 0,0233 | 0,0242 | 0,0148 | 0,0079 | 0,0014 | 0,0122 | 0,0005 |
| Metabolism | Lipid Metabolism | Steroid hormone biosynthesis | 0,0247 | 0,0450 | 0,0330 | 0,0424 | 0,0360 | 0,0023 | 0,0285 | 0,0252 |
| Metabolism | Lipid Metabolism | Synthesis and degradation of ketone bodies | 0,1382 | 0,1457 | 0,1544 | 0,1800 | 0,1981 | 0,2156 | 0,1301 | 0,2226 |
| Metabolism | Lipid Metabolism | alpha-Linolenic acid metabolism | 0,0442 | 0,0384 | 0,0500 | 0,0527 | 0,0491 | 0,0997 | 0,0623 | 0,0654 |
| Metabolism | Metabolism of Cofactors and Vitamins | Biotin metabolism | 0,2030 | 0,1832 | 0,1913 | 0,1647 | 0,1168 | 0,4240 | 0,1967 | 0,0811 |
| Metabolism | Metabolism of Cofactors and Vitamins | Folate biosynthesis | 0,4821 | 0,4694 | 0,4649 | 0,4898 | 0,3939 | 0,5586 | 0,5091 | 0,3832 |
| Metabolism | Metabolism of Cofactors and Vitamins | Lipoic acid metabolism | 0,0651 | 0,0683 | 0,0651 | 0,0674 | 0,0631 | 0,0706 | 0,0631 | 0,0527 |
| Metabolism | Metabolism of Cofactors and Vitamins | Nicotinate and nicotinamide metabolism | 0,4258 | 0,4177 | 0,4043 | 0,3818 | 0,3925 | 0,4004 | 0,3992 | 0,4186 |
| Metabolism | Metabolism of Cofactors and | One carbon pool by folate | 0,5215 | 0,5412 | 0,5274 | 0,5491 | 0,4920 | 0,6014 | 0,5503 | 0,4790 |

| | | | | | | | | | | |
|------------|--------------------------------------|---|--------|--------|--------|--------|--------|--------|--------|--------|
| | Vitamins | | | | | | | | | |
| Metabolism | Metabolism of Cofactors and Vitamins | Pantothenate and CoA biosynthesis | 0,5639 | 0,5787 | 0,5775 | 0,5595 | 0,5486 | 0,5425 | 0,5078 | 0,5301 |
| Metabolism | Metabolism of Cofactors and Vitamins | Porphyrin and chlorophyll metabolism | 0,9564 | 0,9924 | 0,9231 | 0,8413 | 0,9135 | 0,6591 | 0,8898 | 0,9179 |
| Metabolism | Metabolism of Cofactors and Vitamins | Retinol metabolism | 0,0812 | 0,1091 | 0,0920 | 0,0905 | 0,1182 | 0,1131 | 0,0996 | 0,1466 |
| Metabolism | Metabolism of Cofactors and Vitamins | Riboflavin metabolism | 0,2931 | 0,2999 | 0,2910 | 0,2699 | 0,2575 | 0,2863 | 0,2977 | 0,2699 |
| Metabolism | Metabolism of Cofactors and Vitamins | Thiamine metabolism | 0,4002 | 0,4091 | 0,4065 | 0,3272 | 0,3892 | 0,3373 | 0,3726 | 0,3218 |
| Metabolism | Metabolism of Cofactors and Vitamins | Ubiquinone and other terpenoid-quinone biosynthesis | 0,3287 | 0,2952 | 0,3101 | 0,3032 | 0,2495 | 0,3527 | 0,3406 | 0,2837 |
| Metabolism | Metabolism of Cofactors and Vitamins | Vitamin B6 metabolism | 0,1450 | 0,1662 | 0,1516 | 0,1647 | 0,1500 | 0,2103 | 0,1700 | 0,1655 |
| Metabolism | Metabolism of Other Amino Acids | Cyanoamino acid metabolism | 0,1563 | 0,1528 | 0,1712 | 0,2114 | 0,2425 | 0,3092 | 0,1721 | 0,2096 |
| Metabolism | Metabolism of Other Amino Acids | D-Alanine metabolism | 0,0970 | 0,0866 | 0,0889 | 0,0860 | 0,0850 | 0,0721 | 0,0948 | 0,0849 |
| Metabolism | Metabolism of Other Amino Acids | D-Arginine and D-ornithine metabolism | 0,0167 | 0,0128 | 0,0123 | 0,0101 | 0,0140 | 0,0014 | 0,0231 | 0,0241 |
| Metabolism | Metabolism of Other Amino Acids | D-Glutamine and D-glutamate metabolism | 0,1079 | 0,1061 | 0,1139 | 0,1249 | 0,1089 | 0,2016 | 0,1159 | 0,0949 |
| Metabolism | Metabolism of Other Amino Acids | Glutathione metabolism | 0,3588 | 0,4293 | 0,3373 | 0,3773 | 0,4467 | 0,3705 | 0,4654 | 0,5433 |
| Metabolism | Metabolism of Other Amino Acids | Phosphonate and phosphinate metabolism | 0,0239 | 0,0566 | 0,0326 | 0,0610 | 0,0766 | 0,0376 | 0,0542 | 0,0641 |
| Metabolism | Metabolism of Other Amino Acids | Selenocompound metabolism | 0,3319 | 0,3427 | 0,3430 | 0,4298 | 0,3341 | 0,5193 | 0,3399 | 0,2723 |
| Metabolism | Metabolism of Other Amino Acids | Taurine and hypotaurine metabolism | 0,1312 | 0,1423 | 0,1196 | 0,1456 | 0,1729 | 0,1114 | 0,1337 | 0,2115 |

| | | | | | | | | | | |
|------------|--|---|--------|--------|--------|--------|--------|--------|--------|--------|
| Metabolism | Metabolism of Other Amino Acids | beta-Alanine metabolism | 0,4695 | 0,5056 | 0,5159 | 0,5405 | 0,7013 | 0,3332 | 0,4747 | 0,7316 |
| Metabolism | Metabolism of Terpenoids and Polyketides | Biosynthesis of 12-, 14- and 16-membered macrolides | 0,0043 | 0,0016 | 0,0049 | 0,0018 | 0,0000 | 0,0001 | 0,0000 | 0,0000 |
| Metabolism | Metabolism of Terpenoids and Polyketides | Biosynthesis of ansamycins | 0,0637 | 0,0704 | 0,0702 | 0,0521 | 0,0533 | 0,0721 | 0,0532 | 0,0498 |
| Metabolism | Metabolism of Terpenoids and Polyketides | Biosynthesis of siderophore group nonribosomal peptides | 0,0147 | 0,0126 | 0,0203 | 0,0324 | 0,0383 | 0,0421 | 0,0198 | 0,0103 |
| Metabolism | Metabolism of Terpenoids and Polyketides | Biosynthesis of type II polyketide backbone | 0,0003 | 0,0010 | 0,0004 | 0,0044 | 0,0079 | 0,0000 | 0,0036 | 0,0076 |
| Metabolism | Metabolism of Terpenoids and Polyketides | Biosynthesis of type II polyketide products | 0,0000 | 0,0002 | 0,0000 | 0,0000 | 0,0000 | 0,0000 | 0,0003 | 0,0003 |
| Metabolism | Metabolism of Terpenoids and Polyketides | Biosynthesis of vancomycin group antibiotics | 0,0680 | 0,0614 | 0,0688 | 0,0630 | 0,0449 | 0,0662 | 0,0466 | 0,0262 |
| Metabolism | Metabolism of Terpenoids and Polyketides | Carotenoid biosynthesis | 0,0372 | 0,0313 | 0,0336 | 0,0423 | 0,0294 | 0,0956 | 0,0242 | 0,0211 |
| Metabolism | Metabolism of Terpenoids and Polyketides | Geraniol degradation | 0,3940 | 0,4273 | 0,4485 | 0,4828 | 0,5789 | 0,4340 | 0,4184 | 0,6566 |
| Metabolism | Metabolism of Terpenoids and Polyketides | Limonene and pinene degradation | 0,3897 | 0,4462 | 0,4465 | 0,5061 | 0,5953 | 0,7269 | 0,4504 | 0,6772 |
| Metabolism | Metabolism of Terpenoids and Polyketides | Polyketide sugar unit biosynthesis | 0,1730 | 0,1709 | 0,1765 | 0,1741 | 0,1201 | 0,2301 | 0,1389 | 0,0803 |
| Metabolism | Metabolism of Terpenoids and Polyketides | Prenyltransferases | 0,3790 | 0,3409 | 0,3557 | 0,3157 | 0,2607 | 0,2572 | 0,3101 | 0,2293 |
| Metabolism | Metabolism of Terpenoids and Polyketides | Sesquiterpenoid biosynthesis | 0,0000 | 0,0000 | 0,0000 | 0,0000 | 0,0000 | 0,0000 | 0,0000 | 0,0000 |
| Metabolism | Metabolism of Terpenoids and Polyketides | Terpenoid backbone biosynthesis | 0,5890 | 0,5484 | 0,5941 | 0,5180 | 0,4995 | 0,3807 | 0,5001 | 0,4500 |
| Metabolism | Metabolism of Terpenoids and Polyketides | Tetracycline biosynthesis | 0,1569 | 0,1675 | 0,1587 | 0,1719 | 0,1425 | 0,2099 | 0,1723 | 0,1431 |
| Metabolism | Metabolism of Terpenoids | Zeatin biosynthesis | 0,0347 | 0,0377 | 0,0352 | 0,0340 | 0,0280 | 0,0350 | 0,0347 | 0,0260 |

| | | | | | | | | | | |
|------------|---|---|--------|--------|--------|--------|--------|--------|--------|--------|
| | and Polyketides | | | | | | | | | |
| Metabolism | Nucleotide Metabolism | Purine metabolism | 1,9181 | 1,9038 | 1,9065 | 2,0164 | 1,8597 | 2,0126 | 2,0078 | 1,8669 |
| Metabolism | Nucleotide Metabolism | Pyrimidine metabolism | 1,3089 | 1,3635 | 1,3447 | 1,4889 | 1,2976 | 1,7997 | 1,4006 | 1,1775 |
| Metabolism | Xenobiotics Biodegradation and Metabolism | 1,1,1-Trichloro-2,2-bis(4-chlorophenyl)ethane (DDT) degradation | 0,0006 | 0,0014 | 0,0029 | 0,0222 | 0,0131 | 0,0625 | 0,0074 | 0,0160 |
| Metabolism | Xenobiotics Biodegradation and Metabolism | Aminobenzoate degradation | 0,3909 | 0,4118 | 0,4305 | 0,5046 | 0,6014 | 0,5728 | 0,3830 | 0,5990 |
| Metabolism | Xenobiotics Biodegradation and Metabolism | Atrazine degradation | 0,0601 | 0,0346 | 0,0453 | 0,0722 | 0,0892 | 0,1059 | 0,0455 | 0,0993 |
| Metabolism | Xenobiotics Biodegradation and Metabolism | Benzoate degradation | 0,4877 | 0,5147 | 0,5595 | 0,6407 | 0,7621 | 0,7149 | 0,4340 | 0,7234 |
| Metabolism | Xenobiotics Biodegradation and Metabolism | Bisphenol degradation | 0,1235 | 0,1597 | 0,1444 | 0,2305 | 0,1850 | 0,3645 | 0,1916 | 0,2126 |
| Metabolism | Xenobiotics Biodegradation and Metabolism | Caprolactam degradation | 0,2786 | 0,3001 | 0,3136 | 0,3020 | 0,3934 | 0,1647 | 0,2703 | 0,4419 |
| Metabolism | Xenobiotics Biodegradation and Metabolism | Chloroalkane and chloroalkene degradation | 0,2576 | 0,3647 | 0,2923 | 0,3120 | 0,3747 | 0,4265 | 0,3436 | 0,4384 |
| Metabolism | Xenobiotics Biodegradation and Metabolism | Chlorocyclohexane and chlorobenzene degradation | 0,0600 | 0,0796 | 0,0682 | 0,1120 | 0,1420 | 0,1049 | 0,0752 | 0,1431 |
| Metabolism | Xenobiotics Biodegradation and Metabolism | Dioxin degradation | 0,0209 | 0,0332 | 0,0250 | 0,0418 | 0,0678 | 0,0053 | 0,0230 | 0,0306 |
| Metabolism | Xenobiotics | Drug metabolism - cytochrome P450 | 0,1318 | 0,2159 | 0,1423 | 0,1516 | 0,2514 | 0,1237 | 0,2128 | 0,3594 |

| | | | | | | | | | | |
|------------|---|--|--------|--------|--------|--------|--------|--------|--------|--------|
| | Biodegradation and Metabolism | | | | | | | | | |
| Metabolism | Xenobiotics Biodegradation and Metabolism | Drug metabolism - other enzymes | 0,1597 | 0,1658 | 0,1747 | 0,2352 | 0,2397 | 0,3471 | 0,1976 | 0,2653 |
| Metabolism | Xenobiotics Biodegradation and Metabolism | Ethylbenzene degradation | 0,0885 | 0,0991 | 0,1079 | 0,1364 | 0,1280 | 0,3303 | 0,1015 | 0,1241 |
| Metabolism | Xenobiotics Biodegradation and Metabolism | Fluorobenzoate degradation | 0,0418 | 0,0429 | 0,0436 | 0,0547 | 0,0720 | 0,0390 | 0,0389 | 0,0617 |
| Metabolism | Xenobiotics Biodegradation and Metabolism | Metabolism of xenobiotics by cytochrome P450 | 0,1253 | 0,2090 | 0,1346 | 0,1457 | 0,2364 | 0,1223 | 0,2100 | 0,3294 |
| Metabolism | Xenobiotics Biodegradation and Metabolism | Naphthalene degradation | 0,2306 | 0,3074 | 0,2708 | 0,3420 | 0,3944 | 0,6149 | 0,2962 | 0,4089 |
| Metabolism | Xenobiotics Biodegradation and Metabolism | Nitrotoluene degradation | 0,1843 | 0,1474 | 0,1796 | 0,1271 | 0,1420 | 0,0714 | 0,0861 | 0,1417 |
| Metabolism | Xenobiotics Biodegradation and Metabolism | Polycyclic aromatic hydrocarbon degradation | 0,1005 | 0,1466 | 0,1368 | 0,1749 | 0,1911 | 0,3374 | 0,1427 | 0,2199 |
| Metabolism | Xenobiotics Biodegradation and Metabolism | Styrene degradation | 0,0669 | 0,0670 | 0,0676 | 0,1032 | 0,1336 | 0,1107 | 0,0686 | 0,1166 |
| Metabolism | Xenobiotics Biodegradation and Metabolism | Toluene degradation | 0,1895 | 0,1817 | 0,1931 | 0,2219 | 0,2159 | 0,1484 | 0,2006 | 0,1993 |
| Metabolism | Xenobiotics Biodegradation and Metabolism | Xylene degradation | 0,0166 | 0,0233 | 0,0184 | 0,0461 | 0,0458 | 0,0031 | 0,0185 | 0,0208 |

| | Metabolism | | | | | | | | | |
|--------------------|--------------------------|---|--------|--------|--------|--------|--------|--------|--------|--------|
| Organismal Systems | Circulatory System | Cardiac muscle contraction | 0,0536 | 0,0645 | 0,0469 | 0,0473 | 0,0509 | 0,0088 | 0,0936 | 0,0773 |
| Organismal Systems | Circulatory System | Vascular smooth muscle contraction | 0,0000 | 0,0000 | 0,0000 | 0,0000 | 0,0000 | 0,0000 | 0,0000 | 0,0000 |
| Organismal Systems | Development | Axon guidance | 0,0000 | 0,0000 | 0,0000 | 0,0000 | 0,0000 | 0,0000 | 0,0000 | 0,0000 |
| Organismal Systems | Digestive System | Bile secretion | 0,0016 | 0,0040 | 0,0010 | 0,0051 | 0,0093 | 0,0001 | 0,0030 | 0,0097 |
| Organismal Systems | Digestive System | Carbohydrate digestion and absorption | 0,0084 | 0,0072 | 0,0072 | 0,0125 | 0,0075 | 0,0327 | 0,0033 | 0,0014 |
| Organismal Systems | Digestive System | Fat digestion and absorption | 0,0000 | 0,0000 | 0,0000 | 0,0000 | 0,0000 | 0,0000 | 0,0000 | 0,0000 |
| Organismal Systems | Digestive System | Gastric acid secretion | 0,0006 | 0,0019 | 0,0000 | 0,0002 | 0,0000 | 0,0000 | 0,0000 | 0,0000 |
| Organismal Systems | Digestive System | Mineral absorption | 0,0049 | 0,0048 | 0,0043 | 0,0022 | 0,0103 | 0,0015 | 0,0032 | 0,0162 |
| Organismal Systems | Digestive System | Pancreatic secretion | 0,0006 | 0,0019 | 0,0000 | 0,0002 | 0,0000 | 0,0000 | 0,0000 | 0,0000 |
| Organismal Systems | Digestive System | Protein digestion and absorption | 0,0022 | 0,0045 | 0,0043 | 0,0213 | 0,0028 | 0,0316 | 0,0125 | 0,0095 |
| Organismal Systems | Digestive System | Salivary secretion | 0,0006 | 0,0019 | 0,0000 | 0,0002 | 0,0000 | 0,0000 | 0,0000 | 0,0000 |
| Organismal Systems | Endocrine System | Adipocytokine signaling pathway | 0,1250 | 0,0892 | 0,1255 | 0,0996 | 0,1028 | 0,0406 | 0,0605 | 0,0673 |
| Organismal Systems | Endocrine System | GnRH signaling pathway | 0,0005 | 0,0026 | 0,0018 | 0,0019 | 0,0061 | 0,0005 | 0,0030 | 0,0243 |
| Organismal Systems | Endocrine System | Insulin signaling pathway | 0,0814 | 0,0578 | 0,0766 | 0,0571 | 0,0430 | 0,0346 | 0,0734 | 0,0435 |
| Organismal Systems | Endocrine System | Melanogenesis | 0,0000 | 0,0000 | 0,0000 | 0,0000 | 0,0000 | 0,0000 | 0,0000 | 0,0000 |
| Organismal Systems | Endocrine System | PPAR signaling pathway | 0,2411 | 0,2131 | 0,2519 | 0,2377 | 0,2668 | 0,0875 | 0,1757 | 0,2283 |
| Organismal Systems | Endocrine System | Progesterone-mediated oocyte maturation | 0,0247 | 0,0187 | 0,0217 | 0,0236 | 0,0136 | 0,0340 | 0,0275 | 0,0097 |
| Organismal Systems | Endocrine System | Renin-angiotensin system | 0,0006 | 0,0013 | 0,0012 | 0,0005 | 0,0009 | 0,0000 | 0,0060 | 0,0089 |
| Organismal Systems | Environmental Adaptation | Circadian rhythm - mammal | 0,0000 | 0,0000 | 0,0000 | 0,0000 | 0,0000 | 0,0000 | 0,0000 | 0,0000 |
| Organismal Systems | Environmental Adaptation | Circadian rhythm - plant | 0,0028 | 0,0027 | 0,0051 | 0,0039 | 0,0107 | 0,0322 | 0,0039 | 0,0000 |
| Organismal Systems | Environmental Adaptation | Plant-pathogen interaction | 0,1555 | 0,1567 | 0,1497 | 0,1331 | 0,1191 | 0,0812 | 0,1457 | 0,1320 |
| Organismal Systems | Excretory System | Aldosterone-regulated sodium reabsorption | 0,0050 | 0,0035 | 0,0049 | 0,0019 | 0,0000 | 0,0000 | 0,0000 | 0,0000 |
| Organismal Systems | Excretory System | Endocrine and other factor-regulated calcium reabsorption | 0,0006 | 0,0019 | 0,0000 | 0,0002 | 0,0000 | 0,0000 | 0,0000 | 0,0000 |
| Organismal Systems | Excretory System | Proximal tubule bicarbonate reclamation | 0,0286 | 0,0308 | 0,0250 | 0,0279 | 0,0346 | 0,0661 | 0,0234 | 0,0419 |
| Organismal Systems | Excretory System | Vasopressin-regulated water reabsorption | 0,0023 | 0,0024 | 0,0008 | 0,0037 | 0,0033 | 0,0002 | 0,0008 | 0,0005 |
| Organismal Systems | Immune System | Antigen processing and presentation | 0,0247 | 0,0187 | 0,0217 | 0,0236 | 0,0136 | 0,0340 | 0,0275 | 0,0097 |
| Organismal Systems | Immune System | Complement and coagulation cascades | 0,0000 | 0,0000 | 0,0000 | 0,0000 | 0,0000 | 0,0000 | 0,0000 | 0,0000 |
| Organismal Systems | Immune System | Cytosolic DNA-sensing pathway | 0,0000 | 0,0000 | 0,0000 | 0,0000 | 0,0000 | 0,0000 | 0,0000 | 0,0000 |

| | | | | | | | | | | |
|--------------------|----------------------------------|---|--------|--------|--------|--------|--------|--------|--------|--------|
| Organismal Systems | Immune System | Fc epsilon RI signaling pathway | 0,0000 | 0,0000 | 0,0000 | 0,0000 | 0,0000 | 0,0000 | 0,0000 | 0,0000 |
| Organismal Systems | Immune System | Fc gamma R-mediated phagocytosis | 0,0005 | 0,0026 | 0,0018 | 0,0019 | 0,0061 | 0,0005 | 0,0030 | 0,0243 |
| Organismal Systems | Immune System | Hematopoietic cell lineage | 0,0000 | 0,0000 | 0,0000 | 0,0000 | 0,0000 | 0,0000 | 0,0000 | 0,0000 |
| Organismal Systems | Immune System | Leukocyte transendothelial migration | 0,0000 | 0,0000 | 0,0000 | 0,0000 | 0,0000 | 0,0000 | 0,0000 | 0,0000 |
| Organismal Systems | Immune System | NOD-like receptor signaling pathway | 0,0247 | 0,0187 | 0,0217 | 0,0237 | 0,0136 | 0,0340 | 0,0275 | 0,0103 |
| Organismal Systems | Immune System | RIG-I-like receptor signaling pathway | 0,0001 | 0,0003 | 0,0008 | 0,0012 | 0,0065 | 0,0016 | 0,0006 | 0,0011 |
| Organismal Systems | Nervous System | Cholinergic synapse | 0,0000 | 0,0000 | 0,0000 | 0,0000 | 0,0000 | 0,0000 | 0,0000 | 0,0000 |
| Organismal Systems | Nervous System | Glutamatergic synapse | 0,0627 | 0,0806 | 0,0705 | 0,0813 | 0,1009 | 0,1066 | 0,0829 | 0,1390 |
| Organismal Systems | Nervous System | Long-term depression | 0,0000 | 0,0000 | 0,0000 | 0,0000 | 0,0000 | 0,0000 | 0,0000 | 0,0000 |
| Organismal Systems | Nervous System | Long-term potentiation | 0,0000 | 0,0000 | 0,0000 | 0,0000 | 0,0000 | 0,0000 | 0,0000 | 0,0000 |
| Organismal Systems | Nervous System | Neurotrophin signaling pathway | 0,0000 | 0,0000 | 0,0000 | 0,0000 | 0,0000 | 0,0000 | 0,0000 | 0,0000 |
| Organismal Systems | Sensory System | Olfactory transduction | 0,0000 | 0,0000 | 0,0000 | 0,0000 | 0,0000 | 0,0000 | 0,0000 | 0,0000 |
| Organismal Systems | Sensory System | Phototransduction | 0,0000 | 0,0000 | 0,0000 | 0,0000 | 0,0000 | 0,0000 | 0,0000 | 0,0000 |
| Organismal Systems | Sensory System | Phototransduction - fly | 0,0000 | 0,0000 | 0,0000 | 0,0000 | 0,0000 | 0,0000 | 0,0000 | 0,0000 |
| Unclassified | Cellular Processes and Signaling | Cell division | 0,0887 | 0,0932 | 0,0801 | 0,0704 | 0,0607 | 0,0687 | 0,0806 | 0,0773 |
| Unclassified | Cellular Processes and Signaling | Cell motility and secretion | 0,3765 | 0,3587 | 0,3488 | 0,2679 | 0,2224 | 0,2147 | 0,3322 | 0,2337 |
| Unclassified | Cellular Processes and Signaling | Electron transfer carriers | 0,0676 | 0,0533 | 0,0662 | 0,0488 | 0,0551 | 0,0054 | 0,0206 | 0,0557 |
| Unclassified | Cellular Processes and Signaling | Germination | 0,0001 | 0,0000 | 0,0014 | 0,0001 | 0,0280 | 0,0157 | 0,0002 | 0,0000 |
| Unclassified | Cellular Processes and Signaling | Inorganic ion transport and metabolism | 0,3648 | 0,4006 | 0,3557 | 0,3897 | 0,3551 | 0,3311 | 0,4283 | 0,4308 |
| Unclassified | Cellular Processes and Signaling | Membrane and intracellular structural molecules | 0,8182 | 0,7526 | 0,7125 | 0,6745 | 0,6014 | 0,6573 | 0,8590 | 0,7426 |
| Unclassified | Cellular Processes and Signaling | Other ion-coupled transporters | 0,9446 | 0,9089 | 0,9310 | 0,9712 | 0,9742 | 1,2714 | 1,0478 | 1,0372 |
| Unclassified | Cellular Processes and Signaling | Other transporters | 0,2483 | 0,2143 | 0,2370 | 0,2099 | 0,2126 | 0,2777 | 0,2558 | 0,2118 |
| Unclassified | Cellular Processes and Signaling | Pores ion channels | 0,5956 | 0,4858 | 0,5249 | 0,4764 | 0,3841 | 0,6508 | 0,6389 | 0,5141 |

| | | | | | | | | | | |
|--------------|----------------------------------|--|--------|--------|--------|--------|--------|--------|--------|--------|
| | Signaling | | | | | | | | | |
| Unclassified | Cellular Processes and Signaling | Signal transduction mechanisms | 0,5981 | 0,4059 | 0,5005 | 0,4231 | 0,2990 | 0,4638 | 0,4749 | 0,4584 |
| Unclassified | Cellular Processes and Signaling | Sporulation | 0,0481 | 0,0239 | 0,0563 | 0,0324 | 0,1486 | 0,0635 | 0,0221 | 0,0095 |
| Unclassified | Genetic Information Processing | Protein folding and associated processing | 1,0307 | 0,8607 | 0,9337 | 0,8861 | 0,8037 | 0,8883 | 0,8910 | 0,8835 |
| Unclassified | Genetic Information Processing | Replication, recombination and repair proteins | 0,8231 | 0,7481 | 0,7549 | 0,6443 | 0,7228 | 0,7312 | 0,6308 | 0,6664 |
| Unclassified | Genetic Information Processing | Restriction enzyme | 0,2195 | 0,1388 | 0,1866 | 0,1211 | 0,0453 | 0,3159 | 0,1464 | 0,0381 |
| Unclassified | Genetic Information Processing | Transcription related proteins | 0,0058 | 0,0073 | 0,0039 | 0,0036 | 0,0056 | 0,0018 | 0,0011 | 0,0108 |
| Unclassified | Genetic Information Processing | Translation proteins | 0,8131 | 0,7586 | 0,7889 | 0,7777 | 0,6415 | 0,8807 | 0,8305 | 0,6574 |
| Unclassified | Metabolism | Amino acid metabolism | 0,3112 | 0,2952 | 0,3078 | 0,2735 | 0,2682 | 0,3834 | 0,2733 | 0,2842 |
| Unclassified | Metabolism | Biosynthesis and biodegradation of secondary metabolites | 0,0445 | 0,0456 | 0,0506 | 0,0600 | 0,0673 | 0,0737 | 0,0758 | 0,0892 |
| Unclassified | Metabolism | Carbohydrate metabolism | 0,0913 | 0,0858 | 0,0838 | 0,0682 | 0,0785 | 0,1066 | 0,0638 | 0,1071 |
| Unclassified | Metabolism | Energy metabolism | 0,9523 | 0,8965 | 0,9269 | 0,9331 | 0,7836 | 0,8825 | 0,9613 | 0,9252 |
| Unclassified | Metabolism | Glycan biosynthesis and metabolism | 0,0926 | 0,0751 | 0,0846 | 0,0698 | 0,0617 | 0,0380 | 0,0833 | 0,0768 |
| Unclassified | Metabolism | Lipid metabolism | 0,0999 | 0,1024 | 0,1010 | 0,0843 | 0,0841 | 0,0780 | 0,0832 | 0,1117 |
| Unclassified | Metabolism | Metabolism of cofactors and vitamins | 0,2393 | 0,2085 | 0,2206 | 0,2432 | 0,1986 | 0,1893 | 0,2482 | 0,2426 |
| Unclassified | Metabolism | Nucleotide metabolism | 0,0291 | 0,0177 | 0,0283 | 0,0229 | 0,0075 | 0,0020 | 0,0215 | 0,0187 |
| Unclassified | Metabolism | Others | 0,9212 | 1,0029 | 1,0085 | 1,5291 | 1,2083 | 4,2271 | 1,1118 | 1,2105 |
| Unclassified | Poorly Characterized | Function unknown | 1,7350 | 1,4927 | 1,5989 | 1,5933 | 1,5485 | 1,6406 | 1,8226 | 1,8655 |
| Unclassified | Poorly Characterized | General function prediction only | 3,3816 | 3,1066 | 3,3610 | 3,5606 | 3,3212 | 3,6420 | 3,3555 | 3,0344 |
| | | | 100 | 100 | 100 | 100 | 100 | 100 | 100 | 100 |

Supplementary Table S5 Complete information for catabolic network reconstruction.

(A) In-house codes used for graphical visualization of degradation networks. As described in text, each query sequence from the metagenome that matches a given protein family of the AromaDeg²⁴ is associated to a key catabolic enzyme for an aromatic degradation reaction. Based on bibliographic records²⁴⁻²⁷, the substrates and intermediates products can be linked to form a biodegradation network²⁵⁻²⁷. For network reconstruction, each query sequence encoding a catabolic enzyme (with an in-house given “ec code”) was assigned to a degradation reaction involving a metabolic substrate and a product with appropriated in-house assigned codes (“sp” codes”). The codes were further used for the network reconstruction using appropriated scripts and commands described in the Supplementary Methods. Panel A also shows the relative abundance (rel. ab.) of genes encoding each of the catabolic enzymes (to avoid artifacts due to differences in sample size) as found in the DNA (used for creating Supplementary Fig. S2) or 16 rRNA (used for creating Supplementary Fig. S3) data sets. The total rel. ab. for the both previous data sets ($\Sigma_{\text{DNA+16SrRNA}}$) is also shown (used to create Fig. 3). The data sets (only for DNA sequences) regarding Deepwater OV11 and BM058 sites, are also shown. Note that in all cases, the absolute number of genes corresponding to each rel. ab. is also shown. Genes/enzymes name abbreviations, corresponding to those mentioned in the text, are shown in brackets in the column D “Enzyme”.

(B) List of substrate pollutants or intermediates possibly degraded by each of the communities herein examined, as inferred from the rel. ab. level (and absolute number, also shown) of genes encoding enzymes involved in their biodegradation in DNA (see Supplementary Fig. S2), 16S rRNA (Supplementary Fig. S3) and $\Sigma_{\text{DNA+16SrRNA}}$ (Fig. 3) data sets. Presumptive pollutants degraded by communities at Deepwater OV11 and BM058 sites (based on DNA data sets) are also shown. The total number of chemicals being potentially degraded by each of the communities, as well as the total number of ORF examined in each dataset, is shown at the bottom in the three datasets. Those pollutants from which validation were conducted are shown in shadowed grey color (column A, Panel B). The confidence value, that gives an estimation of the possibility that a given chemical is degraded, is also given, based on the data statistics reported in Supplementary Fig. S4.

The Table has been provided as a separate Excel table due to the extensive size. For raw data, please contact authors directly.

Supplementary Table S6 Data statistics for samples obtained by Illumina or 454 sequencing from the bacterial communities in the polluted sediments collected in the Mediterranean Sea and the Aqaba Gulf (Red Sea). For comparison data regarding samples at the Deepwater Horizon oil spill (panel E).

Supplementary Table S6A Raw sequencing data

| Sample name | Insert size (bp) | Sequence type (bp) | Raw reads (Mbp) | High quality reads (Mbp) | Clean data rate (%) |
|-------------|------------------|--------------------|-----------------|--------------------------|---------------------|
| MGS-HAV | 170 | Index 91 PE | 2,000 | 1,981 | 99.00 |
| MGS-MES | 170 | Index 91 PE | 2,000 | 1,982 | 99.00 |
| MGS-MCh | 170 | Index 91 PE | 2,000 | 1,982 | 99.00 |
| MGS-PRI | 170 | Index 91 PE | 2,000 | 1,981 | 99.00 |
| MGS-BIZ | 170 | Index 91 PE | 1,987 | 1,962 | 99.00 |
| | 350 | Index 91 PE | 1,266 | 1,100 | 86.88 |
| MGS-ELMAX | 170 | Index 91 PE | 1,584 | 1,420 | 89.64 |
| | 350 | Index 91 PE | 1,149 | 1,100 | 95.73 |
| MGS-AQ | 564 | 454 GS FLX Ti | 0.207 | 0.0517 | 24.98 |
| | 350 | Index 91 PE | 1,163 | 1,100 | 94.60 |

Supplementary Table S6B Data statistics for the best assembly results

| Sample name | Contig | Total bp | N50 | N90 | Max | Min | Map to own |
|-------------|--------|------------|--------|-----|---------|-----|------------|
| MGS-HAV | 4,412 | 5,426,170 | 1,611 | 574 | 66,436 | 500 | 3.29 |
| MGS-MES | 20,103 | 28,484,805 | 2,019 | 593 | 102,834 | 500 | 15.86 |
| MGS-MCh | 24,955 | 27,378,482 | 1,164 | 572 | 241,119 | 500 | 20.42 |
| MGS-PRI | 1,855 | 4,379,134 | 7,634 | 710 | 62,941 | 500 | 4.35 |
| MGS-BIZ | 16,792 | 16,779,454 | 1,034 | 558 | 50,777 | 500 | 6.76 |
| | 12,691 | 19,364,101 | 2,076 | 622 | 62,304 | 500 | 66.99 |
| MGS-ELMAX | 3,133 | 2,982,628 | 1,629 | 367 | 14,075 | 200 | 4.50 |
| | 12,814 | 20,253,283 | 2,117 | 667 | 73,362 | 500 | 77.39 |
| MGS-AQ | 11,041 | 15,528,589 | 1,888 | | 22,380 | 500 | 63.53 |
| | 8,371 | 21,504,196 | 12,101 | 753 | 273,210 | 500 | 86.23 |

Supplementary Table S6C Number of Open Reading Frames (ORF) and total assembled sequence

| Sample name | ORFs | Total length (bp) | Avg. length (bp) |
|-------------|--------|-------------------|------------------|
| MGS-HAV | 8,388 | 4,695,330 | 560.00 |
| MGS-MES | 40,077 | 25,562,526 | 638.00 |
| MGS-MCh | 44,522 | 24,811,614 | 557.00 |
| MGS-PRI | 5,858 | 3,872,385 | 661.00 |
| MGS-BIZ | 27,708 | 15,323,475 | 553.00 |
| | 27,893 | 17,270,982 | 619.19 |
| MGS-ELMAX | 3,481 | 2,346,126 | 674.00 |
| | 28,698 | 17,782,842 | 619.65 |
| MGS-AQ | 24,958 | 15,528,589 | 435.00 |
| | 26,866 | 19,154,985 | 712.98 |

Supplementary Table S6D Number of Open Reading Frames (ORF) with assigned function

| Sample name | ORFs | Assigned to COG | Assigned to KEGG | Nr of COG | Nr of KEGG |
|-------------------|--------|-----------------|------------------|-----------|------------|
| MGS-HAV | 8,388 | 4,500 | 3,797 | 1,990 | 1,719 |
| MGS-MES | 40,077 | 23,458 | 19,654 | 3,167 | 3,049 |
| MGS-MCh | 44,522 | 25,079 | 20,397 | 2,935 | 2,999 |
| MGS-PRI | 5,858 | 2,602 | 1,893 | 1,308 | 914 |
| MGS-BIZ (total) | 55,601 | 34,439 | 28,456 | 2,954 | 2,925 |
| MGS-ELMAX (total) | 32,179 | 41,869 | 38,223 | 3,125 | 3,245 |
| MGS-AQ (total) | 51,824 | 29,871 | 24,434 | 2,948 | 3,307 |

Supplementary Table S6E Number of Open Reading Frames (ORF) for samples BM058 (Longitude: -88.4375; Latitude: 28.672222; JGI project ID 403207; taxon IDs 2088090017 and 2081372002) and OV011 (Longitude: -88.4375; Latitude: 28.672222; JGI project ID 403191; taxon ID 2081372001) obtained from the Joint Genome Institute webpage (<https://img.jgi.doe.gov/>).

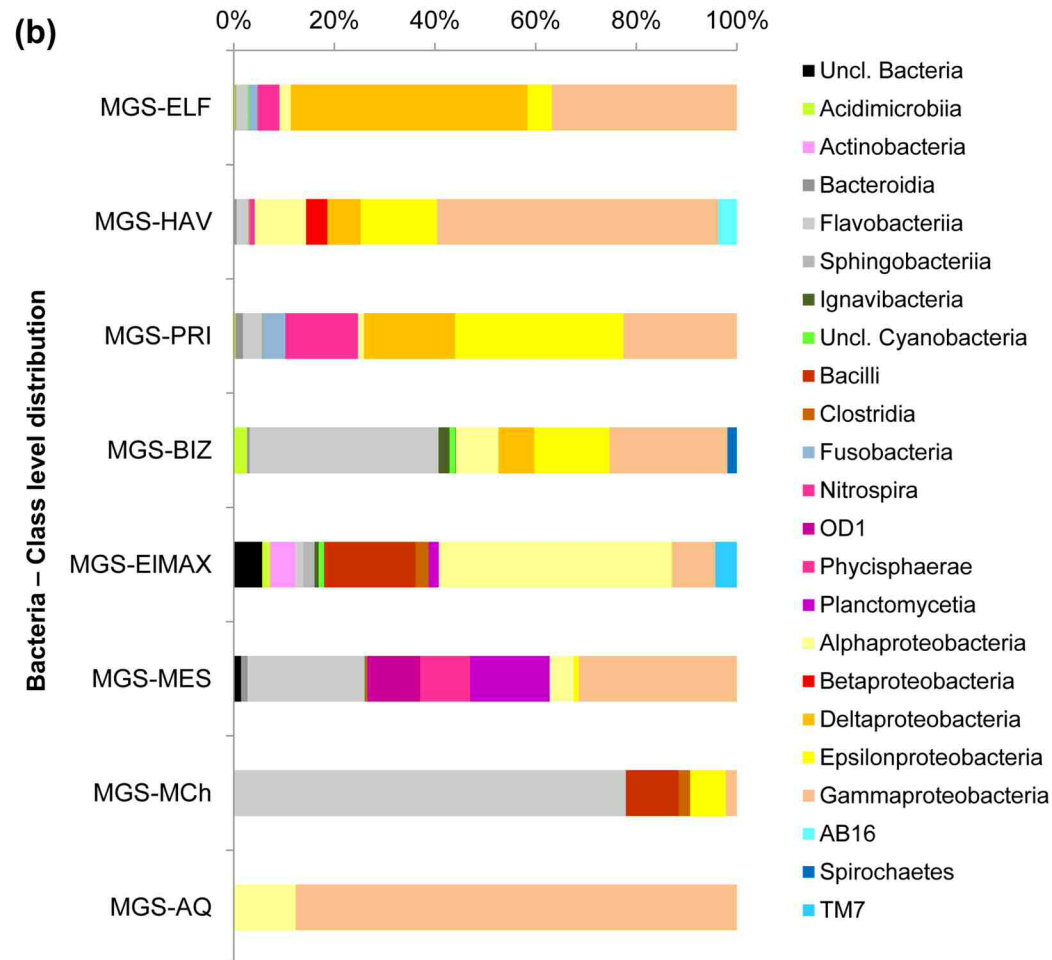
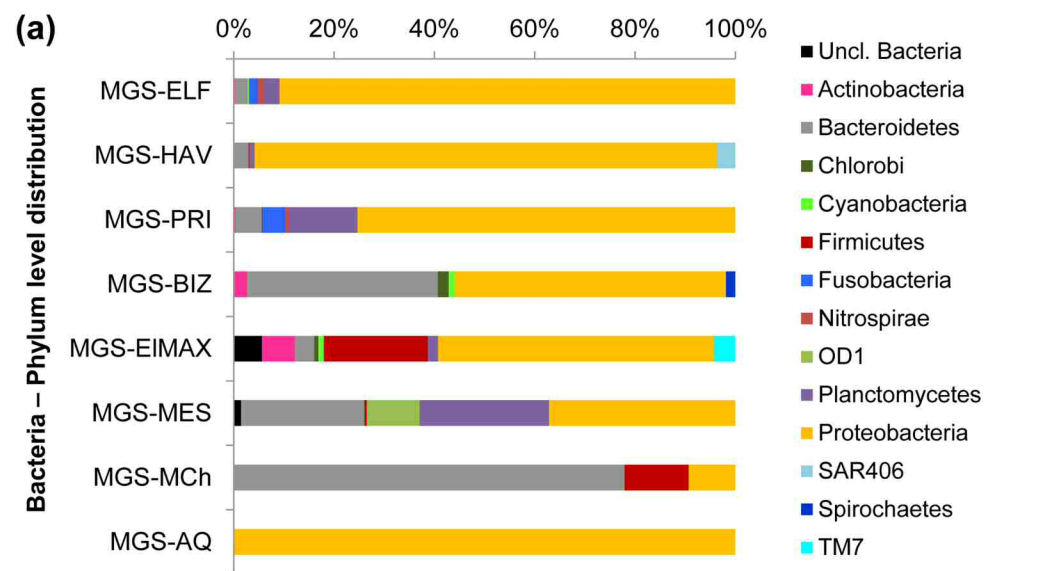
| Sample name | ORFs | Total length (bp) |
|-------------|--------|-------------------|
| BM058 | 83,920 | 50,620,616 |
| OV011 | 54,273 | 23,846,686 |

Supplementary Table S7 Metabolomic target data sets displaying the relative degradation of initial substrate pollutants (A) and the relative presence of key chemical intermediates (B), in the investigated enrichments. In panel A, the remaining relative concentration of the initial pollutants (referred to as “P” in the table) used to set up enrichment cultures is shown; 100%, no degradation of initial substrate pollutant; 0%, total degradation (absence of pollutant). In Panel B, values represent the area of the peak area (abbreviated as PA in the table) of key degradation intermediates (referred to as “I” in the table) in arbitrary units (a.u.), calculated on the basis of appropriate standards. The values were calculated, in triplicates per each of the duplicates sediment samples, by comparing the presence and abundance level after 3-weeks of the microcosm experiment compared to the initial point and after considering the controls assays. Standard deviations (SD) are shown.

| Panel A | | PRI | | HAV | | MES | | MCh | | BIZ | | ELMAX | | AQ | |
|---------------------------------|--|--------------|-------|--------------|-------|--------------|-------|--------------|-------|--------------|-------|--------------|-------|--------------|------|
| | | Rel. ab. (%) | SD | Rel. ab. (%) | SD | Rel. ab. (%) | SD | Rel. ab. (%) | SD | Rel. ab. (%) | SD | Rel. ab. (%) | SD | Rel. ab. (%) | SD |
| Benzoic acid (P) | | 100.00 | 0.00 | 36.17 | 7.03 | 10.86 | 1.60 | 44.96 | 4.78 | 21.85 | 4.61 | 22.49 | 11.75 | 5.24 | 3.83 |
| Chlorobenzoic acid (P) | | 100.00 | 0.00 | 100.00 | 0.00 | 47.24 | 3.79 | 100.00 | 0.00 | 50.30 | 2.41 | 38.12 | 6.59 | 7.30 | 2.19 |
| Nitrobenzoic acid (P) | | 62.14 | 5.01 | 69.61 | 5.16 | 16.91 | 0.37 | 28.18 | 2.45 | 51.50 | 2.86 | 26.07 | 1.77 | 4.77 | 0.77 |
| Hydroxybenzoic acid (P) | | 63.06 | 7.11 | 66.89 | 5.28 | 15.18 | 1.18 | 31.57 | 1.91 | 48.87 | 3.06 | 34.20 | 2.07 | 4.63 | 0.54 |
| Phthalic acid (P) | | 59.75 | 8.41 | 51.49 | 6.01 | 52.94 | 4.22 | 43.93 | 4.03 | 61.72 | 5.50 | 16.01 | 0.90 | 12.65 | 0.77 |
| Isophthalic acid (P) | | 57.81 | 7.82 | 50.85 | 5.63 | 49.55 | 0.75 | 36.09 | 5.65 | 56.78 | 3.83 | 23.82 | 1.65 | 8.60 | 0.64 |
| Terephthalic acid (P) | | 14.34 | 1.90 | 55.87 | 21.96 | 11.80 | 0.20 | 100.00 | 0.00 | 25.08 | 1.78 | 24.23 | 1.58 | 17.32 | 1.56 |
| Anthracene (P) | | 69.86 | 4.80 | 100.00 | 0.00 | 100.00 | 0.00 | 24.26 | 12.09 | 5.18 | 1.52 | 14.92 | 4.85 | 5.96 | 0.67 |
| 2,3-Dihydroxybiphenyl (P) | | 100.00 | 0.00 | 95.61 | 10.61 | 17.15 | 0.40 | 45.97 | 0.13 | 57.74 | 9.89 | 60.51 | 4.36 | 16.42 | 1.68 |
| 4-Hydroxyphenylpyruvic acid (P) | | 70.34 | 4.15 | 69.59 | 24.05 | 10.38 | 10.46 | 16.77 | 1.72 | 27.35 | 5.88 | 29.13 | 4.38 | 3.10 | 0.03 |
| Phenoxybenzoic acid (P) | | 11.25 | 1.01 | 73.63 | 5.96 | 10.51 | 0.45 | 23.12 | 2.23 | 30.95 | 2.02 | 70.86 | 6.23 | 58.70 | 4.45 |
| Carbazole (P) | | 100.00 | 0.00 | 100.00 | 0.00 | 100.00 | 0.00 | 100.00 | 0.00 | 96.31 | 12.12 | 100.00 | 4.19 | 56.25 | 0.27 |
| Phenol (P) | | 42.72 | 26.76 | 100.00 | 0.00 | 12.54 | 2.06 | 19.17 | 3.70 | 9.11 | 0.33 | 15.32 | 19.53 | 5.34 | 8.46 |
| Trihydroxytoluene (P) | | 11.80 | 5.09 | 1.62 | 0.94 | 1.44 | 0.57 | 4.22 | 1.43 | 2.94 | 0.67 | 2.37 | 2.53 | 1.04 | 1.63 |
| Gallic acid (P) | | 13.54 | 3.57 | 3.13 | 1.30 | 3.25 | 0.72 | 4.01 | 0.74 | 3.46 | 0.14 | 2.61 | 0.88 | 4.45 | 9.59 |
| Panel B | | PRI | | HAV | | MES | | MCh | | BIZ | | ELMAX | | AQ | |
| | | PA (a.u.) | SD | PA (a.u.) | SD | PA (a.u.) | SD | PA (a.u.) | SD | PA (a.u.) | SD | PA (a.u.) | SD | PA (a.u.) | SD |
| Catechol (I) | | 10.76 | 0.78 | 9.51 | 1.34 | 6.53 | 0.87 | 8.46 | 1.48 | 5.22 | 2.05 | 6.18 | 2.30 | 6.93 | 2.23 |
| Chlorocatechol (I) | | 3.15 | 0.08 | 2.67 | 0.28 | 0.75 | 0.00 | 0.50 | 0.01 | 0.43 | 0.09 | 0.57 | 0.10 | 1.27 | 0.28 |
| Salicylic acid (I) | | 0.05 | 0.04 | 10.54 | 1.56 | 9.57 | 0.27 | 6.53 | 1.05 | 6.12 | 1.73 | 7.53 | 1.19 | 11.12 | 1.80 |
| Muconic acid (I) | | 0.42 | 0.02 | 0.34 | 0.07 | 0.67 | 0.03 | 0.20 | 0.04 | 0.33 | 0.01 | 0.20 | 0.01 | 0.10 | 0.14 |
| Gentisic acid (I) | | 2.03 | 0.96 | 0.00 | 0.00 | 21.02 | 0.48 | 14.07 | 1.41 | 17.10 | 0.88 | 16.89 | 1.08 | 19.96 | 1.69 |
| Protocatechuic acid (I) | | 1.13 | 0.64 | 1.00 | 0.05 | 9.89 | 0.04 | 5.98 | 0.50 | 2.45 | 0.19 | 9.44 | 0.84 | 7.05 | 0.76 |
| Homogentisic acid (I) | | 2.15 | 0.29 | 1.89 | 0.04 | 8.11 | 0.12 | 7.45 | 0.50 | 9.16 | 0.48 | 7.27 | 0.65 | 12.69 | 1.43 |
| Myristic acid (I) | | 9.11 | 1.41 | 3.65 | 4.10 | 15.28 | 0.26 | 8.70 | 1.19 | 12.07 | 1.37 | 11.36 | 0.84 | 15.65 | 1.45 |
| Homoprotocatechuic acid (I) | | 1.69 | 0.23 | 1.50 | 0.07 | 1.01 | 0.03 | 0.92 | 0.08 | 1.13 | 0.10 | 0.87 | 0.15 | 1.53 | 0.18 |

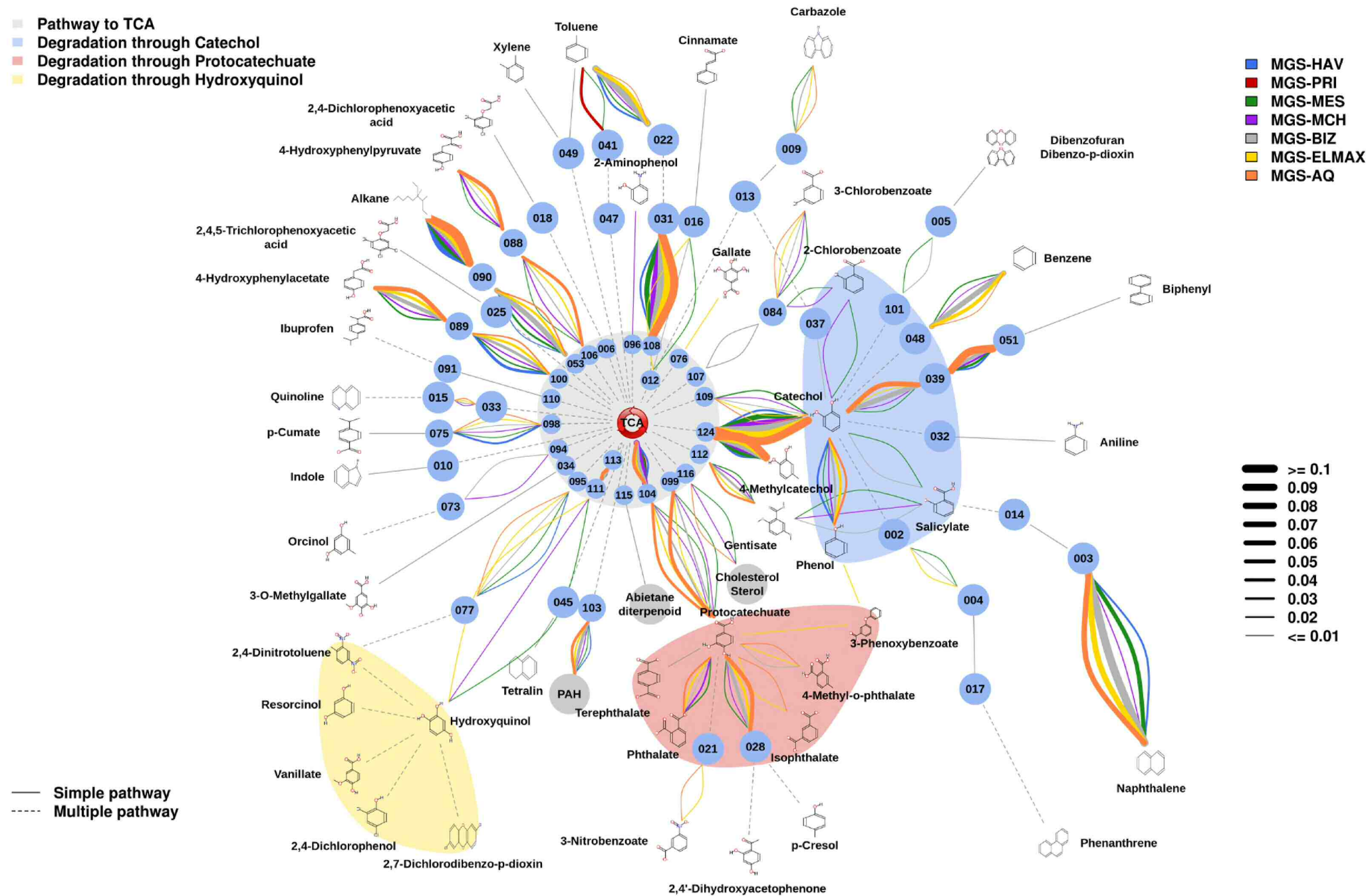
Supplementary Table S8 Putative metabolites identified and quantified by metabolomic approaches by LC-MS (-) and LC-MS (+) in the sediment samples. For differential quantitative metabolomics, we compared the metabolomes (in triplicates) of sediment samples by evaluating the peak area from the chromatographic peaks. A list of masses identified by LC-MS using positive and negative polarities following alignment are presented for samples HAV, MES, PRI and AQ. Because the samples interact during the separation technique and MS, it is crucial to employ quality controls (QCs) during LC-MS to ensure analytical reproducibility. Indeed, QC samples are required throughout the analytical runs at periodic intervals of time to monitor variations in signal across time and at the beginning of the sequence to stabilize the system QC samples were prepared for LC-MS by pooling and mixing equal volumes of each sample⁸³. After gently vortexing, the mix was also filtered and subsequently transferred to an analytical vial and analysed. In all cases, the technique (LC-MS positive (+) or negative (-) mode), mass (in ppm) and retention time (RT; as ppm@RT), and the abundance level per sample are shown. Panel abbreviations and content as follows: LC(-) total and LC(+) total, list of statistically different masses obtained after alignment in LC-MS using negative (-) and positive (+) polarities, respectively; LC(-) HAV, LC(-)MES, LC(-)PRI and LC(-)AQ, list of statistically different masses obtained after alignment identified in HAV, MES, PRI and AQ samples as obtained using LC-MS using negative polarity; LC(+) HAV, LC(+)MES, LC(+)PRI and LC(+)AQ, list of statistically different masses obtained after alignment identified in HAV, MES, PRI and AQ samples in LC-MS using positive polarity. The Table has been provided as a separate Excel table due to the extensive size. For raw data, please contact authors directly.

Supplementary Fig. S1 Relative abundances of the different bacterial taxonomic groups at the (a) phylum and (b) class levels identified in the polluted sediments collected in the Mediterranean Sea and the Aqaba Gulf (Red Sea), as determined by pyrosequencing targeting the 16S rRNA gene. Bacterial sequences were classified based on the RDP Classifier through Qiime 1.6 (<http://www.qiime.org/>).



Supplementary Fig. S2 Potential key catabolic networks of alkanes and aromatics via di- and trihydroxylated intermediates in the investigated communities based on the metagenome sequences derived from sequenced DNA. The color code used for the respective pathways is shown. Codes for chemical species per pathway, as follows. *Napthalene biodegradation*: 3, 1,2-dihydroxynapthalene; 14, 2-hydroxychromene-2-carboxylate. *Aniline biodegradation*: 32, 4-aminobenzene-1,2-diol. *Biphenyl biodegradation*: 51, biphenyl-2-3-diol; 39, benzoate. *Benzene biodegradation*: 48, cis-1,2-dihydrobenzene-1,2-diol. *Dibenzofuran/Dibenzo-p-dioxin biodegradation*: 5, 2,2',3-trihydroxybiphenyl; 101, 2-hydroxy-6-oxo-(2-hydroxyphenyl)-hexa-2,4-dienoic acid. *Chlorobenzoate biodegradation*: 84, 2-chlorocatechol; 107, chloromuconate. *Gallate biodegradation*: 76, (1E)-4-oxobut-1-ene-1,2,4-tricarboxylate. *Carbazole biodegradation*: 9, 2'-aminobiphenyl-2,3-diol; 13, 2-Hydroxy-6-oxo-6-(2'-aminophenyl)-hexa-2,4-dienoate (HOADA); 12, 2-hydroxypenta-2,4-dienoate; 37, anthranilate. *Cinnamate biodegradation*: 16, 2,3-dihydroxycinnamate. *Toluene and Xylene biodegradation*: 49, benzyl alcohol; 41, benzylsuccinate; 47, benzoyl-CoA; 22, toluene-cis-dihydrodiol; 31, 3-methylcatechol; 108, cis,cis-2-hydroxy-6-oxohepta-2,4-dienoate. *2-Aminophenol biodegradation*: 96, 2-aminomuconate 6-semialdehyde. *2,4-Dichlorophenoxyacetic acid biodegradation*: 18, 2,4-chlorophenol; 6, 2-chloromaleylacetic acid. *4-Hydroxyphenylpyruvate biodegradation*: 88, homogentisate; 106, maleylacetoacetate. *Alkane biodegradation*: 90, hydroxy alkane; 53, fatty acid. *2,4,5-Trichlorophenoxyacetic acid biodegradation*: 25, 2,4,5-trichlorophenol / 4-chlorocatechol / chlorohydroquinone. *4-Hydroxyphenylacetate biodegradation*: 89, homoprotocatechuate; 100, 2-hydroxy-5-carboxymethylmuconate semialdehyde. *Ibuprofen biodegradation*: 91, ibuprofen-CoA; 110, cis-1,2-diol-2-hydroibuprofen-CoA. *Quinoline biodegradation*: 15, 2-oxo-1,2-dihydroquinoline; 33, 8-hydroxy-2-oxo-1,2-dihydroquinoline. *p-Cumate biodegradation*: 75, 2,3-dihydroxy-p-cumate; 98, 2-hydroxy-3-carboxy-6-oxo-7-methylocta-2,4-dienoate. *Indole biodegradation*: 10, 2-formylaminobenzaldehyde. *Orcinol biodegradation*: 73, 2,3,5-trihydroxytoluene; 94, 2,4,6-trioxoheptanoate. *3-Methylgallate biodegradation*: 34, 4-carboxy-2-hydroxy-6-methoxy-6-oxohexa-2,4-dienoate; *2,4-Dinitrotoluene biodegradation*: 77, 2,4,5-trihydroxytoluene; 95, 2,4-dihydroxy-5-methyl-6-oxohexa-2,4-dienoate. *Hydroxyquinol biodegradation*: 111, 2-maleylacetate; 113, 3-oxoadipate. *Tetralin biodegradation*: 45, cis-1,2-Dihydroxy-1,2,5,6,7,8-hexahydronaphthalene. *PAH biodegradation*: 103, PAH dihydrodiol. *Abietane diterpenoid biodegradation*: 115, abietane diterpenoid intermediate (abietic acid/pallustric acid). *3-Nitrobenzoate biodegradation*: 21, p-hydroxyaminobenzoate. *2,4'-Dihydroxyacetophenone and p-Cresol biodegradation*: 28, 4-hydroxybenzoate. *Cholesterol/Sterol biodegradation*: 116, cholesterol/sterol intermediate. *Gentisate biodegradation*: 112, maleylpyruvate. *Phenanthrene biodegradation*: 17, 3,4-dihydroxyphenanthrene; 4, 1-hydroxy-2-naphthoate; 2, 2-carboxy-4-(2'-oxo-3,5-cyclohexadienyl)-buta-2,4-dienoic acid.

Protocatechuate biodegradation: 104, 3-carboxy-cis,cis-muconate; 99, 2-hydroxy-4-carboxymuconate-6-semialdehyde. *Catechol and 4-Methylcatechol biodegradation:* 124, cis,cis-2-hydroxy-6-oxohexa-2,4-dienoate; 109, cis,cis-muconic acid. The rel. ab. of each catabolic gene assigned to degradation reactions, as represented by the thickness of the lines in the figure, and the complete list of substrates possibly degraded by the communities are summarized in Supplementary Table S5.

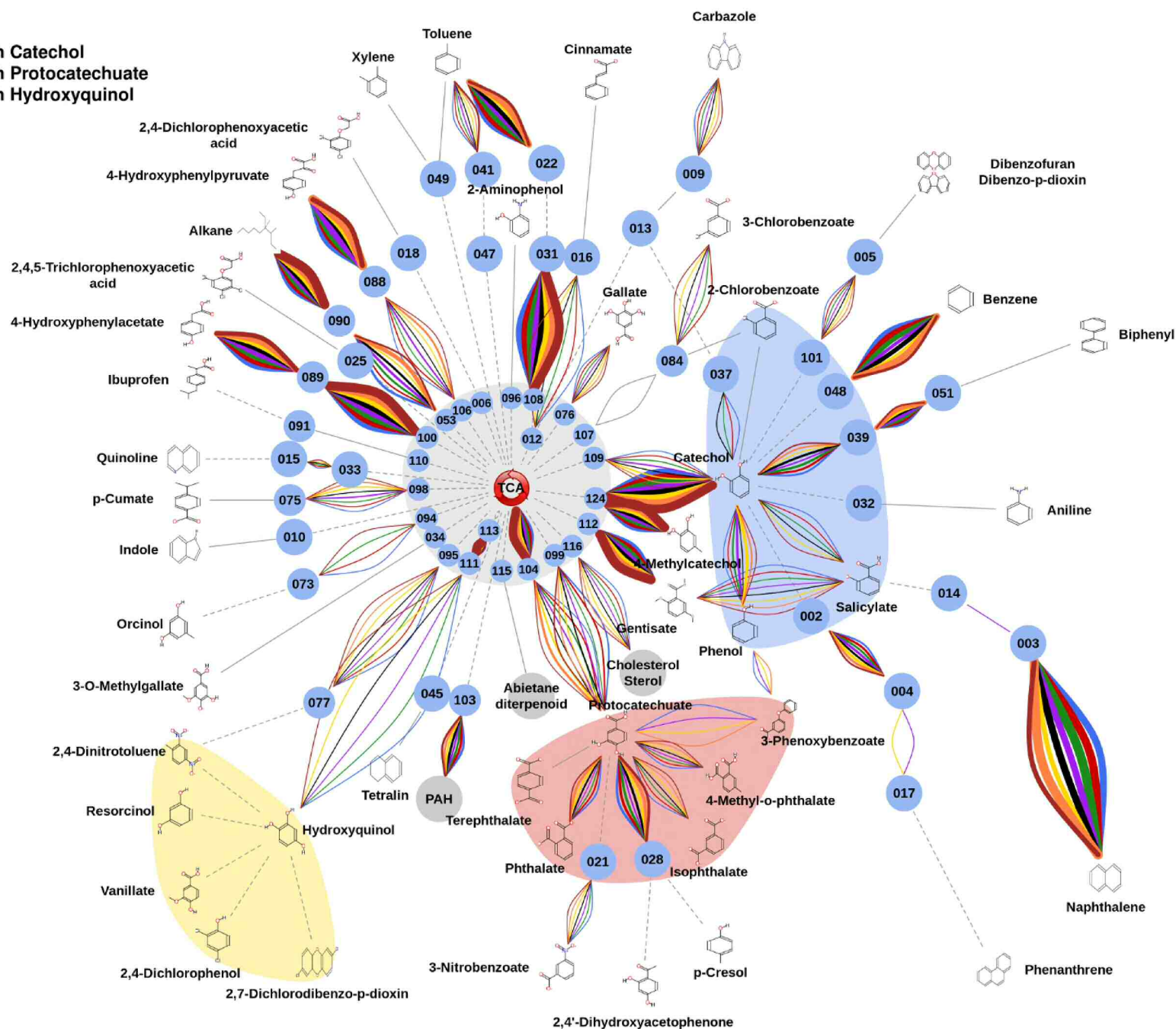


Supplementary Fig. S3 Potential key catabolic networks of alkanes and aromatics via di- and trihydroxylated intermediates in the investigated communities based on the 16S rRNA *in silico*-based metagenome. The color code used for the respective pathways is shown. The codes for the chemical species in each pathway are as described in Supplementary Fig. S2. The rel. ab. of each catabolic gene assigned to degradation reactions, as represented by the thickness of the lines in the figure, and the complete list of substrates possibly degraded by the communities are summarized in Supplementary Table S5. Note that the presumptive network includes an additional sample (ELF) for which DNA sequences could not be obtained.

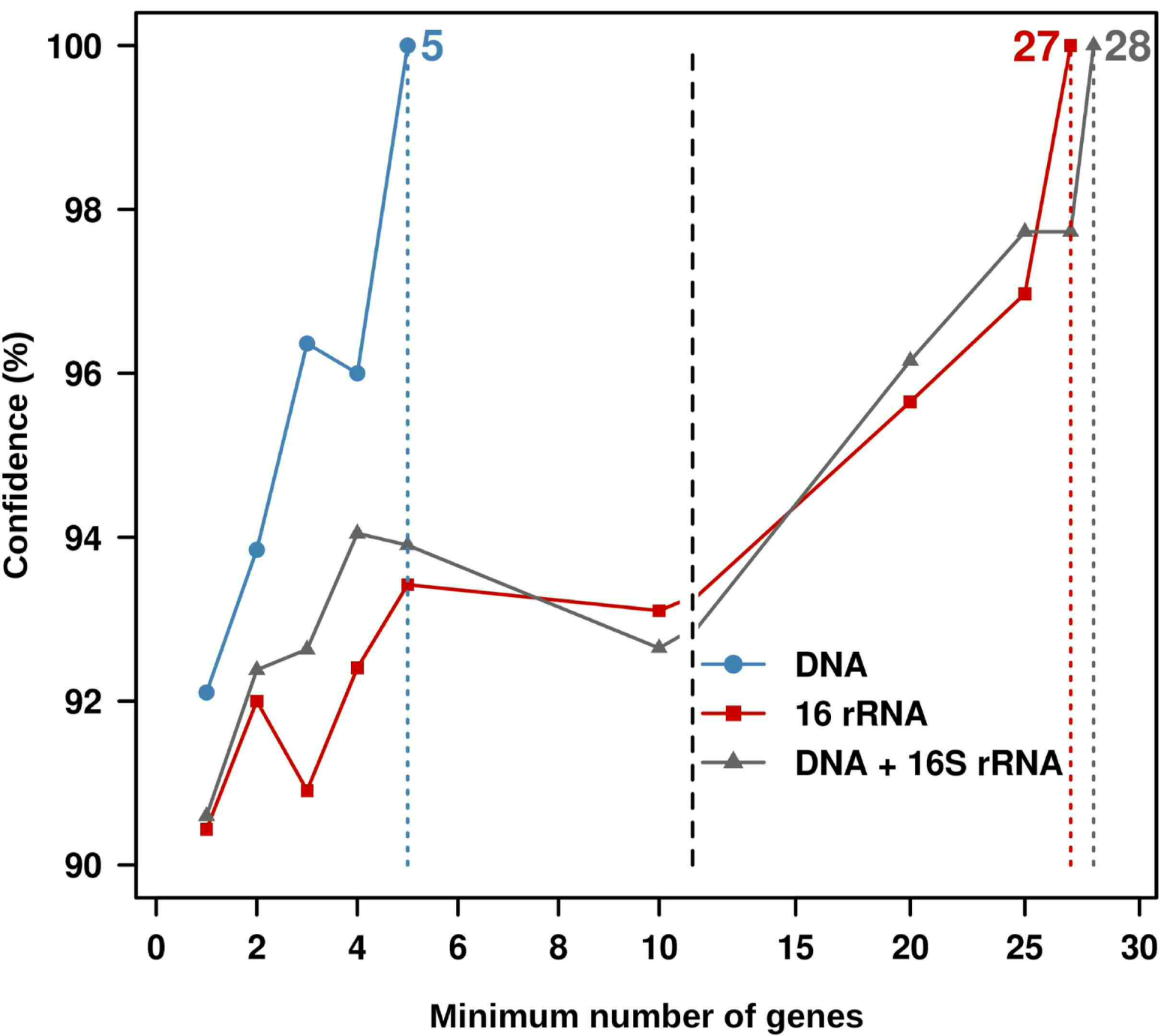
- Pathway to TCA
- Degradation through Catechol
- Degradation through Protocatechuete
- Degradation through Hydroxyquinol

- MGS-HAV
- MGS-PRI
- MGS-MES
- MGS-MCH
- MGS-BIZ
- MGS-ELMAX
- MGS-AQ
- MGS-ELF

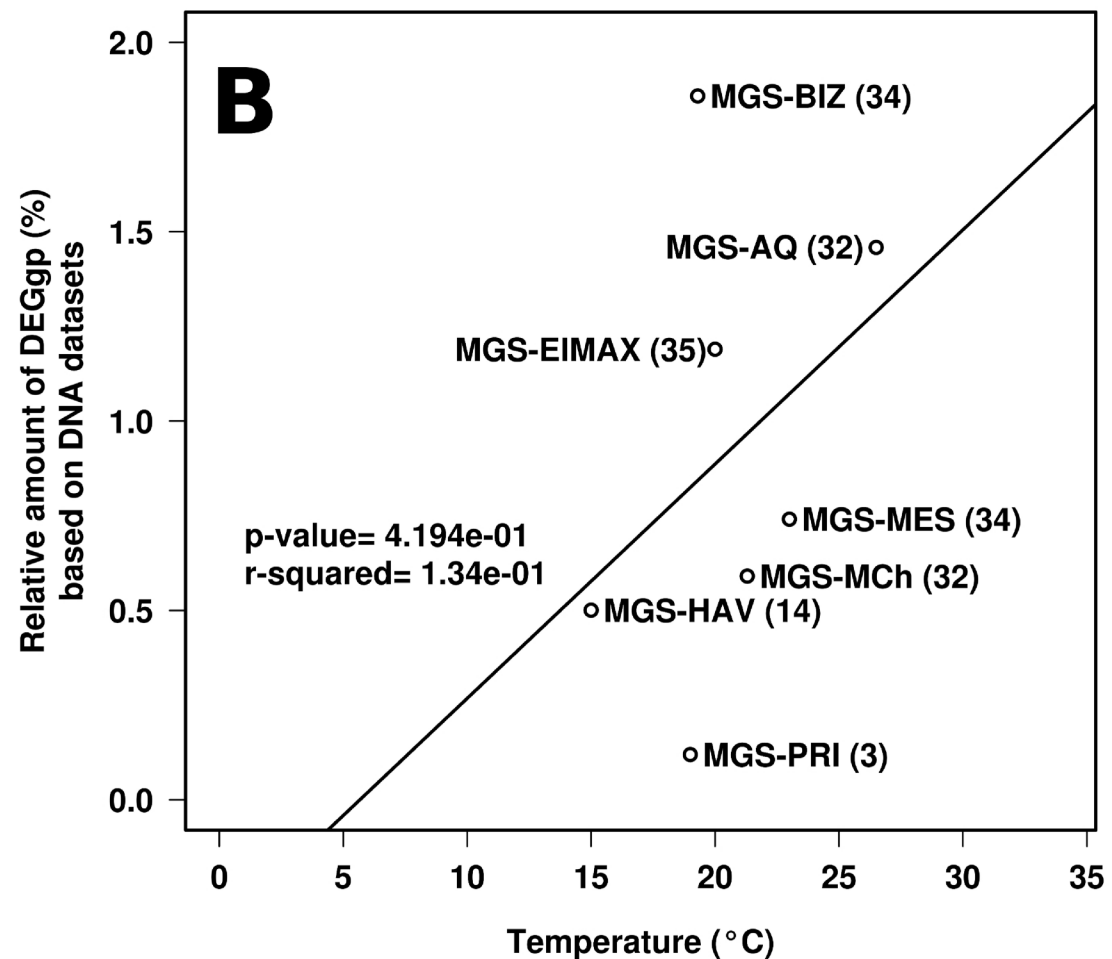
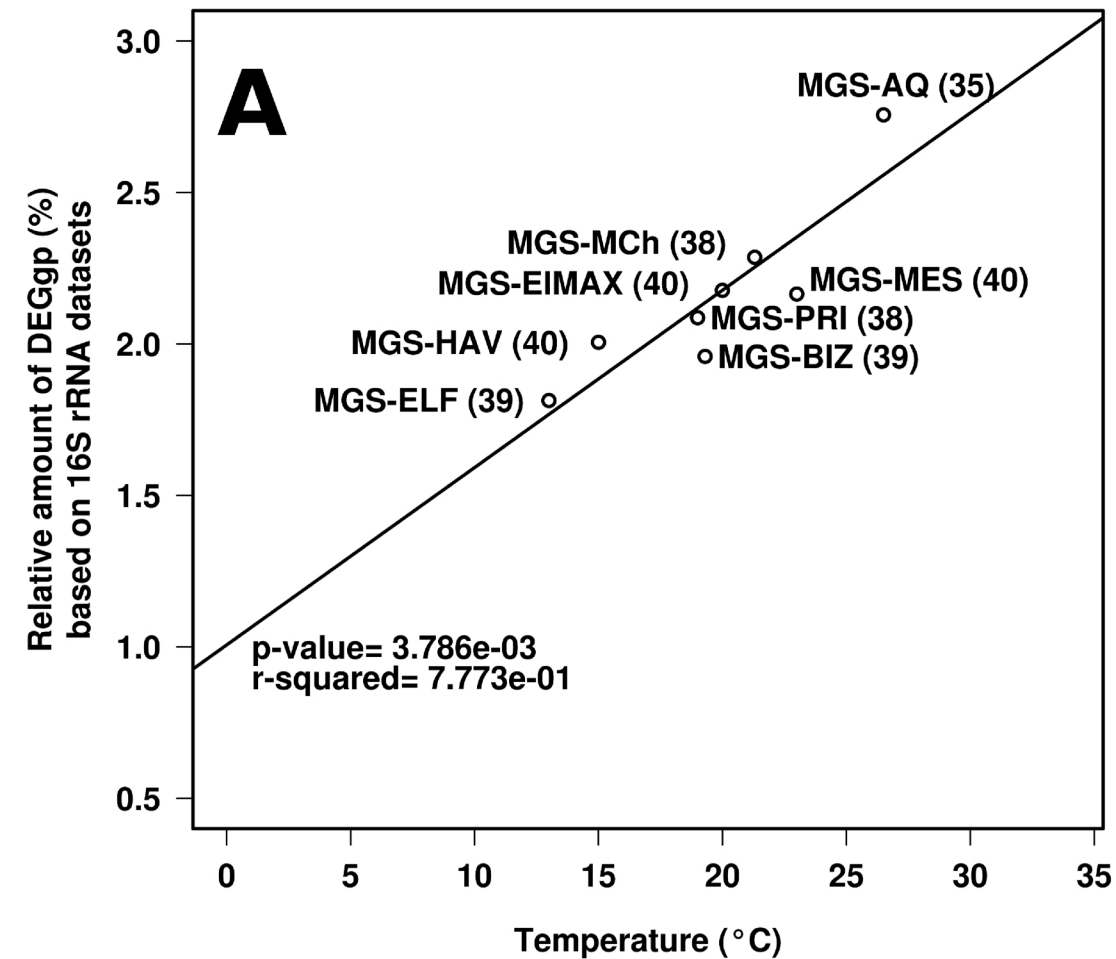
- Simple pathway
- Multiple pathway



Supplementary Fig. S4 Summary statistics on the distribution of the confidence scores based on the number of genes associated to the degradation of a given chemical. Confidence was calculated on the basis of the minimum number of genes encoding catabolic enzymes involved in the degradation of a given chemical, and for which experimental metabolomics evidences were found (see Fig. 2). Based on the calculations, confidence intervals for each of the genes associated with pollutant degradation can be obtained and are given in Supplementary Table S5. As example, as shown in the figure, depending on the number of genes confidence can be calculated, and above a certain threshold a 100% confidence was achieved (the number above which pollutant degradation was confirmed in all cases). Statistics are given considering independent DNA, 16S rRNA and DNA + 16S rRNA datasets.



Supplementary Fig. S5 Temperature as environmental factor driving the size of biodegradation meta-webs at the eight studied sites. A significant positive correlation ($r^2 \sim 0.8$; $P = 3.78 \times 10^{-3}$; t -test) has been found between the relative percentage of genes encoding enzymes participating in biodegradation steps (DEGgp) based on the total number of genes (to avoid artifacts due to differences in sample size) identified as using 16S rRNA data sets (Panel A). When only gene percentages based on DNA datasets were considered (Panel B), the correlation was found at lower extend ($r^2 \sim 0.42$; $P = 4.194 \times 10^{-1}$; t -test); this is most likely due to the differences in sequence coverage. Both, the R-squared (r^2) and the P -value (t -test) for the regression are shown for data in Panels A and B.



Supplementary Fig. S6 Multi-panel map of the spatial distribution of the relative abundance level of genes encoding catabolic enzymes in the study area, referred to the total number of genes, as detected in the meta-sequences. Values are represented by colored dots. See legend in each panel as a reference. Spatial distributions of genes encoding catabolic enzyme percentages (on the basis of DNA + 16S rRNA data sets) in the study area were produced using Golden Software Surfer 8.0. The data are plotted as colored dots showing the true values at each sampling station. Note that, genomic evidence for the conversion of carbazole to anthranilate (via CarA and 2'-aminobiphenyl-2,3-diol 1,2-dioxygenase) was observed at all sites; however, further conversion to catechol (via AndA) was not detected in the MCh, ELMAX, ELF and AQ samples, suggesting that the complete mineralization of this pollutant most likely does not occur at those sites. Site temperatures are indicated in the panels. Reactions associated to genes encoding enzymes in panels, as follows:

Phenol hydroxylase (PhO): phenol \Rightarrow catechol

Carbazol dioxygenase (CarA): carbazol \Rightarrow 2'-aminobiphenyl-2,3-diol (code 009, Fig. 3)

Antranilate-1,2-dioxygenase (AndA): anthranilate (code 37, Fig.3) \Rightarrow catechol

Benzene dioxygenase (Ben): benzene \Rightarrow cis-1,2-dihydrobenzene-1,2-diol (code 048, Fig. 3)

Benzoate-1,2-dioxygenase: benzoate (code 039, Fig. 3) \Rightarrow catechol

2-Chlorobenzoate-1,2-dioxygenase: 2-chlorobenzoate (code 044, Fig. 3) \Rightarrow 2-chlorocatechol (code 084, Fig. 3)

Aromatic demethylase: 4-methyl-o-phthalate \Rightarrow protocatechuate

3-Nitrobenzoate-1,2-dioxygenase: 3-nitrobenzoate \Rightarrow *p*-hydroxyaminobenzoate (code 021, Fig. 3)

4-Hydroxybenzoate 3-monoxygenase: 4-hydroxybenzoate (code 028, Fig. 3) \Rightarrow protocatechuate

Toluene dioxygenase: toluene \Rightarrow toluene-cis-dihydrodiol (code 049, Fig. 3)

Benzyl succinate synthase: benzylsuccinate (code 041, Fig. 3) \Rightarrow benzoyl-CoA (code 047, Fig. 3).

